

**ION MICROPROBE ISOTOPIC STUDIES OF Ca-Al-RICH
INCLUSIONS FROM PRIMITIVE METEORITES**

THESIS SUBMITTED

to

THE MAHARAJA SAYAJI RAO UNIVERSITY OF BARODA

FOR THE DEGREE OF

Doctor of Philosophy

in

Physics

by

G. SRINIVASAN

May 1994

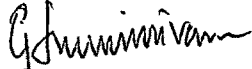
**PHYSICAL RESEARCH LABORATORY
NAVRANGPURA
AHMEDABAD- 380 009
INDIA**




P/Th
7890

Certificate


This is to certify that the contents of this thesis is original work of the candidate and no time has been submitted for any other degree or diploma.


(G. Srinivasan)

Candidate


(Dr. Madhuben Shah)

Co-Guide


(Dr. B.G.A. Anand Rao)

Guide

" Fire is this burning and radiant Sun,
he is the One lustre and all-knowing Light,
he is the highest heaven of spirits.
With a thousand rays he burns and exists in a
hundred existences; lo this Sun that rises,
he is the Life of all his creatures"

(Prashna Upanishad 1.8)

Dedicated to
Amma, Appa,
Lakshmi & Krishna

Acknowledgements

I am grateful to my thesis supervisors Drs. B.G.A. Ananda Rao and Madhuben Shah for their guidance and encouragement. I am beholden to Dr. J. N. Goswami for support and advice, and for providing excellent laboratory facilities. I sincerely appreciate his active involvement in every stage of my research and critiquing my work. He has taught me to appreciate keen attention to detail and has inspired me to excel.

I have been fortunate to receive help and guidance from many experts. I express my heartfelt thanks to Drs. S.V.S. Murty, S.K. Bhattacharya and Profs. S. Krishnaswami and N. Bhandari.

The manuscript for this thesis would not have attained its present form but for the critical comments from Drs. I.D. Hutcheon, A.M. Davis, E. Zinner, G. Lugmair and Prof. K. Gopalan. The work would not have been possible without the meteoritic samples from Vernadsky Institute. Suitable terrestrial standards were provided by Drs. I. D. Hutcheon, G.J. MacPherson, E. Zinner and A.A. Ulyanov.

I want to thank the faculty of PRL who provided me with advice and useful discussions. Prof. B.L.K Somayajulu, Dr. M.M. Sarin for always being accessible and allowing to use the facilities in Chem. Lab. Dr. R Ramesh for stimulating my thought process. Drs.A.Sinhgvi, T.R.Venkateshan, Kanchan Pande, J.R.Trivedi , S. Kusumgar and P. N. Shukla for materials and timely help. I also thank Drs. S. Sitaram and Sai Iyer for assistance with computer related matters. I express my gratitude to Prof. Lal for taking an interest in my work.

I am deeply appreciative for the helpful and congenial atmosphere of PRL facilities particularly the friendly staff of the library. Thanks are due to Shri Ranpura and Shri Bhavsar for their skilful photography and drafting. Thanks also to staff members of

the workshop , glass blowing, liquid nitrogen, computer center, despatch and canteen. I acknowledge Bhavsar, Pandian, Panchal, Ravi and Kameshwar Rao for their ever ready cooperative spirits and help extended over all these years with my heartfelt thanks. I will always remember with fondness the staff members of PRL who give the lab its charm and conducive atmosphere to work.

The sanity, or lack of it, of those around me in the ion probe lab , especially Nirjhari, Deomurari, V.G. Shah, Anjan, Sandeep, Micheal and Sanjeev, enabled me to keep my work in (or out of) perspective.

I owe more appreciation than I can ever put into words to some very special friends who have provided moral support and encouragement and kept me going when the end was not in sight. Devashis, Sandeep, Shailaja, Supriya and Venkatraman for helping me in various stages of thesis preparation. Special thanks to Nambiar for typing my manuscript, often at a rushed pace. I would like to thank all my fellow research students and PostDocs for making my stay in PRL memorable.

Finally, I thank my parents, relatives and innumerable other people who have nurtured my spirit to explore. Last but not the least I thank the tax payers of this nation for providing research funds.

To any one else I may have missed out : Hey ! no offence meant. I am doing this at four in the morning and its due at the binders at seven thirty !!

Contents

Acknowledgement	(i)
Contents	(iii)
List of Tables	(v)
List of Figures	(vi)
1 Introduction	1
1.1 Ca-Al-Rich Inclusions (CAIs)	3
1.2 Isotopic Studies of CAIs	5
1.2.1 Studies of Stable Isotope Anomalies	6
1.2.2 Mg Isotopic Studies	7
1.3 Extinct Radionuclides as “Chronometers” of Early Solar System Processes . .	10
1.4 Aim and Scope of this work	11
2 Experimental Techniques	14
2.1 The Cameca Ims-4f Ion Microprobe	14
2.1.1 Primary Ion Column	16
2.1.2 Secondary Ion Column	18
2.2 High Mass Resolution Isotopic Analysis	22
2.2.1 Interferences and Corrections	23
2.2.2 Dynamic Stability of the Instrument	23
2.2.3 Stability of the Counting System	27
2.3 Isotopic Analysis of Terrestrial Standards	29
2.3.1 Mass Fractionation	29
2.3.2 Mg Isotopic Analysis	34
2.3.3 K-Ca Isotopic Analysis	38

3	Sample Description	43
3.1	Efremovka CAIs	43
3.2	Grosnaja CAIs	45
4	Results	61
4.1	Results from Mg-Al Isotopic Studies	61
4.2	Results from K-Ca Isotopic Studies	78
5	Discussion	83
5.1	Processes Affecting the Formation of CAIs	84
5.2	Relict Spinel and Nebular Environment for the Formation of CAIs	91
5.3	Mg-Al Isotopic Systematics and Isotopic Heterogeneity in the Nebula	99
5.4	^{41}Ca In The Early Solar System	105
5.5	Extinct Radionuclides and Time Scales for Early Solar System Process	110
6	Summary and Conclusions	114
6.1	Scope for Future Work	117
7	References	120
8	List of Publications	129

List of Tables

1.1	Mineralogical Compositions of CAIs	4
2.1	Mg Isotopic Data for Terrestrial Standards	35
2.2	Mg-Al Sensitivity Factors	35
2.3	Mg Composition of Isotopically Spiked Samples	37
2.4	K-Ca Sensitivity Factors	42
2.5	K Isotopic Analyses of Terrestrial Minerals	42
3.1	CAIs analyzed in this work	57
3.2	Composition of mineral phases in CAIs	57
3.3	Electron Microprobe Analysis of Melilite in Efremovka CAIs	58
3.4	Electron Microprobe Analysis of Pyroxene in Efremovka CAIs	59
3.5	Electron Microprobe Analyses of Mineral Phases in E50	60
3.6	Major element composition of mineral phases in Grosnaja CAIs	60
4.1	Mg-Al Data	66
4.2	Mg-Al Data	67
4.3	Mg-Al Data	68
4.4	Mg-Al Data	69
4.5	Mg-Al DATA	70
4.6	K-Ca DATA	81

List of Figures

2.1	A schematic of the ion microprobe (Cameca Ims-4f).	15
2.2	Schematic of the primary column of the ion microprobe.	17
2.3	Schematic of the secondary ion column of the ion microprobe.	19
2.4	Ideal traces of the secondary ions from the sample surface.	20
2.5	High mass resolution spectra.	24
2.6	Dynamic stability test in the peak-jumping mode.	26
2.7	Dead time of the integrated pulse counting system.	28
2.8	Static background of the pulse counting system.	30
2.9	Magnesium isotopic mass fractionation in terrestrial spinel as a function of time.	36
2.10	High mass resolution spectrum at mass 41 in terrestrial perovskite.	40
2.11	The values of $[^{40}\text{Ca}^{43}\text{Ca}]^{++}/^{43}\text{Ca}^{+}$ in terrestrial perovskite and meteoritic and terrestrial pyroxenes.	41
3.1	Photomicrographs of Efremovka and Grosnaja CAIs.	56
4.1	Mg-Al evolution diagram for the Efremovka and Grosnaja CAIs.	77
5.1	Intrinsic Mg isotopic mass fractionation in Efremovka CAIs.	85
5.2	Magnesium isotopic mass fractionation in melilite from compact type A Efremovka CAI E2.	87
5.3	Akermanite content and Mg isotopic composition in melilite along a nearly radial traverse in type B1 Efremovka CAI E40.	88
5.4	Photomicrographs of spinels from the boundary and interior regions of E40.	92
5.5	Magnesium isotopic mass fractionation in melilite and spinel from Efremovka CAI E40 measured along two radial traverses.	93
5.6	Initial $^{26}\text{Al}/^{27}\text{Al}$ in eight Efremovka CAIs.	101
5.7	K-Ca evolution diagram for Efremovka CAIs E44, E50 and E65.	107

Chapter 1

Introduction

The solar system originated from a cloud of gas and dust, the so called solar nebula, about 4.6 billion years ago. Our present day understanding of the solar system is based mainly on studies of various constituent members of the solar system : the Sun, the planets and their satellites, meteorites and comets. Amongst all the constituent members, samples from our own planet are most easily accessible for scientific studies.

Samples from the three major reservoirs of the Earth, the landmass (continents), the oceans and the atmosphere have been extensively studied to understand their evolution over geological time scales. Geophysical techniques and laboratory based simulation experiments have also helped us to decipher the internal structure of the Earth. However the records of events that took place during the very early epochs of Earth's history are difficult to obtain as the terrestrial samples have undergone extensive geological alteration and weathering that led to obliteration of the records of the earliest era. The oldest dated terrestrial sample has an age of about $\sim 4.27\text{Ga}$ (Compston and Pidgeon 1986), much lower than the formation age of the Earth and the solar system. The situation is similar in the case of the lunar rocks which have been studied extensively following the successful Apollo and Luna missions. Most of the returned lunar samples from the Mare regions have ages between 3.3 to 3.9Ga, and only a few of the anorthositic highland rocks are older than 4.2Ga, but none of them closer to 4.6Ga. On the other hand, most of the meteorites have formation ages close to 4.6Ga (Tilton 1988) and many of these have not been disturbed since their

time of formation. The antiquity of meteorites gives them a position of prime importance in the investigation of the early evolutionary history of the solar system.

Meteorites are rock bodies that have mostly originated from the present day asteroid belt although some may be of cometary origin. Gravitational perturbations by Mars and Jupiter can disturb their orbits and this can lead to their capture by Earth or other planets (Wetherill and Chapman, 1988 and references therein). On the basis of their composition, meteorites have been classified broadly into three different types: stones, stony-iron and iron. The stones are like rocks on the surface of the earth made primarily of silicate minerals, irons are pieces of metal (essentially Fe-Ni alloys) and stony irons are a mix of both silicates and metals. Meteorites belonging to each type exhibit great diversity in their physical and chemical properties, and this leads to further classification of each type. On the basis of presence or absence of small (0.1 - 1 mm) rounded objects, known as chondrules, the stones have been classified into two groups: chondrites and achondrites. As a group chondrites display a very important property which sets them apart from other classes of meteorites. Their bulk chemical composition, except for several highly volatile elements and Li, is similar to solar composition and this is particularly true of the carbonaceous chondrites (Sears and Dodd 1988). This bears testimony to the fact that these meteorites have preserved primitive signatures from the time of their formation and makes studies of chondritic meteorites and particularly that of carbonaceous chondrites extremely important for our understanding of the early evolution of the solar system.

A great deal of information about the earliest stages of evolution of the solar system comes from the study of a particular group of objects, the so called Ca-Al-rich refractory inclusions or CAIs, that are found only in carbonaceous chondrites belonging to CV, CO and CM groups. The CAIs are composed of refractory oxides and silicates like hibonite ($\text{CaAl}_{12}\text{O}_6$), perovskite (CaTiO_3), spinel (MgAl_2O_4), melilite ($\text{Ca}_2\text{Al}_2\text{SiO}_7$ - $\text{Ca}_2\text{MgSi}_2\text{O}_7$), anorthite ($\text{CaAl}_2\text{Si}_2\text{O}_8$), fassaite ($\text{Ca}(\text{Mg}, \text{Ti}, \text{Al})_2(\text{Al}, \text{Si})_2\text{O}_6$) and diopside ($\text{CaMgSi}_2\text{O}_6$), and have high concentrations of refractory major and trace elements like Ca, Al, Mg, Ti, and Sc, V, refractory rare earth elements etc. The CAIs were first observed in the carbonaceous

chondrite Allende (Marvin et al. 1970) which fell in 1969 and were subsequently identified in other carbonaceous chondrites. The present thesis exclusively deals with the study of early solar system processes based on isotopic studies of CAIs using the ion microprobe.

1.1 Ca-Al-Rich Inclusions (CAIs)

The CAIs are refractory objects with sizes ranging from submillimeter to a couple of centimeters. Their chemical and mineralogical composition are in general accord with those expected for the first solids to form during the cooling of a hot nebular gas with average solar system composition (Grossman 1972). Many workers have reviewed the properties of CAIs found in different types of carbonaceous chondrites (Grossman 1980, McDougall and Goswami 1981, MacPherson et al. 1988), and a brief summary of these are presented here.

On the basis of the sizes of the constituent minerals, CAIs can be classified into two groups: fine-grained (typical grain size 1-20 μm) and coarse-grained (grain size upto 0.5 mm). The coarse grained CAIs, found generally in CV and CO meteorites like Allende, Efremovka, Vigarano, Ornans etc. range in size from < 1mm to \sim 2cm. The coarse-grained CAIs can be further classified on the basis of their petrographic and mineralogical composition (Grossman 1980, Wark and Lovering 1982, and Wark 1987). The generally accepted sub-types and their constituent phases are: type A (melilite + Spinel), type B (melilite + spinel + fassaite + anorthite), and type C (anorthite + melilite + spinel) (Table 1.1). The type B inclusions are further divided into B1 and B2, the former having an outer mantle consisting mostly of melilite while it is absent in the latter. CAIs can also be classified by their bulk chemical composition and REE patterns (Mason and Taylor 1982). An alternative scheme of classification of CAIs was also proposed by Kornacki and Fegley (1984). It has been observed that chemical classification and petrographic classification do not necessarily correlate and there is significant overlapping of different petrographic types with different types based on chemical composition. However the petrographic classification is more commonly used to describe the CAIs and we shall follow this terminology here. In

Table 1.1: Mineralogical Compositions of CAIs*

Mineral	CV meteorites			CM meteorites	
	Type A [†]	Type B [†]	Type C [‡]	Hibonite-Rich [†]	Spinel-Rich [†]
Corundum	-	-	-	Trace	-
Hibonite	~ 5	-	-	5-85	0
Perovskite	1-3	-	-	1-10	1-20
Spinel	5-20	15-30	2-12	10-80	60-90
Melilite	> 75	5-20	0-25	-	-
Fassaite	-	35-60	18-34	0-5	-
Diopside	-	-	-	2-5	2-5
Anorthite	-	5-25	45-60	-	-
[†] Grossman 1980, MacDougall and Goswami 1981					
[‡] Wark 1987 *Abundance is in percentage					

addition, it is important to note that there are differences in the mineralogical composition of CAIs from different groups of carbonaceous chondrites; hibonite which is one of the most refractory phase is rarely seen in CAIs from CV or CO meteorites whereas they are more common in CM meteorites.

Petrographic, chemical and isotopic studies, as well as laboratory based simulation experiments, carried out over the last two decades, have revealed that CAIs are a complex and diverse group of objects that are some of the first solids to have formed in the solar system. Some of the CAIs could be direct nebular condensates while others must have undergone complex formation history with one or more episodes of evaporation, melting, and recrystallization. Some of them have also been subjected to late stage secondary alteration. A brief summary of isotopic studies of CAIs and important conclusions obtained from these studies are presented in the following section before describing the scope and the aim of the present work.

1.2 Isotopic Studies of CAIs

Isotopic studies of CAIs have been carried out using mass spectrometric techniques for more than a decade. The main emphasis in these studies was to look for possible deviations in the isotopic compositions of constituent elements of bulk CAIs and/or individual refractory phases in them from “solar system” values. Such deviations, if present, allow us to decipher several important aspects related to the early evolution of the solar system that includes: the state of the solar nebula, the processes responsible for the formation of some of the first solar system solids (CAIs), time scales for the formation of CAIs etc. Presence of non-solar isotopic composition in CAIs, commonly termed as isotopic anomaly, can be due to one or more of the following reasons:

- (i) mass dependent isotopic fractionation at the time of formation of CAIs resulting from the physical or chemical processes responsible for their formation,
- (ii) presence of non-solar nucleosynthetic components from distinct stellar sources in the nebula in the region of CAI formation,
- (iii) incorporation of radioactive nuclei into the CAI at the time of its formation and their subsequent *in situ* decay resulting in an anomalous concentration of the daughter nuclei,
- (iv) enhancement of particular isotope caused by interaction of energetic particle (cosmic rays) with CAIs in interplanetary space.

Identification of the observed isotopic anomaly in CAIs with any one of the above causes can provide useful information to understand processes operating in the formative stages of the solar system. For example, identification of isotopic mass fractionation effects can help us to understand the processes leading to the formation of CAIs and the nature of their parent material, the second type of anomaly allow us to identify specific astrophysical sites that have contributed matter to the solar nebula and the radiogenic isotopic anomalies allow us to infer about times scales of early solar system processes.

Isotopic analyses of major elements like Ca, Mg, Ti, O and Si in CAIs have been carried out using different types of mass spectrometers like thermal ionization mass spectrometer, gas source mass spectrometer and secondary ion mass spectrometer. The isotopic composition of the noble gases (e.g. neon, krypton and xenon) in CAIs have also been studied extensively. The progress made in the field of isotopic studies of CAIs has been reviewed in a series of articles (Clayton 1978; Podosek 1978; Lee 1979, 1988; Begemann 1980; Wasserburg et al 1980; Wasserburg and Papanastassiou 1982; Wasserburg 1985; Clayton et al. 1988; Thiemens 1988; Harper 1993). We briefly summarize some of the main results that emerged from studies of isotopic composition of the major elements.

1.2.1 Studies of Stable Isotope Anomalies

Oxygen and silicon isotopic studies have been carried out using gas source mass spectrometers primarily at the University of Chicago (Clayton et al. 1973, Clayton et al. 1993). Oxygen which consists of three isotopes ^{16}O (99.756%), ^{17}O (0.039%) and ^{18}O (0.205%) is one of the major elements in the solar system. Studies of oxygen isotopes have revealed enormous variations in oxygen isotopic compositions of individual mineral phases in CAIs that cannot be explained by mass dependent fractionation process (Clayton 1973, Clayton et al. 1993 and references therein). This observation shattered the earlier belief of a well mixed isotopically homogeneous solar nebula. It was soon realized that CAIs are in general derived from an oxygen reservoir (dust) enriched in ^{16}O which later reequilibrated with gaseous reservoir depleted in ^{16}O . Initial data from Allende CAIs suggested an enrichment of $\sim 5\%$ in their $^{16}\text{O}/^{18}\text{O}$ compared to the reference value of O (498.70337).

The observation of oxygen isotopic anomaly led to the search for isotopic anomalies in other elements. Silicon isotopic studies have shown that the coarse-grained CAIs are enriched in the heavy isotopes of Si (i.e. ^{29}Si and ^{30}Si) compared to ^{28}Si (Molini-Velsko 1983, Clayton et al. 1985). This enrichment that ranges upto $\sim 5\%$ /amu, relative to the solar value can be explained by normal mass dependent fractionation, and unlike oxygen, the silicon isotopic composition is similar in all the mineral phases. This observation can be

explained by postulating that source material of the coarse-grained CAIs are evaporative residues that are preferentially depleted in the lighter isotopes.

Studies of isotopic composition of elements in the iron group, e.g. Ca, Ti and Cr, have shown that there is a general enrichment in the neutron rich isotopes (e.g. ^{48}Ca , ^{50}Ti and ^{54}Cr). The most prominent signatures (isotopic anomalies of large magnitude) of Ca and Ti isotopic anomalies are mainly seen in hibonite. The CAIs from CV meteorites have hibonite only as a minor phase and in general these CAIs do not show large anomalies in Ti or Ca. In contrast hibonite from CM meteorites show large isotopic anomalies in both Ca and Ti (Zinner et al. 1986b, Fahey et al. 1987a, Hinton et al. 1987, Ireland 1988, 1990). The studies of Ca and Ti isotopic anomalies in CAIs also brought into fore the advantages of secondary ion mass spectrometer or the ion microprobe over thermal ionization mass spectrometer (TIMS) in analyzing individual microphases within the CAIs. Although the data for CAIs obtained by TIMS suggested the isotopic anomalies in ^{48}Ca and ^{50}Ti to be linearly correlated with a few exceptions (Jungck et al. 1984, Niederer and Papanastassiou 1984), the conclusive evidence in this regard came from the ion microprobe study of individual hibonite grains from CM meteorites (Zinner et al. 1986b). The enrichment in the neutron-rich isotopes of Ca, Ti and Cr and their qualitative correlation have led to the theoretical investigation of plausible astrophysical sites whose nucleosynthetic output may give rise to the observed features. At present these observations are best explained by considering contribution from neutron-rich nuclear statistical equilibrium process taking place in the expanding supernova envelope (Hartman et al. 1985). Interstellar grains are considered to be the most likely carriers of these isotopic anomalies to the solar nebula. However, no definite signatures of such grains were obtained during the study of the hibonites (Fahey et al. 1985, 1987a).

1.2.2 Mg Isotopic Studies

Magnesium isotopic composition of CAIs has been studied most extensively as most of the initial thermal ionization and ion microprobe studies of CAIs concentrated on magnesium

isotopic analysis. These studies were carried out mainly to identify intrinsic isotopic mass fractionation effect and the possible presence of excess ^{26}Mg due to the decay of the short-lived radioisotope ^{26}Al that could have been incorporated into the CAIs at the time of their formation.

The studies of magnesium isotopic composition in CAIs, particularly identification of intrinsic mass fractionation effect, have helped in elucidating the nature of precursor material and/or the processes leading to the formation of the CAIs. For example, most of the coarse-grained CAIs are characterized by enrichment in the heavy isotopes of magnesium suggesting their source material to be evaporative residues. On the otherhand, the fine-grained CAIs are generally enriched in the lighter isotopes indicating that they are comprised of refractory components that may have condensed from a gas depleted in the heavier isotopes (Esat and Taylor, 1984; Niederer and Papanastassiou, 1984; Clayton et al., 1988 and references therein). Many of the inclusions however show complex petrographic and isotopic features and it is difficult to rule out multistage processes leading to their formation. Petrographic studies of the coarse-grained CAIs indicate that most of them are formed by crystallization from refractory melts of appropriate composition and some constraints on the initial temperature of such melts as well as their cooling rate were derived from mineralogical and laboratory simulation studies (Nagasawa et al., 1977; MacPherson and Grossman, 1981; Stolper, 1982; Wark and Lovering, 1982; MacPherson et al., 1984; Kornacki and Fegley, 1984; Stolper and Paque, 1986). Occurrence of additional processes like evaporation/volatilization that could leave their imprint in both petrographic and magnesium isotopic records found in CAIs have also been proposed (e.g., MacPherson et al., 1988). However, instances for sympathetic behaviour of petrographic and magnesium isotopic data are rare and data for only a couple of very special type of CAIs, the so called FUN inclusions, are suggestive of such a trend (Clayton et al., 1984; Davis et al., 1991).

Studies of Mg-Al isotopic systematics in CAIs from primitive meteorites and the observed excess in ^{26}Mg in many CAIs have provided strong evidence for the presence of the now-extinct nuclide ^{26}Al (meanlife $\sim 1.1\text{Ma}$) in the solar nebula at the time of CAI

formation (Lee et al. 1977, Wasserburg 1985). An extensive data set on magnesium isotopic composition have been obtained by ion microprobe studies of CAIs belonging to different petrographic types (A, B1 and B2) from CV and CO meteorites and hibonite grains from CM meteorites (Hutcheon, 1982; Huneke et al., 1983; Armstrong et al., 1984; Clayton et al., 1984; Hutcheon et al., 1986; Ireland et al., 1986; Fahey et al., 1987a,b; Brigham et al., 1988; Hinton et al., 1988; Ireland, 1990; Davis et al., 1991; Podosek et al., 1991; see also reviews by Clayton et al., 1988; and MacPherson et al., 1988). The studies of the coarse-grained CAIs, in particular, showed some specific trends between magnesium isotopic composition and petrographic type. For example, some type B1 CAIs are characterized by the presence of ^{26}Mg excess due to the decay of ^{26}Al , and yield ($^{26}\text{Al}/^{27}\text{Al}$) at the time of formation of these inclusions (initial $^{26}\text{Al}/^{27}\text{Al}$) clustering around the value of 5×10^{-5} , commonly referred to as the canonical value. The Mg-Al systematics in the type B2 CAIs, on the other hand, are often disturbed and are characterized by lower values for initial ($^{26}\text{Al}/^{27}\text{Al}$). This is suggestive of either a heterogeneous distribution of ^{26}Al in the nebula or late disturbances in the magnesium isotopic systematics in these CAIs due to exchange/reequilibrium of magnesium isotopes. Relatively few type A CAIs have been studied and the Mg-Al systematics in these inclusions also show disturbances except for a couple of cases (e.g., Fahey et al., 1987b). In addition, hibonite grains from CM meteorites like Murchison, that have large isotopic anomalies in Ca and Ti, either have very low initial ($^{26}\text{Al}/^{27}\text{Al}$) compared to the canonical value or are characterized by near absence of ^{26}Al . Most of these variations were generally considered to represent an extremely heterogeneous distribution of ^{26}Al in the nebula. There are however alternative suggestions (e.g. Podosek et al. 1991) that these differences may be due to secondary processes affecting these objects. Thus the idea of an extremely heterogeneous distribution of ^{26}Al in the solar nebula need not necessarily be correct.

1.3 Extinct Radionuclides as “Chronometers” of Early Solar System Processes

Isotopic studies of Mg, Cr, Ni, Ag and Xe in early solar system objects have established the presence of several short-lived now-extinct radionuclides with meanlife $\geq 1\text{Ma}$ in the early solar system (Wasserburg 1985, Cameron 1993). The presence of such short-lived radionuclides manifests itself through an excess in the daughter isotopes (e.g., ^{26}Mg in the case of ^{26}Al). Although a fossil origin for these excesses have also been suggested (Clayton 1977, 1982, 1986), there are good reasons (particularly the correlation of excess in daughter nuclide with the abundance of the parent element in the analyzed phases) to believe that these extinct nuclides were present in the early solar system and were incorporated ‘live’ into these early solar system objects.

In general, if the meanlife of a radionuclide is $\leq 35\text{Ma}$ then such nuclides will be extinct today. The primary criteria to demonstrate the presence of extinct radionuclides at the time of formation of early solar system objects like CAIs are: (i) to establish the presence of an excess in the daughter nuclide concentration, and (ii) show that this excess is well correlated with abundances of parent element in the object. The second observation suggests *in situ* decay of the now-extinct nuclide within the object.

Evidence for the presence of extinct radionuclides in the early solar system can give us valuable information about the time interval ‘ Δ ’ between the input of freshly synthesized matter to the solar nebula and the formation of some of the first solar system solids (e.g. CAIs). Obviously, the presence of the radionuclide with shortest mean life will provide the most stringent constraint on Δ . At present, ^{26}Al with a meanlife of $\sim 1.1\text{Ma}$ is the shortest lived radionuclide whose presence in the early solar system has been conclusively established. Search for extinct nuclides with even shorter meanlife like ^{36}Cl , ^{41}Ca and ^{99}Tc have not yielded conclusive results (Gobel et al. 1982; Yin et al. 1992), although the data of Hutcheon et al. (1984) provided a hint for the possible presence of excess ^{41}K due to ^{41}Ca decay in Allende CAIs. In addition, if one can establish that the initial distribution

of any one of the extinct nuclides was homogeneous in the nebula, it can also be used as a relative chronometer for studying the evolution of objects that formed at different times during the early history of the solar system. In the following, we describe the aim and scope of the present work keeping in view the above background information already available in the area of isotopic studies of CAIs directed towards understanding early solar system processes.

1.4 Aim and Scope of this work

A majority of the earlier isotopic studies of CAIs were restricted to samples from the Allende carbonaceous chondrite in which the CAIs were first identified. Only a few CAIs from the other carbonaceous chondrites belonging to CV or CO group have been studied in some detail (Clayton et al., 1986; Davis and Hinton, 1986; Hutcheon et al., 1986; Fahey et al., 1986, 1987b; Caillet et al., 1991). It is well known that most of the Allende CAIs show distinct signs of secondary alteration and present difficulties for an unambiguous interpretation of their isotopic records (e.g., Hutcheon, 1982; Podosek et al., 1991). Inclusions from some other meteorites (e.g., Ornans, Vigarano and Leoville) are less altered, but they are also less abundant. The refractory inclusions in the Efremovka CV chondrite are however an exception in this regard; they show very little evidence for secondary alteration, they are generally large (mm to cm in size), and one can easily find all the different inclusion types. In fact, petrographic and trace element studies (Ulyanov et al., 1982, 1988; Nazarov et al., 1982, 1984) suggest that the Efremovka CAIs are more pristine than the Allende inclusions. Thus, the Efremovka CAIs are expected to be better suited for isotopic studies to decipher early solar system processes than the Allende CAIs. However, no systematic isotopic study of Efremovka CAIs have been attempted to date.

In this work, isotopic studies of a set of Efremovka CAIs were carried out to determine their magnesium, calcium and potassium isotopic compositions using an ion microprobe. In addition a set of CAIs from the Grosnaja meteorite, which show distinct signatures of secondary alteration, were also studied for their Mg-Al isotopic systematics. The CAIs

from Grosnaja were studied to look for possible effects of secondary alteration on isotopic systematics vis-a-vis the Efremovka CAIs that were almost free from secondary alteration. Inclusions from all the major petrographic types (A, B1, B2, hibonite-rich and C) have been included in this study so that we can generalize upon our results.

As already noted there are several advantages of isotopic studies using the ion microprobe technique as compared to thermal ionization mass spectrometric method. Most importantly the ion microprobe offers the distinct advantage of *in situ* analyses of microphases with a spatial resolution of $\sim 10\mu\text{m}$. This allows us to carry out isotopic analyses of small mineral grains within the CAIs and also to correlate the isotopic data from different mineral phases within a CAI. Additionally, it is also possible to carry out repeat analyses of the same phase to determine isotopic composition of different elements with relative ease. This helps us to discern possible relationship between isotopic anomalies in different elements.

Application of the ion microprobe technique for high resolution and high precision isotopic studies depends upon the capability of the instrument to resolve interferences at mass(es) of interest and the dynamical stability of the instrument during isotopic analysis. Since the commercially available ion microprobes barely manage to reach the high resolutions and stability needed, it is very important to carry out detailed parametric investigations to establish the capability of individual instrument for precise isotopic studies. We have therefore performed extensive check-tests of our ion microprobe (Cameca Ims-4f) to ensure that conditions necessary for high resolution high precision isotopic studies are adequately met by it. The major goals of the present study and the work approach followed to achieve these are:

- (i) to delineate the processes leading to the formation of CAIs and the nebular environment in which they have formed. Studies of magnesium isotopic mass fractionation were carried out on all the Efremovka CAIs towards this end. Special efforts were made to look for possible correlation between Mg isotopic mass fractionation and

petrographic features with a view to improve our understanding of CAI forming processes. In addition we also searched for possible presence of isotopic disequilibrium between coexisting mineral phases within individual CAIs that may lead to identification of “relict” grains. Presence of such grains can provide us with important clues towards understanding the thermal evolutionary history of the CAI and constrain the nebular environment compatible with the inferred thermal history,

- (ii) to look for possible presence of excess ^{26}Mg due to the in-situ decay of the short-lived now-extinct radionuclide ^{26}Al in the CAIs. Studies of Mg-Al isotopic systematics were carried out on all the Efremovka and Grosnaja CAIs to achieve this objective. Possible relationship between disturbance in Mg-Al isotopic systematics and secondary alteration of the CAIs and its effect on the inferred distribution of ^{26}Al in the solar nebula was also investigated.
- (iii) to look for the possible presence of ^{41}Ca , that has a much smaller meanlife ($\sim 0.15\text{Ma}$) than ^{26}Al , in the early solar system. Studies of potassium and calcium isotopic composition in Efremovka CAIs having ^{26}Mg excess were carried out to look for ^{41}K excess due to *in situ* decay of ^{41}Ca . Mineral phases with high Ca/K ratios (pyroxene and perovskite) were chosen for these studies. As already noted the presence of ^{41}Ca can be used to provide a stringent constraint on the time interval between the last injection of nucleosynthetic matter to the solar nebula and the formation of the CAIs.

In the next chapter (Chapter 2) we describe the experimental techniques used for isotopic analysis by the ion microprobe. This chapter contains a brief description of the working principles of the Cameca Ims-4f ion microprobe followed by the results obtained from different check tests conducted to test its suitability for high resolution high precision isotopic studies. A brief description of the samples analyzed in this study is given in Chapter 3. The results obtained from magnesium, aluminium, potassium and calcium isotopic studies of Efremovka and Grosnaja CAIs are presented in Chapter 4. The implications of these results in conjunction with other known properties of the analyzed CAIs are discussed in Chapter 5. We summarize the results obtained from this study and discuss the scope for future work in Chapter 6.

Chapter 2

Experimental Techniques

This chapter describes the experimental procedures followed for studies of isotopic composition of solids using the secondary ion mass spectrometer or the ion microprobe. A brief description of the working principle of the Cameca Ims-4f ion microprobe used in this work is provided along with results obtained from parametric studies that confirm the suitability of the ion microprobe for high precision, high mass resolution isotopic studies. Basic principles used in data synthesis are discussed and results obtained from isotopic analyses of terrestrial standards and isotopically doped silicate glasses are also presented to illustrate the precision and reproducibility that may be obtained with our ion microprobe.

2.1 The Cameca Ims-4f Ion Microprobe

The Cameca Ims-4f ion microprobe is a double focussing mass spectrometer which also has the unique capability of ion imaging. It uses energetic (keV) primary ion beam to bombard the sample surface and generate secondary ions. The secondary ions are energized, energy filtered and mass analyzed and are detected using suitable ion counting system. A general schematic of the ion microprobe is shown in Fig. 2.1. The principles of secondary ion mass spectrometry have been reviewed by Benninghoven et al. (1987) and the details of optical design of the Cameca Ims-3f ion microprobe have been presented by Lapareur (1980).

Cameca Ims-4f Ion Microprobe

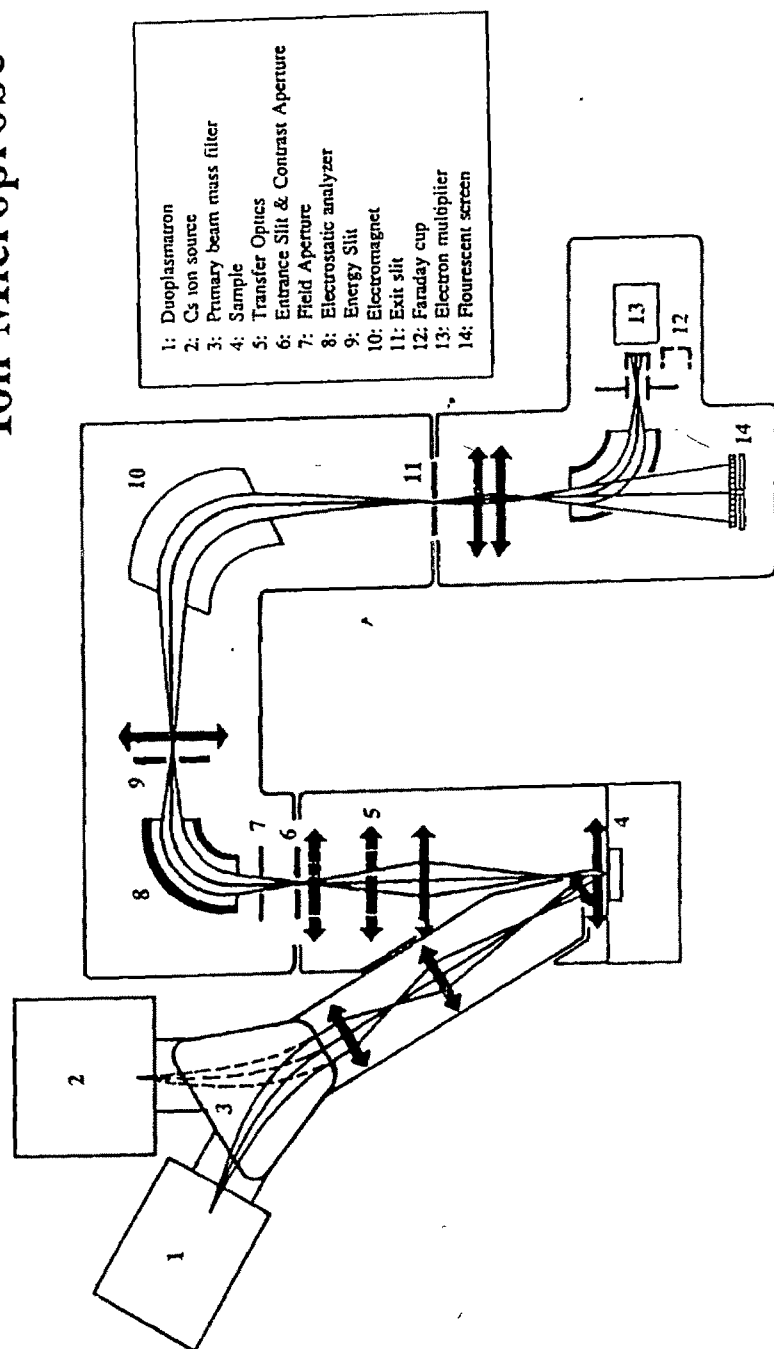


Figure 2.1: A schematic of the ion microprobe (Cameca Ims-4f). The important sub-systems are labelled and ideal traces of both primary and secondary ion optics are shown.

2.1.1 Primary Ion Column

The primary ion column consists of the primary beam source and is followed by a flight tube which consists of a set of lenses and apertures which can be used to control the size and strength of primary beam impinging on the sample surface (Fig. 2.2). There are two primary ion beam sources, a Duoplasmatron (DP) and a thermal ionization source (TI).

The Duoplasmatron can be used to generate both positive and negative ions of a variety of atomic and molecular species (e.g. O, Ar, Xe); we use oxygen to produce $^{16}\text{O}^-$ and O_2^+ beam. Ions are produced in a cold hollow Ni cathode by arc-discharge. Energetic positive or negative primary ions are extracted by floating the source at a higher/lower potential with respect to the grounded extraction lens.

A conical lens (CL) is used to focus the primary ions extracted from the source. A set of deflectors (D2) is used to align the beam along the central path of the magnetic prism. The magnetic prism, known as the primary beam mass filter (PBMF), is used to deflect the primary ions into the flight tube. It also helps to clean the primary beam of impurities (e.g. H_2O , N_2 , and NO in the case of Duoplasmatron).

A set of electrostatic lenses and apertures placed after the magnetic prism are used to focus the beam onto the sample surface. An electrostatic lens (L2), after the primary magnet focusses the beam at the position of the mass selection aperture (MSA). Deflector plates (D1) beyond this aperture align the primary beam along the principle axis of lens L1 which follows lens L2. The lens L1 is used to change the diameter of the beam at the position of primary beam aperture (PBA) thus allowing one to adjust the primary beam current on the sample surface. A set of stigmators (S1) and beam position deflectors (BPD) are placed immediately after the primary beam aperture. The beam position deflector is used to position the beam on the sample surface or to divert it into the Faraday cup (FC) to measure the primary current. The stigmators are in general used to produce a circular beam spot on the sample surface. Finally the lens L3 is used to focus the beam on the sample surface.

Cameca Ims-4f Primary Ion Optical System

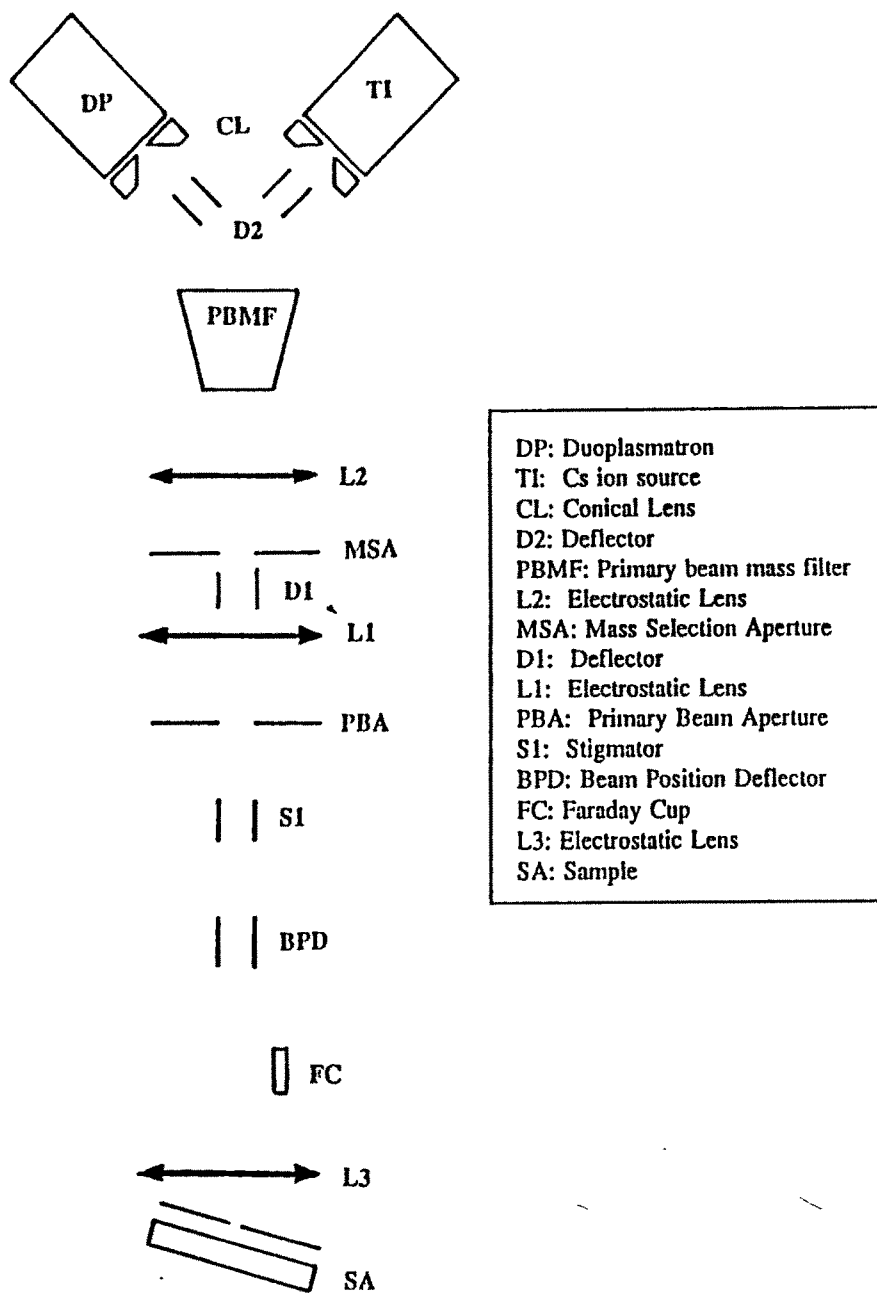


Figure 2.2: Schematic of the primary column of the ion microprobe. The important subsystems are labelled.

The choice of the primary beam and its polarity is made depending upon the elements to be analyzed. A combination of $^{16}\text{O}^-$ beam from the Duoplasmatron and positive secondary ions is used for analyzing elements like Mg, Al, K, Ca, Ti etc., while the combination of a Cs^+ beam from the thermal ionization source and negative secondary ions is used for analyzing electronegative elements like O, C, N, S etc.

In this study, isotopic analyses were carried out with a 17 keV $^{16}\text{O}^-$ focussed primary ion beam, with current in the nanoampere range. The corresponding size of the beam spot is generally $\leq 10\mu\text{m}$, that allowed the analysis of microphases. Studies of negative secondaries from insulating samples using Cs^+ beam is made difficult by the problem of sample charging and no attempt was made to study isotopic composition of elements (e.g. O) where this mode of operation is necessary. However, this problem can be overcome, in principle, by flooding the sample surface with low energy electron cloud (Slodzian et al. 1987).

2.1.2 Secondary Ion Column

The secondary ion column consists of the sample chamber, the transfer optics, the electrostatic and magnetic sectors, and a set of slits and apertures through which the secondary ions are transported and mass resolved. The mass resolved ions are detected using either a Faraday cup or pulse counting system. A schematic of the secondary ion optics is shown in Fig. 2.3.

The sample is kept at a potential of $\pm 4.5\text{keV}$ with respect to the grounded extraction plate (GP), the polarity depending on whether positive or negative secondary ions are chosen for analysis. The secondary ions are accelerated towards the grounded extraction plate that is placed 4.5mm away from the sample surface. The extraction plate that has a circular hole, also acts as the immersion lens of the transfer optics system which collimates the secondary ion beam towards the entrance slit of the mass spectrometer.

The immersion lens produces virtual images of the sample surface and the crossover

Cameca Ims-4f Secondary Ion Optical System

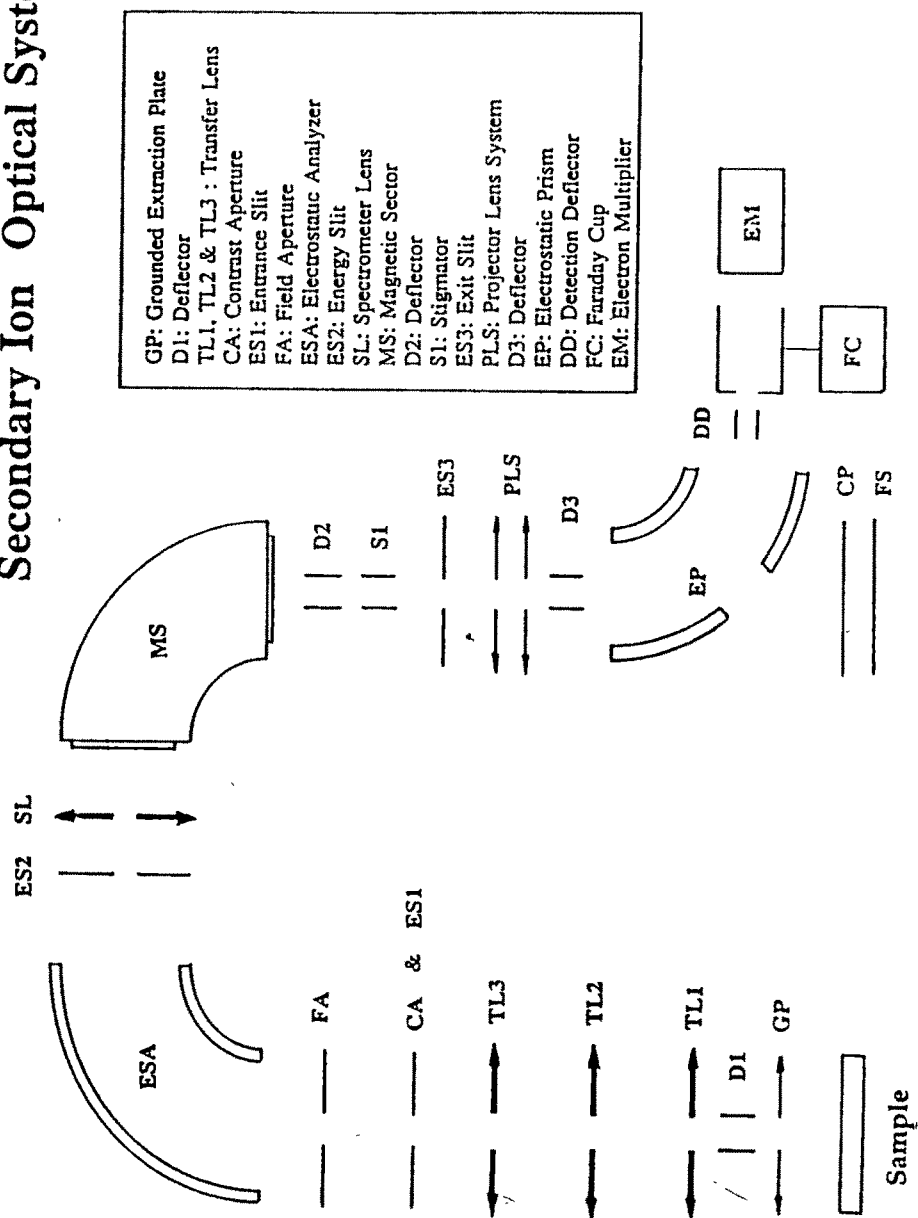


Figure 2.3: A schematic of the secondary ion column of the ion microprobe; the important subsystems are labelled.

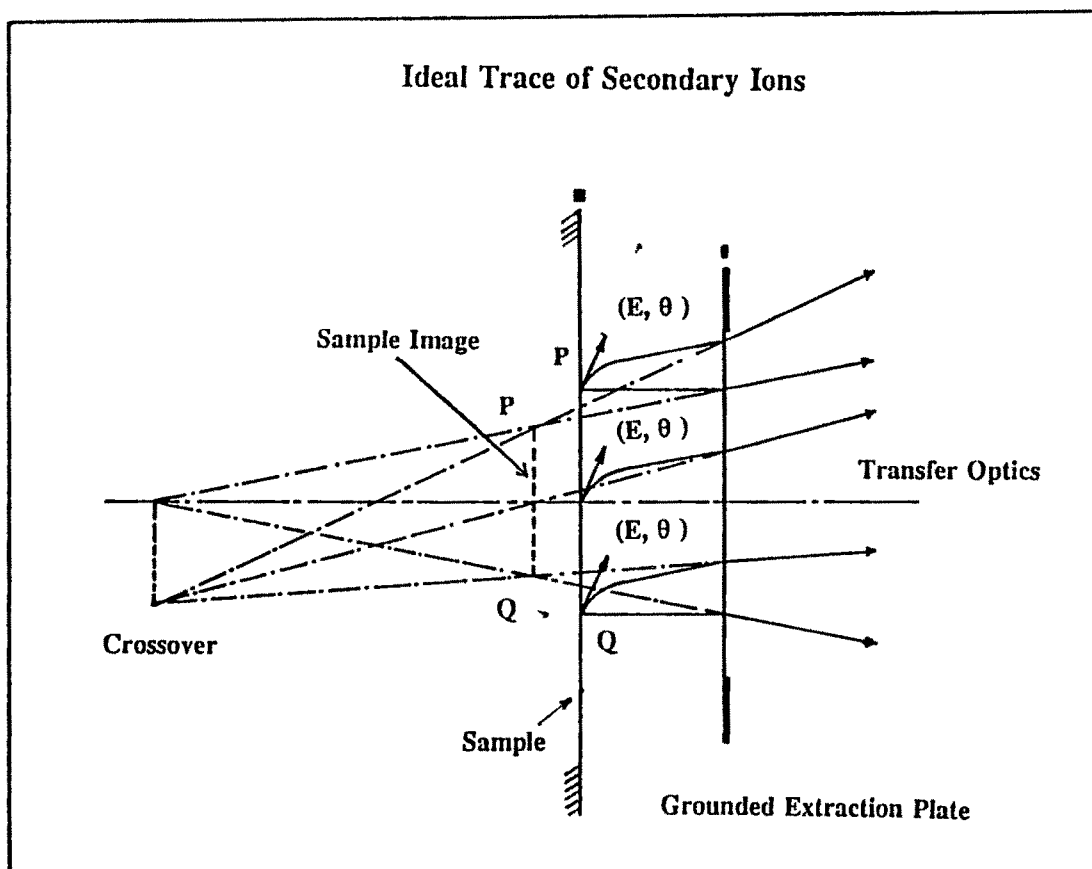


Figure 2.4: Ideal traces of the secondary ions from the sample surface are shown to illustrate the virtual image of the crossover or the illumination pupil.

(the illumination pupil) (Fig. 2.4). The size of the crossover is dependent on the lateral energy distribution of the secondary ions. A deflector (D1) placed after the immersion lens allows one to adjust the beam position with respect to the optic axis. The three lenses (TL1, TL2 and TL3) that follow the deflector are used to produce real image of the sample surface and the crossover in the plane of field aperture (FA) and contrast aperture (CA) respectively. These apertures are used to restrict the size of the crossover and the field of view as seen by the rest of the mass spectrometer. The ion microprobe transfer optics system can be used to provide preset imaged fields of $25\mu\text{m}$, $150\mu\text{m}$ and $200\mu\text{m}$. The $150\mu\text{m}$ imaged field is generally used for high mass resolution isotopic analyses [mass resolving power (MRP) $(M/\Delta M)$: 3000-10000]. Use of suitable field aperture allows one to restrict the sampling of ions from as small an area as $10\mu\text{m}$ of the sample surface.

The contrast aperture is used to restrict the size of the crossover thereby allowing only those ions with lateral energy below a certain value to enter the electrostatic analyzer (ESA). This not only reduces spherical aberrations but also improves the spatial resolution of the image. Additionally, the entrance slit (ES1) to the mass spectrometer system is also placed nearly coincident with the contrast aperture. The field aperture placed after the contrast aperture is coincident with the focal plane of the ESA and is used to restrict the transmission of ions only from a selected area.

The secondary ions sputtered from the sample surface have an energy spread of about 130eV. If all these ions are allowed to pass through the magnet they would be dispersed both in energy and mass. In order to avoid the chromatic aberration due to such an energy spread a double focussing system is used. It consists of a combination of an ESA which disperses ions in energy and a magnetic sector (MS) which disperses them in mass. Ions emanating from a single point with same mass but different energies are dispersed in energy by the ESA and are brought back to the same focus by the magnetic sector. The ESA consists of two concentric electrodes which are held at fixed potentials such that ions with energy $\sim 4.5\text{keV}$ are transmitted along the principal axis while other ions are dispersed on either side depending on their energies. This produces an image of the crossover along the radial direction of the ESA. The energy slit (ES2) placed after the ESA allows ions of only certain energy bandwidth to reach the magnetic sector. These ions are then mass analyzed in the magnetic sector which has a radius of curvature of 12.5cm. The exit slit (ES3), placed after the magnet, allows mass(es) of interest to enter the detection system. One of the important criteria for isotopic analysis is symmetric peak shape and this is achieved by using the deflector (D2) and stigmator (S1) which allow one to make the entrance slit image parallel to the exit slit. The entrance and exit slits can be suitably adjusted to achieve the desired mass resolution.

There are several options at the detection end. Since the instrument can transport image, one can use the projector lens system (PLS) to produce image of the sample surface or the image of the crossover on the fluorescent screen (FS) which is coupled to the channel

plate (CP). This allows us to use this instrument as an ion microscope. However this arrangement is generally used by us only to tune the instrument for isotopic analysis. The electrostatic deflector (EP) placed after the projector lens deflects the ions to the ion counting system where one has the choice of either using the Faraday cup (FC) or the electron multiplier (EM).

An electron multiplier (Balzer SEV217) is used for all isotopic analysis in this study. It consists of 17 stages and a potential of $\sim 2750\text{V}$ is applied across it when it is fresh (however this potential needs to be increased as the electron multiplier ages with time). The most important parameters of the electron multiplier that need routine checking are the efficiency and the dead time. However, instead of measuring the dead time of the electron multiplier, we opt to obtain the effective dead time of the total counting system (EM, preamplifier, discriminator and counting electronics) by measuring isotopic ratios in standard samples; this is described in a later section in this chapter.

2.2 High Mass Resolution Isotopic Analysis

The basic approach used for high precision, high mass resolution isotopic analysis using the ion microprobe has been discussed by many workers (Hutcheon 1982, Huneke et al. 1983, McKeegan et al. 1985, Ireland 1985 and Fahey et al. 1987a). The primary criteria to be satisfied for such an analysis are:

- (i) resolution of isobaric, hydride, oxide and other molecular interferences at the mass(es) of interest,
- (ii) dynamic stability of the magnet, and other instrument parameters during analysis,
- (iii) suitable dead time ($< 30\text{nsec}$) of the counting system that is stable over a period of a few weeks or more,
- (iv) proper sample preparation to avoid charging of the sample surface,

- (v) a stable primary ion beam to minimize secular variation in secondary ion intensity.

2.2.1 Interferences and Corrections

The secondary ions that are generated from the sample surface consist of both atomic and molecular species (primarily hydrides, oxides, dimers and trimers) which may be singly or multiply charged. In addition, neutral species and electrons are also emitted from the sample surface. Any one of the charged species with a mass to charge ratio similar to the mass(es) of interest can act as an interfering species.

In general, hydride and oxide interferences in the low mass region ($A \leq 60$) can be resolved with a mass resolving power ($M/\Delta M$) of few thousand (where ΔM is the width of the peak at 10% of the peak count rate at mass M). However, separation of true isobaric interference (e.g. ^{48}Ti and ^{48}Ca) require a much higher mass resolution of $\sim 10,000$. We have been able to resolve interference that require mass resolving power of upto 10,000 quite routinely with our ion microprobe. Several cases of resolved interferences, accomplished at high mass resolution with peak shapes having excellent flat tops and steep shoulders, are shown in Fig. 2.5.

In certain cases it is not possible to resolve the isobaric interferences (e.g. ^{46}Ca and ^{46}Ti ; ^{50}Ti and ^{50}V ; ^{40}K and ^{40}Ca etc.) and one has to indirectly correct such interferences. Additionally, when the mass of interest has a very low count rate compared to its neighbouring mass one has to correct for interference from the tail of the neighbouring peak, known as the tail correction and also take into account possible contribution from the dynamic background of the counting system. It is therefore necessary to consider all these aspects for each isotopic system carefully to resolve and/or correct for possible interference(s).

2.2.2 Dynamic Stability of the Instrument

Isotopic analysis using the ion microprobe is generally done in the flat-top peak-jumping mode. In this mode, the magnetic field values for the masses of interest are preset and the

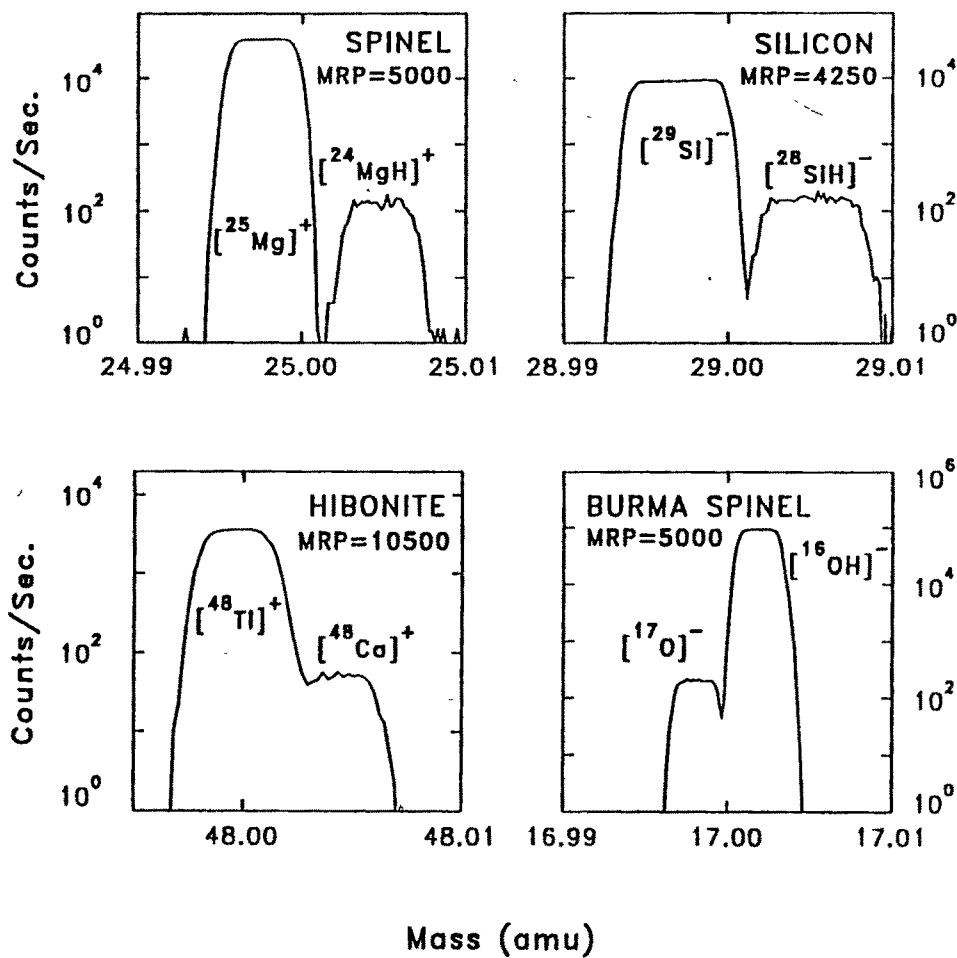


Figure 2.5: High mass resolution spectra at masses 25 (magnesium), 48 (calcium and titanium), 29 (silicon) and 17 (oxygen) showing well resolved hydride and true isobaric interferences. The mass resolving power ($\text{MRP} = M/\Delta M$) and sample analyzed in each case are also indicated. Oxygen isotopic analysis was carried out using the Cs^+ primary ion beam in the negative secondary mode while the rest were analyzed as positive secondary ions with $^{16}\text{O}^-$ primary ion beam.

magnet is cycled through these masses with appropriate counting time for each mass. Five to eight such cycles constitute a block of data and each analysis typically comprises of data from 20 to 30 blocks. The magnetic field control of the Cameca Ims-4f has $\sim 2.6 \times 10^5$ field bits that can be used for any one of the preselected mass ranges (1-20, 1-80, 1-280 amu). At high mass resolution ($M/\Delta M \geq 5000$), the flat top peak represents a small magnetic field interval ΔB , which is generally of the order of 10-15 field bits in the 1-80 mass range. Any instability in the instrument, especially in the magnet can alter the preset values for analyzed mass(es) beyond the flat top region leading to erroneous count rates. Therefore, several precautions have been taken to ensure a high degree of dynamic stability of the instrument; these include:

- (i) extremely stable power supply for the ESA and other instrument sub-systems,
- (ii) optimum temperature ($\sim 18 \pm 0.5^\circ\text{C}$) for the magnet and ESA environments,
- (iii) use of pre-adjusted voltages for the ESA,
- (iv) a thick gold coating ($\sim 1000\text{\AA}$) of the sample to avoid progressive sample charging,
- (v) an extremely stable counting system.

Since all these factors have a combined effect on the instrument performance, the dynamic stability of the instrument is measured in terms of the effective stability of the magnetic field in the peak-jumping mode of operation. Two mass regions (24-27) and (46-50) were investigated at a mass resolution of ~ 5000 and count rates were measured at the peak centers of the chosen masses and at the left shoulder of the peaks where the count rate is approximately half that of the peak value. Since the count rate on the rising shoulder is extremely sensitive to changes in the effective magnetic field, the variation in the count rate at this position, relative to the peak center, provides an estimate of the fluctuation ($\Delta M/M$) in the mass which in turn can be related to the fluctuation ($\Delta B/B$) in the magnetic field. The value of $\Delta B/B$ provides a measure of the effective stability of the magnet (and hence the instrument) in the dynamic (peak-jumping) mode of operation.

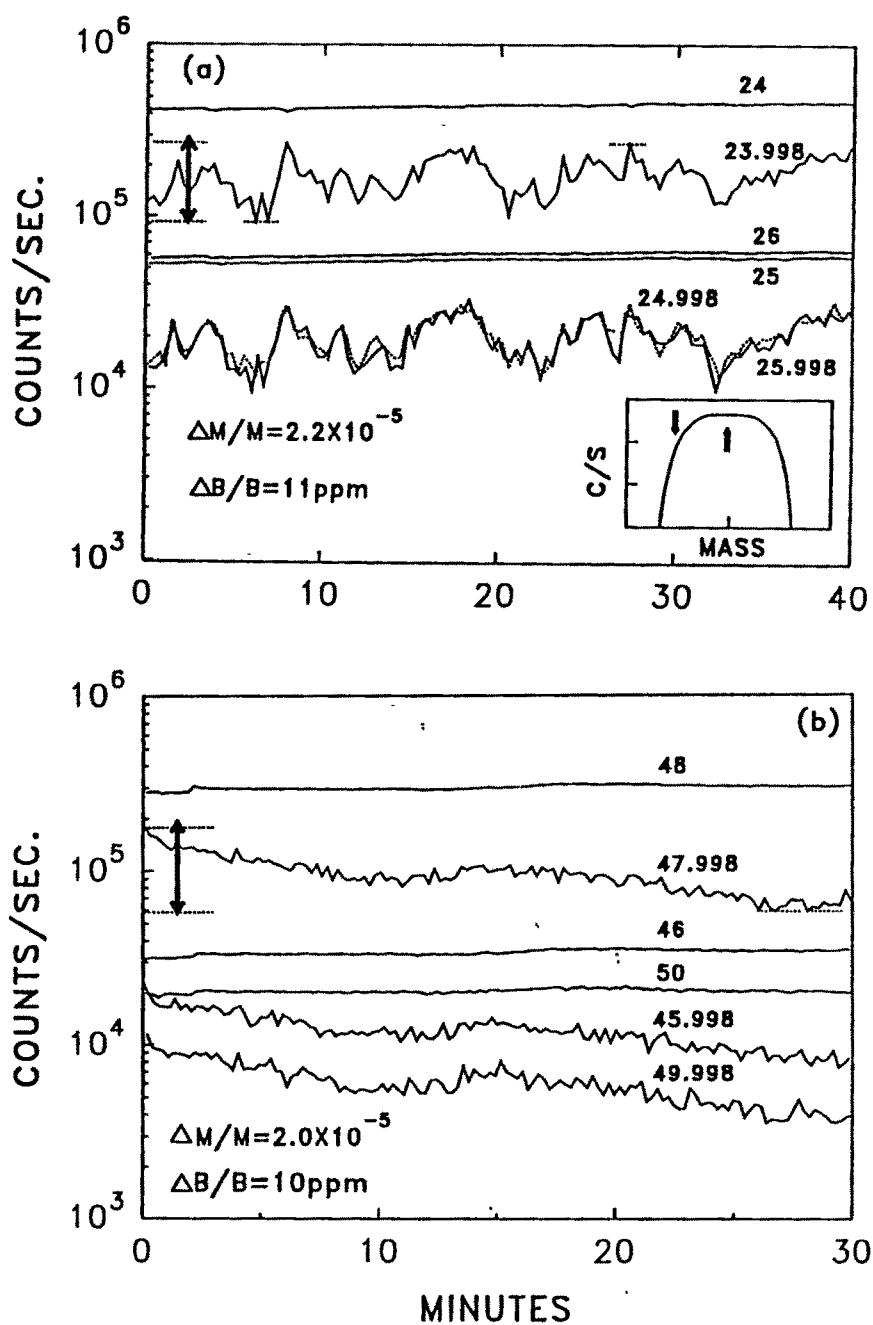


Figure 2.6: Count rates at the peak center (integer masses) and to the left of the peak center (non-integer masses) plotted as a function of time (see inset for approximate positions at which count rates are monitored). Two mass ranges: 24-26 (fig.a) and 46-50 (fig.b) are investigated in the dynamic (peak-jumping) mode of analysis. The values of $\Delta M/M$ and $\Delta B/B$ obtained from the maximum variation in count rate at the peak edge (marked by the vertical arrow) are shown in both the figures.

The results of these experiments are shown in Fig. 2.6. The “effective” value of $\Delta M/M$ is $\sim 2 \times 10^{-5}$ which translates into an effective stability of the magnetic field of about ~ 10 ppm for duration ranging from 30-40 minutes. In terms of magnetic field bits, e.g. at mass 24 this corresponds to about 3 field bits which is much less than the width of the flat top peak (about 15 field bits). Although the dynamic stability of our instrument is extremely good, the magnetic field values for the analyzed masses are automatically recalibrated during actual analysis after each block of data acquisition which generally takes ≤ 10 minutes. The shift in magnetic field during such recalibration is 1 to 2 field bits; this ensures that isotopic analyses do not suffer from temporal drift in the magnetic field and associated uncertainties.

2.2.3 Stability of the Counting System

The pulse counting system is used for all isotopic analyses carried out in this study. The stability of the counting system is extremely important for high precision measurement, and it is important to routinely monitor the efficiency, dead time and the background of the counting system. Tests are conducted to check the counting system comprising of the electron multiplier, preamplifier, discriminator and the counting electronics in an operative way by analyzing suitable terrestrial standards. The dead time is estimated by making measurements of isotopic composition of magnesium and titanium in terrestrial spinel and Ti-metal respectively at a mass resolution that can clearly resolve the hydride interference. The deviations in isotopic compositions from reference values are then attributed to the combined effect of isotopic mass fractionation and dead time of the counting system. Since the mass fractionation effect can be estimated by using appropriate fractionation law, one can determine the “effective” dead time of the counting system.

The results obtained from magnesium isotopic analysis in terrestrial spinel carried out in 1993 are shown in Fig. 2.7. The “effective” dead time of the counting system is (24 ± 1) nsec for ^{24}Mg count rates ranging from $\sim 4 \times 10^5$ to 1.2×10^6 counts/sec(c/s). The dead time of the counting system generally remains stable over a time scale of several weeks and it is also a

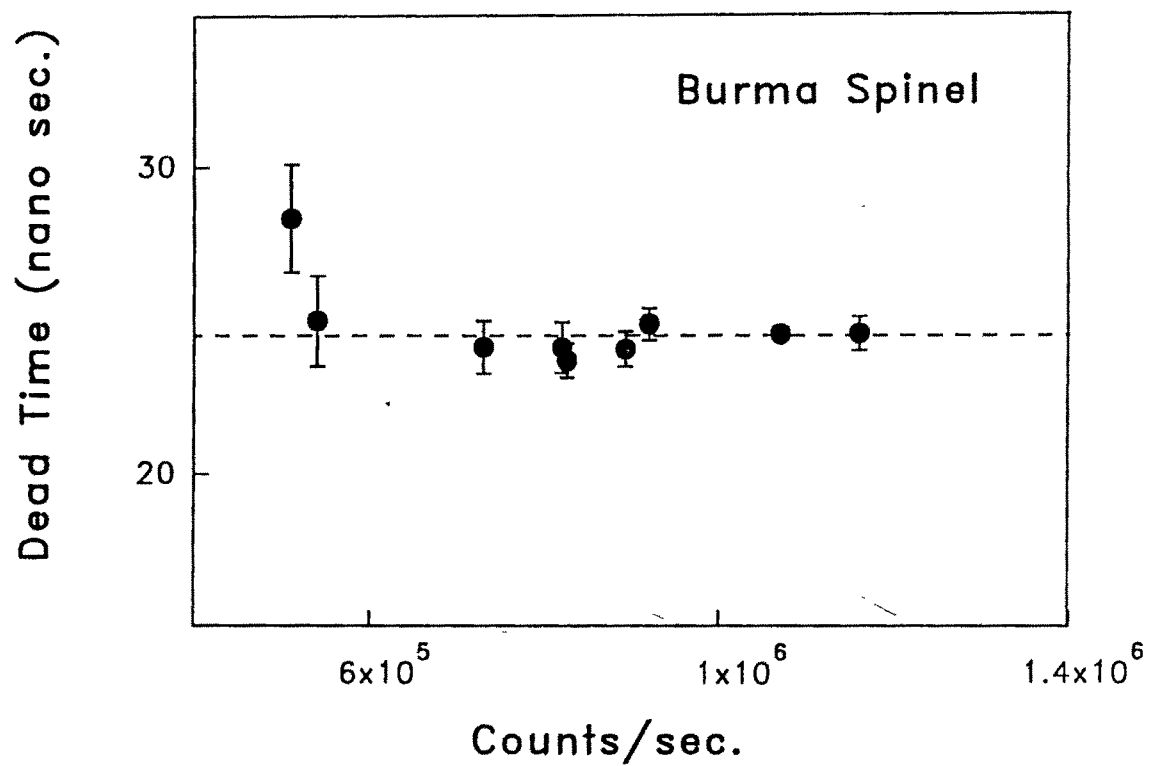


Figure 2.7: Dead time of the integrated pulse counting system as a function of count rate obtained from magnesium isotopic measurements in terrestrial spinel. Error bars are $2\sigma_m$.

function of the age of the electron multiplier. It may be noted that a similar exercise carried out in 1990 with a fresh electron multiplier gave a value of (19 ± 1) nsec. During actual isotopic analysis the maximum count rate at any mass is generally kept below 2×10^5 (c/s) so that uncertainty in isotopic ratios due to uncertainty in the dead time is much below the limit set by counting statistics which is typically $1-2\%$ ($2\sigma_m$).

The background of the counting system is ≤ 0.005 (c/s) in the static mode (Fig. 2.8). In the dynamic (peak jumping) mode the background is monitored by obtaining count rates at a blank mass during isotopic analysis. The value obtained from several runs was ≤ 0.01 (c/s). Since the typical count rates during isotopic analysis are generally higher than this value by more than several orders of magnitude, the counting system background can be neglected during data analysis. The efficiency of the electron multiplier is generally $> 75\%$ and it is replaced when this value reaches $\sim 70\%$. The results obtained from the above parametric investigations of our ion microprobe show that it satisfies all the necessary conditions for carrying out high precision and high mass resolution isotopic analysis.

2.3 Isotopic Analysis of Terrestrial Standards

This section summarizes the results of measurements of isotopic composition of Mg, Ca and K in appropriate terrestrial standards. These analyses are a prerequisite for isotopic analysis of meteoritic phases, the primary aim of this work. Additionally, a set of isotopically doped anorthositic glasses were also analyzed to establish the precision and reproducibility that can be obtained during Mg isotopic analysis. These glasses have been used as internal standards by two other ion microprobe laboratories (Armstrong et al. 1982, McKeegan et al. 1985).

2.3.1 Mass Fractionation

The measured isotopic ratios of an element (e.g. Mg) in a standard can deviate from the reference isotopic ratios because of instrumental and intrinsic isotopic mass fractionation.

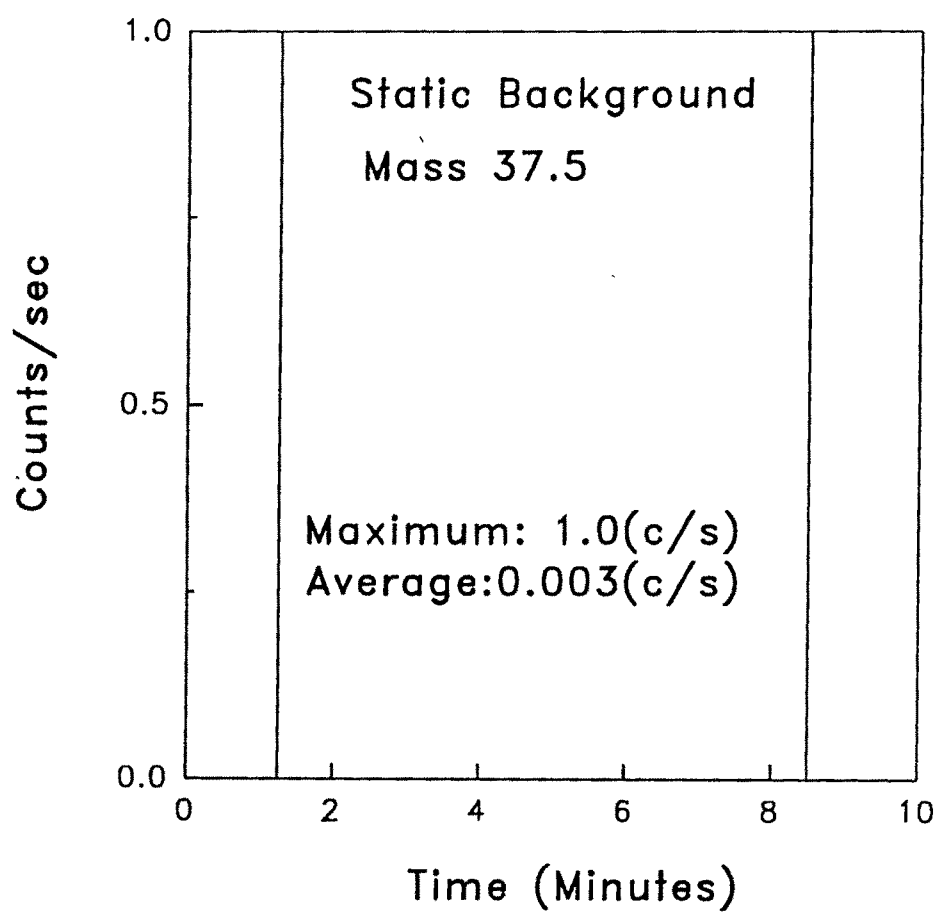


Figure 2.8: The static background of the pulse counting system at a dummy mass 37.5 over a period of ten minutes.

The process of generation, transmission and detection of secondary ions in an ion microprobe lead to instrumental mass fractionation. In addition, the sample itself could have undergone a variety of physico-chemical processes during its formation which could have altered the isotopic composition and this is referred to as the intrinsic mass fractionation or sample mass fractionation.

During the generation of secondary ions by the sputtering process, the lighter isotopes are in general preferentially sputtered compared to the heavier isotopes. Initially, the flux of lighter isotopes is strongly enriched, which decreases with time and finally a steady value is attained (Gnaser and Hutcheon 1987). The enrichment of lighter isotopes in secondary ions is strongly dependent on the sample matrix i.e. the nature of chemical bonding between the constituent atoms of the sample. Since all the ions have the same nominal energy of 4.5keV during transmission, the lighter isotopes with higher velocity are again fractionated preferentially compared to the heavier isotopes. During detection, by the electron multiplier, fractionation favours the lighter isotopes although the effect is very small, $\leq 1\text{‰/amu}$ (Zinner et al. 1986a). It is difficult to decouple the individual effects, and in general the total instrumental mass fractionation is estimated during analysis.

In case of terrestrial sample, the intrinsic fractionation is expected to be extremely small, and thus the measured fractionation in them can be attributed to instrumental mass fractionation. Further, the instrument mass fractionation for a given phase remains nearly the same as long as there are no changes in the ion microprobe tuning/operational conditions.

If we consider an element like Mg, which has three isotopes (24, 25 and 26), with reference isotopic ratios (normalized to ^{24}Mg) of $(^{25}\text{Mg}/^{24}\text{Mg}) = 0.12663$ and $(^{26}\text{Mg}/^{24}\text{Mg}) = 0.13932$ (Catanzaro et al. 1966); the deviations in the measured isotopic ratios from the reference values are generally expressed as:

$$\begin{aligned}\Delta^{25}\text{Mg} &= \left[\frac{\left(\frac{^{25}\text{Mg}}{^{24}\text{Mg}} \right)_{\text{meas.}}}{\left(\frac{^{25}\text{Mg}}{^{24}\text{Mg}} \right)_{\text{ref.}}} - 1 \right] \times 1000 \text{ ‰} \\ \Delta^{26}\text{Mg} &= \left[\frac{\left(\frac{^{26}\text{Mg}}{^{24}\text{Mg}} \right)_{\text{meas.}}}{\left(\frac{^{26}\text{Mg}}{^{24}\text{Mg}} \right)_{\text{ref.}}} - 1 \right] \times 1000 \text{ ‰}\end{aligned}\quad (2.1)$$

Since the total fractionation of any sample is a linear combination of instrumental and intrinsic mass fractionation, the intrinsic or sample mass fractionation of a meteoritic phase can be deduced by measuring isotopic mass fractionation of these phases and their terrestrial analogs under identical instrument operating conditions. If $[\Delta^{25}\text{Mg}]_{\text{met}}$ and $[\Delta^{25}\text{Mg}]_{\text{std}}$ represent the deviations for the meteoritic phase and its terrestrial analog, the intrinsic fractionation $F(\text{Mg})$ for the meteoritic phase is given as:

$$F(\text{Mg}) = [\Delta^{25}\text{Mg}]_{\text{met}} - [\Delta^{25}\text{Mg}]_{\text{std}} \text{ ‰/amu} \quad (2.2)$$

In addition to intrinsic mass fractionation, the measured isotopic ratios in the meteoritic phases may differ from the reference values due to the presence of nuclear effect that can produce the isotope under consideration. Such an effect could be nucleogenic or radiogenic in origin and its presence can be ascertained when more than two isotopes of an element can be analyzed (e.g. Mg). One should however be able to choose at least two isotopes that are independent of the nuclear effect. The measured ratio of this pair of isotopes can be used to obtain the magnitude of isotopic mass fractionation. This will then allow one to infer the magnitude of fractionation effect for the other isotopes using suitable mass fractionation law. If any residual effect is present in the other isotopes, after due correction is made for the fractionation effect, it can be attributed to nuclear effect. The two relations generally used to describe isotopic mass fractionation are:

i) Exponential law:

$$\frac{R_m^{ij}}{R_r^{ij}} = \left(\frac{M^i}{M^j} \right)^p \quad (2.3)$$

ii) Power law:

$$R_m^{ij} = R_r^{ij} (1 + \alpha)^{m_{ij}} \quad (2.4)$$

where R_m^{ij} and R_r^{ij} are the measured and reference isotopic ratios of the isotope i with respect to isotope j , M^i and M^j are the masses of the two isotopes, α and p are the fractionation parameters which are to be determined, and m_{ij} is equal to the difference in the masses of the two isotopes. When the degree of fractionation is small and mass difference m_{ij} is also small, one can use a linear approximation to these laws and they can be replaced by the linear law :

$$R_m^{ij} = R_r^{ij} [1 + \alpha m_{ij}] \quad (2.5)$$

In the case of magnesium the isotopes 24 and 25 are used as the reference pair (free from nuclear effect) and one can use the linear law to show that the fractionation corrected residual, if any, in ^{26}Mg is given by :

$$\delta^{26}\text{Mg} = [\Delta^{26}\text{Mg}] - 2 \cdot [\Delta^{25}\text{Mg}] \quad (2.6)$$

A non-zero value of $\delta^{26}\text{Mg}$ can be attributed to the presence of nuclear effect. In the case of Ca or Ti isotopes where the isotopic masses spread over a large range (40-48), (46-50) one cannot resort to linear approximation and it is necessary to use the exponential law to correct for fractionation and to infer the presence of nuclear isotopic effect (Fahey et al. 1987a).

2.3.2 Mg Isotopic Analysis

A set of terrestrial analogs of meteoritic phases were studied to determine instrumental isotopic mass fractionation ($\Delta^{25}\text{Mg}$) and $\delta^{26}\text{Mg}$ values. In terrestrial phases $\delta^{26}\text{Mg}$ is expected to be zero since no nuclear effects can be present in such samples.

The Mg isotopic analysis of the terrestrial standards were carried out at mass resolution ($M/\Delta M \sim 4000$) which is sufficient to resolve the major interferences from $^{48}\text{Ca}^{++}$, $^{48}\text{Ti}^{++}$, NaH^+ and MgH^+ at the masses of interest. The results of Mg isotopic analyses are shown in Table 2.1. The $\Delta^{25}\text{Mg}$ values for the different mineral phases represent the instrumental isotopic mass fractionation. The difference in these values for the various mineral phases is expected because of the differences in chemical bonding of Mg in them. Since extensive studies of Mg isotopic fractionation were planned on meteoritic phases it is important to establish that there is no significant temporal variation in instrument mass fractionation for magnesium isotopes ($\Delta^{25}\text{Mg}$) for a given phase under similar instrument tuning and operating conditions. We have measured $\Delta^{25}\text{Mg}$ in terrestrial spinel (Burma Spinel) at different time intervals over a 24 hour period. The results obtained in the study are shown in Fig. 2.9. All the values cluster within 1‰ ($2\sigma_m$) of the mean value of 11.7‰, indicating excellent reproducibility of the magnitude of instrumental isotopic mass fractionation under a given instrument operating condition.

The $\delta^{26}\text{Mg}$ in the analyzed phases is indistinguishable from zero within the limit of our experiment uncertainties. The investigation of the possible presence of non-linear excess of ^{26}Mg in meteorite phases also requires the measurement of their Al/Mg ratio. Since the secondary ion yield can be different for different elements and is also dependent on the chemical composition of the sample, the relative yield for different elements has to be determined by using appropriate terrestrial standards of known composition. For example sensitivity factor λ for the Al-Mg system is defined as:

$$\left(\frac{^{27}\text{Al}}{^{24}\text{Mg}} \right)_{\text{EP}} = \left(\frac{^{27}\text{Al}^+}{^{24}\text{Mg}^+} \right)_{\text{IP}} \cdot \lambda \quad (2.7)$$

Table 2.1: Mg Isotopic Data for Terrestrial Standards[†]

Sample	N [†]	$^{27}\text{Al}/^{24}\text{Mg}$ $\pm 2\sigma_m$	$\Delta^{25}\text{Mg}$ $\pm 2\sigma_m$	$\delta^{26}\text{Mg}$ $\pm 2\sigma_m$
Burma Spinel*	4	2.59 ± 0.01	-11.62 ± 0.59	-2.04 ± 1.14
Spinel [®]	5	2.60 ± 0.02	-12.41 ± 0.66	-1.67 ± 1.28
Melilite [®]	6	1.32 ± 0.01	-7.81 ± 0.48	-0.60 ± 0.88
Madagascar Hibonite [#]	4	30.8 ± 1.50	-5.80 ± 0.84	1.25 ± 1.73
Lake County Plagioclase*	2	215.76 ± 8.10	-6.28 ± 1.90	0.72 ± 3.64

[†] $\Delta^{25}\text{Mg}$ and $\delta^{26}\text{Mg}$ values are in permil

[†]Number of repeat measurements

[®]Vernadsky Institute, Moscow

[#]H. Curien et al. (1956)

*National Museum of Natural History, Smithsonian Institution, Washington, D.C.

Table 2.2: Mg-Al Sensitivity Factors

Mineral	λ
Melilite	1.04
Burma Spinel	1.40
Madagascar Hibonite	1.30
Lake County Plagioclase	1.24
Angra Dos rios Pyroxene	1.31

where EP and IP refer to electron probe and ion microprobe data respectively. The values for λ obtained by us for different minerals are given in Table 2.2.

To check the ability of our instrument to precisely measure non-linear excess in Mg isotopic composition, we have analyzed a set of anorthositic glasses doped with known amounts of ^{25}Mg . The Mg concentrations of these glasses are 200 and 1000 ppm. The results obtained by us are given in Table 2.3 and they are in very good agreement with the results obtained by two other ion microprobe laboratories as well as the gravimetric value. A small

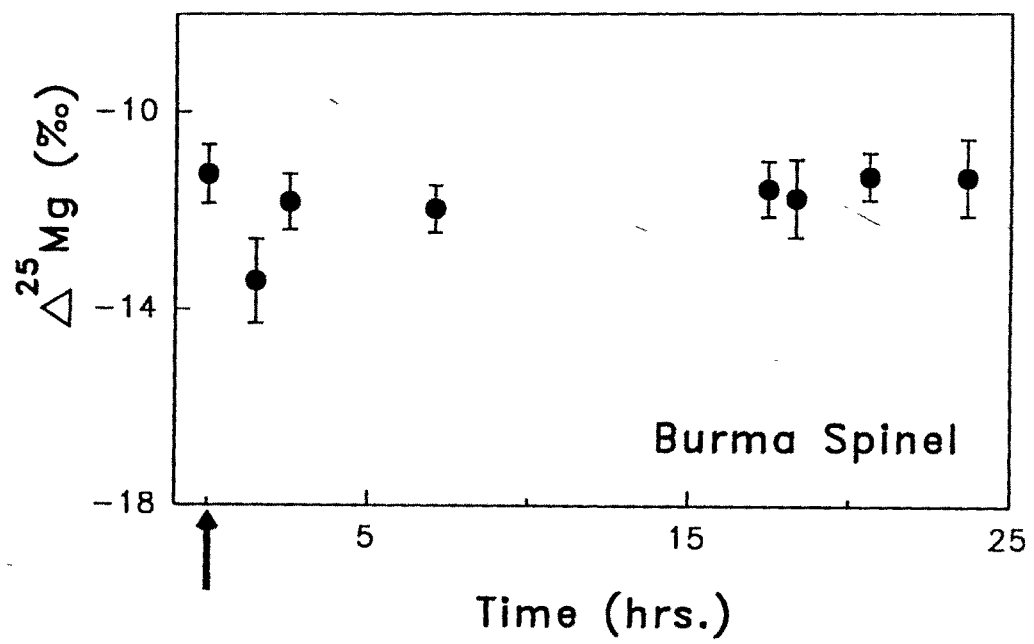


Figure 2.9: Magnesium isotopic mass fractionation in terrestrial spinel obtained from repeated analysis during a 24 hour run period. The arrow marks the start of the run. Error bars are two $2\sigma_m$.

difference can be seen in the case of the sample AN-MG-4, where the gravimetric value is lower than the ion microprobe data; this may probably reflect sample inhomogeneity. These results demonstrate our ability to measure non-linear excess in Mg isotope with a precision of 2‰ ($2\sigma_m$) even when the concentration of Mg is as low as 200ppm.

Table 2.3: Mg Composition of Isotopically Spiked Samples

Sample	Mg	$\delta^{25}\text{Mg}^* (\pm 2\sigma_m) \text{‰}$			
		Grav**	PRL	Panurge [†]	WU [‡]
Anorthositic Glass	ppm				
AN-MG-1	292	0.0	0.3 ± 2.7	3.3 ± 3.4	1.9 ± 1.6
AN-MG-2	292	29.2	28.8 ± 1.9	31.4 ± 5.4	29.5 ± 1.6
AN-MG-3	292	101.7	100.8 ± 2.8	101.2 ± 4.7	99.2 ± 1.6
AN-MG-4	292	318.0	307.2 ± 2.5	310.0 ± 3.7	315.8 ± 1.7
AN-MG-5	1000	0.0	0.7 ± 1.8	2.2 ± 2.9	0.7 ± 2.2
AN-MG-6	1000	9.4	9.8 ± 1.7	9.1 ± 2.3	9.2 ± 1.5
AN-MG-7	1000	28.9	29.7 ± 2.7	29.6 ± 4.8	30.4 ± 1.9
AN-MG-8	1000	97.9	96.9 ± 2.2	96.7 ± 2.1	97.5 ± 1.9

* $\delta^{25}\text{Mg} = \Delta^{25}\text{Mg} - 0.5 \cdot \Delta^{26}\text{Mg}$

**Gravimetric Measurement

[†]Panurge (IMS-3F at Caltech): J. T. Armstrong et al. (1982)

[‡]WU (IMS-3F at Washington Univ.): K. D. McKeegan et al. (1985)

2.3.3 K-Ca Isotopic Analysis

One of the investigations conducted in this work was potassium isotopic studies of suitable meteoritic phases with high Ca/K to look for possible ^{41}K excess due to the decay of short-lived radionuclide ^{41}Ca ($\tau \sim 0.15\text{Ma}$). In order to check our ability to carry out such studies suitable terrestrial standards were analyzed for their K isotopic composition. In this section we summarize the procedures and precautions used in these measurements.

Studies of K-Ca isotopic system involves the determination of the sensitivity factors for K and Ca in suitable terrestrial analogs of meteoritic phases and accurate measurement of ($^{41}\text{K}/^{39}\text{K}$) since the abundance of ^{41}K is extremely small. Although K has three isotopes (39, 40 and 41), it is not possible to resolve ^{40}K from ^{40}Ca when Ca is present. Thus for all practical purpose K can be considered as a two isotope system in the present case.

K-Ca isotopic studies of terrestrial phases with high Ca/K were carried out at a mass resolution of ~ 5000 (Fig. 2.10), which is sufficient to resolve the major interference of ^{40}CaH at mass ^{41}K . However, the interference of $^{40}\text{Ca}^{42}\text{Ca}^{++}$ cannot be resolved at this mass resolution, and was corrected indirectly. The magnitude of the other unresolved doubly charged interference $^{26}\text{Mg}^{56}\text{Fe}^{++}$ is much smaller due to extremely low content of Fe in the Ca-rich phases and can be neglected. Finally, as the count rate at mass ^{41}K is extremely small compared to ^{40}CaH , it is also necessary to check for possible scattering from the tail of the hydride peak. A check of the dynamic background of the counting system is also necessary when the count rate of ^{41}K is $\leq 1(\text{c/s})$. The measured ($^{41}\text{K}/^{39}\text{K}$) can therefore be written as:

$$\left(\frac{^{41}\text{K}^+}{^{39}\text{K}^+}\right)_{\text{meas.}} = \left(\frac{^{41}\text{K}^+}{^{39}\text{K}^+}\right)_{\text{true}} + \frac{(^{40}\text{Ca}^{42}\text{Ca})^{++}}{^{39}\text{K}^+} + \frac{(^{40}\text{CaH})^+_{\text{tail}}}{^{39}\text{K}^+} + \text{background} \quad (2.8)$$

Since it is not possible to directly measure $^{40}\text{Ca}^{42}\text{Ca}^{++}$ count rate, we correct for it indirectly by finding the magnitude of $^{40}\text{Ca}^{43}\text{Ca}^{++}$ signal at mass 41.5 and noting that

$$\frac{(^{40}\text{Ca}^{43}\text{Ca})^{++}}{^{43}\text{Ca}^+} = \frac{(^{40}\text{Ca}^{42}\text{Ca})^{++}}{^{42}\text{Ca}^+} \quad (2.9)$$

The $[^{40}\text{Ca}^{43}\text{Ca}]^{++}$ signal can be monitored at 41.5. Since this signal is extremely low in both terrestrial and meteoritic phases, they were measured independently by using high primary current and large integration time to achieve good counting statistics. The measured values for $[^{40}\text{Ca}^{43}\text{Ca}]^{++}/^{43}\text{Ca}^+$ in terrestrial and meteoritic pyroxenes and terrestrial perovskite are shown in Fig. 2.11. The results clearly demonstrate our ability to reproduce this ratio in these two mineral phases and we can use this ratio with confidence for correction of $[^{40}\text{Ca}^{42}\text{Ca}]^{++}$ interference. For the correction of possible contribution to $^{41}\text{K}^+$ signal from the tail of the hydride peak, we note that the $^{40}\text{CaH}^+$ signal is generally comparable or at times smaller (by a factor of two) than the $^{43}\text{Ca}^+$ count rate. Therefore we measured the count rate at mass ($^{43}\text{Ca} - \Delta M$) for making this correction; where ΔM is given by the relation:

$$\Delta M = \frac{43}{41} \cdot [^{40}\text{CaH} - ^{41}\text{K}] = 0.009 \text{ amu} \quad (2.10)$$

The contribution from the tail of $^{40}\text{CaH}^+$ to $^{41}\text{K}^+$ is estimated as:

$$^{40}\text{CaH}_{\text{tail}}(\text{c/s}) = (^{43}\text{Ca} - \Delta M) (\text{c/s}) \cdot \frac{^{40}\text{CaH}^+}{^{43}\text{Ca}^+} \quad (2.11)$$

The potassium isotopic analysis was carried out by cycling the magnet through the masses ^{39}K , ^{40}CaH , ^{42}Ca , ($^{43}\text{Ca} - \Delta M$) and ^{43}Ca in the usual peak-jumping mode. The counting time for signals at mass 39(^{39}K) and 41(^{41}K) were typically 30 to 60 sec respectively. Each analyses consisted of 10-12 blocks of 5 cycles each, which lasted for a duration of 90 to 120 minutes.

Relative sensitivity factors for Ca and K were measured in terrestrial pyroxenes with widely differing Ca/K ratios. The results are shown in Table 2.4 and we obtain a yield factor of ~ 3.2 favouring K over Ca. We have used this yield factor for the perovskite phases also. The results of potassium isotopic analyses of terrestrial minerals with Ca/K ratios varying over nine orders of magnitude is shown in Table 2.5. The $^{41}\text{K}/^{39}\text{K}$ value in all the cases is

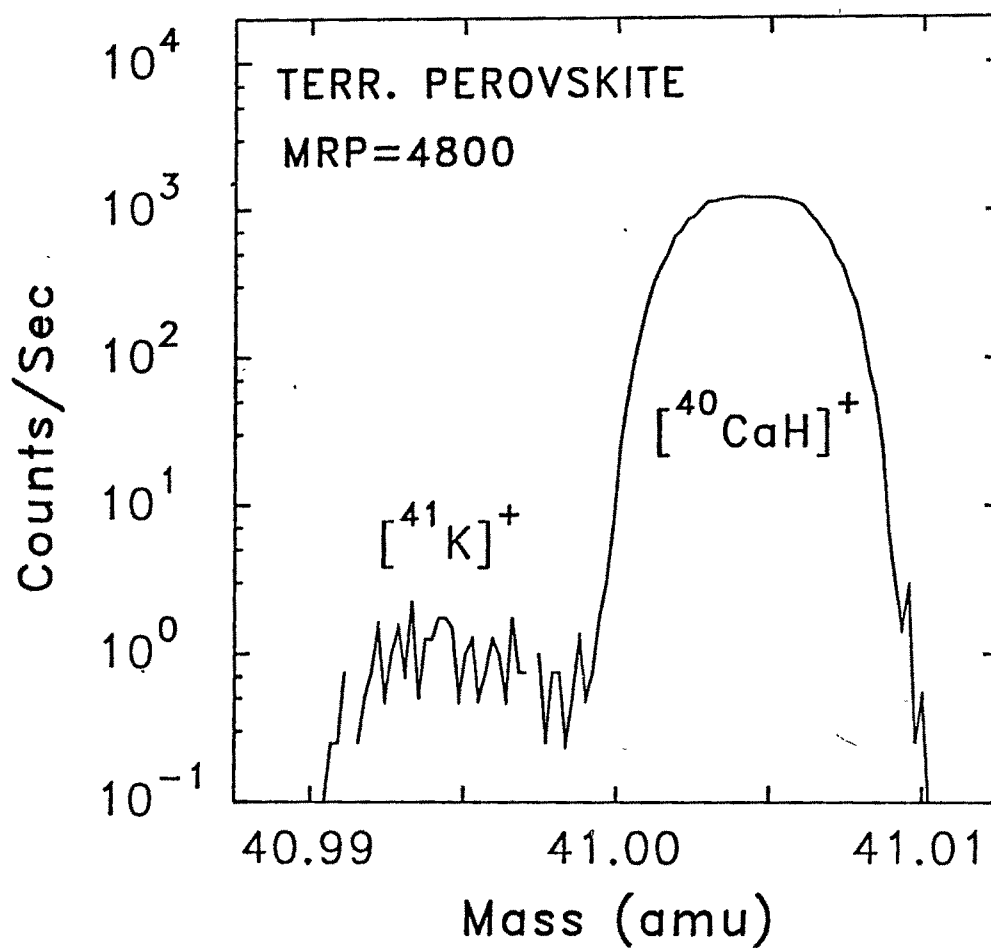


Figure 2.10: High mass resolution (mass resolving power: $M/\Delta M = 4800$) spectrum at mass 41 in terrestrial perovskite with $\text{Ca}/\text{K} > 10^6$ showing clearly resolved $^{41}\text{K}^+$ and $(^{40}\text{CaH})^+$ peaks.

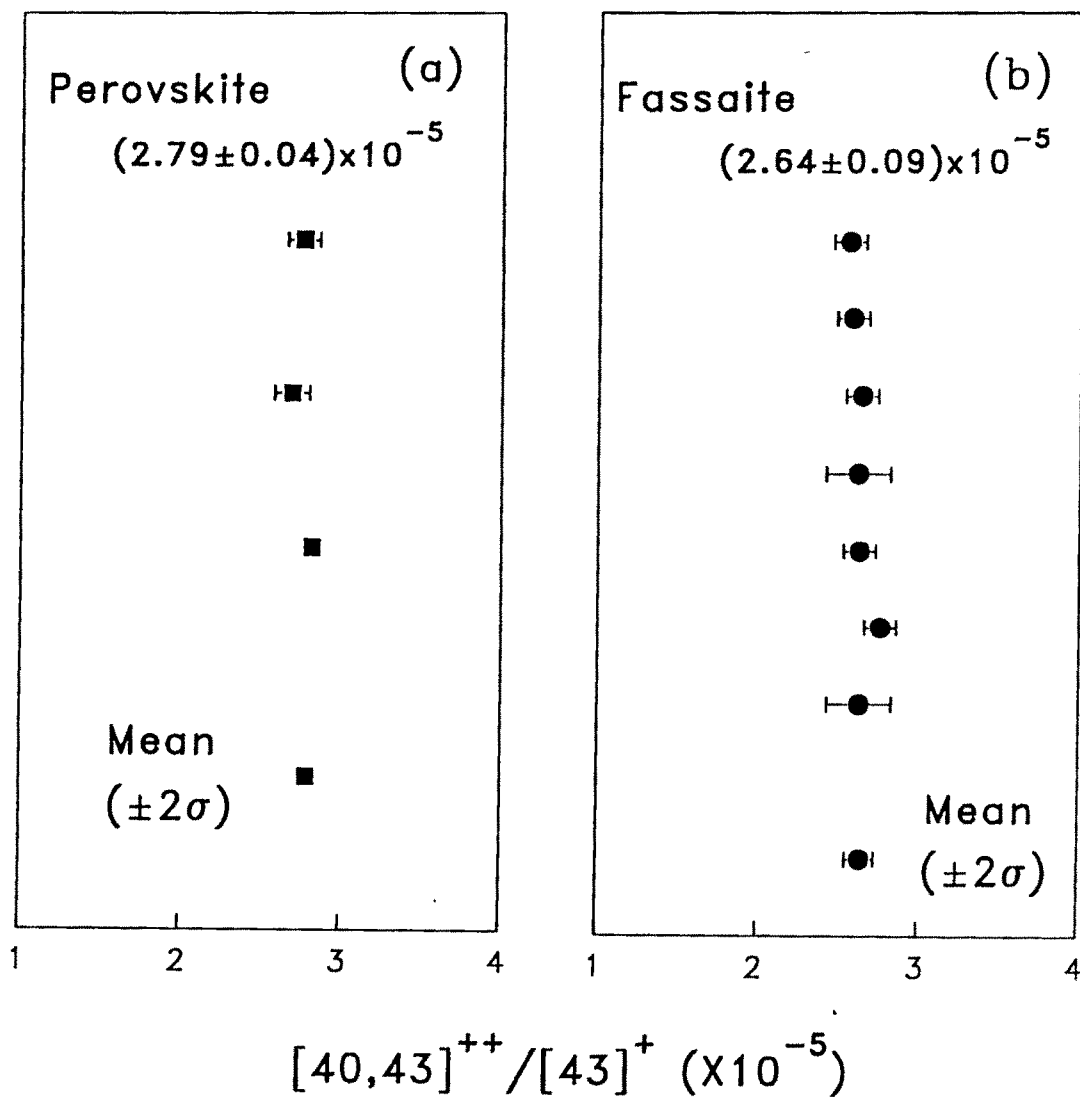


Figure 2.11: The values of $[^{40}\text{Ca}^{43}\text{Ca}]^{++}/^{43}\text{Ca}^+$ for individual runs in terrestrial perovskite [fig(a)] and meteoritic and terrestrial pyroxenes [fig(b)]. The mean values for the two phases are also indicated. Error bars are $2\sigma_m$.

close to the reference value of 0.072, within the limits of experimental uncertainties. These results also suggest that the magnitude of intrinsic or instrumental mass fractionation in the case of potassium isotopes is extremely small.

Table 2.4: K-Ca Sensitivity Factors

Mineral	Ca/K	λ
Pyroxene 1 (Ti-Px-1)	2.1×10^4 -	3.34 ± 0.10 -
Pyroxene 2 (CAI-Px-1)	3×10^6 -	3.08 ± 0.20 -

All errors are $2\sigma_m$

Table 2.5: K Isotopic Analyses of Terrestrial Minerals

Sample	$^{40}\text{Ca}/^{39}\text{K}$	$^{41}\text{K}/^{39}\text{K}^\dagger$ $\pm 2\sigma_m$
Microcline*	$\sim 10^{-3}$	0.07187 ± 0.0001
Anorthositic Glass ** (An-Mg-5)	8.6×10^3	0.07107 ± 0.0013
Pyroxene 1** (Ti-PX-1)	2.1×10^4	0.07301 ± 0.0012
Pyroxene 2** (CAI-PX-1)	3×10^6	0.06999 ± 0.0064
Perovskite®	$\sim 4 \times 10^6$	0.06475 ± 0.0091

* US National Museum Standard (USNM 143966).

**Samples prepared at Caltech (Courtesy I. Hutcheon).

®Sample obtained from Vernadsky Institute, Moscow.

†Corrected for ($^{40}\text{Ca}^{42}\text{Ca}$)⁺⁺ interference.

Chapter 3

Sample Description

The samples analyzed in this study consist of eleven CAIs, of which eight belong to Efremovka and three to Grosnaja meteorite. These samples were studied for their petrographic and chemical composition at the Vernadsky Institute, Moscow, Russia. The inclusions were classified following the petrographic criteria suggested by Grossman (1975, 1980) and Wark and Lovering (1977); this is given in Table 3.1. One of the most important features of the Efremovka CAIs is that they do not show any signature of major secondary petrographic alteration (Ulyanov et al. 1982) attesting to their pristine preservation. This is not the case for Grosnaja CAIs which show distinct signatures of petrographic alteration (Ulyanov 91, Goswami et al., 1993). The documentation of the inclusions were carried out by an electron probe (Cameca Camebax), a scanning electron microscope (Cambridge S4/10) equipped with an energy dispersive X-ray analyzer and a Carl Zeiss optical microscope. The chemical composition of the different primary and secondary phases observed in the CAIs is given in Table 3.2. A brief description of individual CAIs is given below and the elemental composition of individual CAIs is given in Tables 3.3-3.6.

3.1 Efremovka CAIs

E2, E59 : These are compact type A inclusions. E2 which measures ~ 2 cm is one of the largest CAIs seen in Efremovka and E59 (Fig. 3.1a) is ~ 1 cm across. The major mineral

phase in these inclusions are melilite (~ 75%) and spinels (17%) and some minor phases (pervoskite ~3%, Fe-Ni metal ~ 0.4%). Fassaite also occurs as a minor phase in these CAIs. These inclusions have a thick multilayered rim with layer sequence similar to type B1 CAIs (described below). The Akermanite content of melilite in the near rim region is ~ 10 mole % but steadily increases to ~ 35% as one moves to the inclusion interior. Petrographic description of E2 is given by Ulyanov et al. (1982) and Fahey et al. (1987b). This CAI has also been analyzed for REE and oxygen isotopic compositions (Ulyanov et al., 1982, 1988; Nazarov et al., 1982, 1984). Additional REE and Mg isotopic compositions have been reported by Fahey et al. (1987b).

E40, E44, E65 : These are type B1 CAIs (E40: Fig 3.1b; E44: Fig 3.1c and E65 Fig 3.1d) which mainly consist of a melilite mantle and a pyroxene rich core. All the inclusions have a 20 to 30 μm thick multilayered rim with a layer sequence of (as one moves outward from the inclusion) spinel (\pm perovskite), melilite, and an outer layer of pyroxene that is zoned from Ti-Al-rich fassaite to aluminous diopside. Hibonite is also present in some of the spinel-melilite layer of E40 rim. The spinel grains in the interior of E40 are relatively large (up to about ~ 100 μm in the core). The spinel grains are in general isometric crystals that are poikilitically enclosed by pyroxenes and melilite. They are extremely pure and their TiO_2 and FeO content is < 1%. Metal grains and anorthite are generally present in the core region although some times they are also present in the mantle. The abundance of Fe-Ni metal decreases from E65 to E40 to E44.

The pyroxenes in these inclusions show variations in their TiO_2 content from 2.5% in E65 to ~ 14.5% in E40 (Table 3.4). The pyroxenes are zoned; the smaller ones show simple zoning (Ti-rich core and Ti-poor rim) and the larger ones show complex zoning. The compositional data and stoichiometric considerations suggest that a good fraction of Ti in these inclusions is present in the trivalent state. Melilite in all the inclusions show compositional zoning with the core being rich in akermanite content (55-70 mole%) while it decreases in the near rim region (10-30 mole%) (Table 3.3). Mineralogical studies of inclusions E40 and E65 have been carried out by Ulyanov and Kononkova (1990). The REE

composition of E40 was measured by Ulyanov and Kolesov (1984), and oxygen isotopic compositions of bulk samples of E40 were communicated by Ulyanov et al. (1988).

E50 : It is a large ($\sim 1\text{cm}$) multizoned hibonite-rich inclusion (Fig. 3.1e) containing a melilite-perovskite zone, a melilite-spinel zone, a melilite-spinel perovskite zone and the hibonite rich zone. Small ($\leq 10\mu\text{m}$) perovskite grains are extremely abundant in the melilite-perovskite zone. In the interior of the inclusion, where an association of melilite and perovskite is observed, the perovskites are slightly larger. The spinel grains are small and are poikilitically enclosed by the melilite. In the hibonite-rich zone, the hibonite has a lath like structure, and the spinel grains present in this zone are interwoven with melilite. The elemental composition of different mineral phases of E50 is given in Table 3.5.

E36, E60 : These are type B2 CAIs, E36 is a small inclusion ($\sim 5\text{mm}$) across (Fig. 3.1f) while E60 is larger $\sim 1\text{cm}$ across (Fig 3.1g). These inclusions have large melilite and pyroxene grains with smaller spinel grains enclosed in them. The pyroxene composition in E60 is similar to that of type B1 inclusions (Table 3.4). The melilite composition is highly akermanitic except near the outer edge (Table 3.3). There are a couple of localized spots in E60 where the presence of nepheline suggest minor low temperature alteration. There is a single layer diopside rim around the inclusions. The oxygen isotopic compositions of bulk sample of E60, and its mineral separates were reported by Ulyanov et al. (1988).

3.2 Grosnaja CAIs

GR4 : It is a type A inclusion, $\sim 1\text{mm}$ across, and is predominantly composed of melilite (Fig. 3.1h). There are very few spinel grains in the interior of this CAI. The rim does not exhibit distinct layered structure. Secondary alteration products (garnet, Fe-rich olivine and Na-rich plagioclase) are present in some localized areas near the rim region. The average major element composition of the different mineral phases are given in Table 3.6.

GR2 : It is the only Type C inclusion analyzed in this work and is $\sim 2\text{mm}$ across (Fig. 3.1i). It mainly consists of anorthite and pyroxene and its structure indicates that it has

probably originated from a melt. The chemical composition of different mineral phases is given in Table 3.6. The pyroxenes in the core have higher Al and lower Mg content compared to mantle pyroxenes. The TiO₂ content of the core pyroxenes is higher than the mantle pyroxenes. This inclusion has secondary alteration phases near the rim which mainly comprises of garnets, calcite, Na-rich plagioclase.

GR7: This is the largest inclusion from Grosnaja meteorite analyzed in this work and is ~ 1cm across (Fig. 3.1j). It belongs to the type B petrographic class. It is mainly composed of melilite with occasional pyroxenes. The REE data show a pattern that is similar to Group VI with enrichment in Eu and Yb. Melilite composition shows a broad range of akermanite content (15-55 mole%).

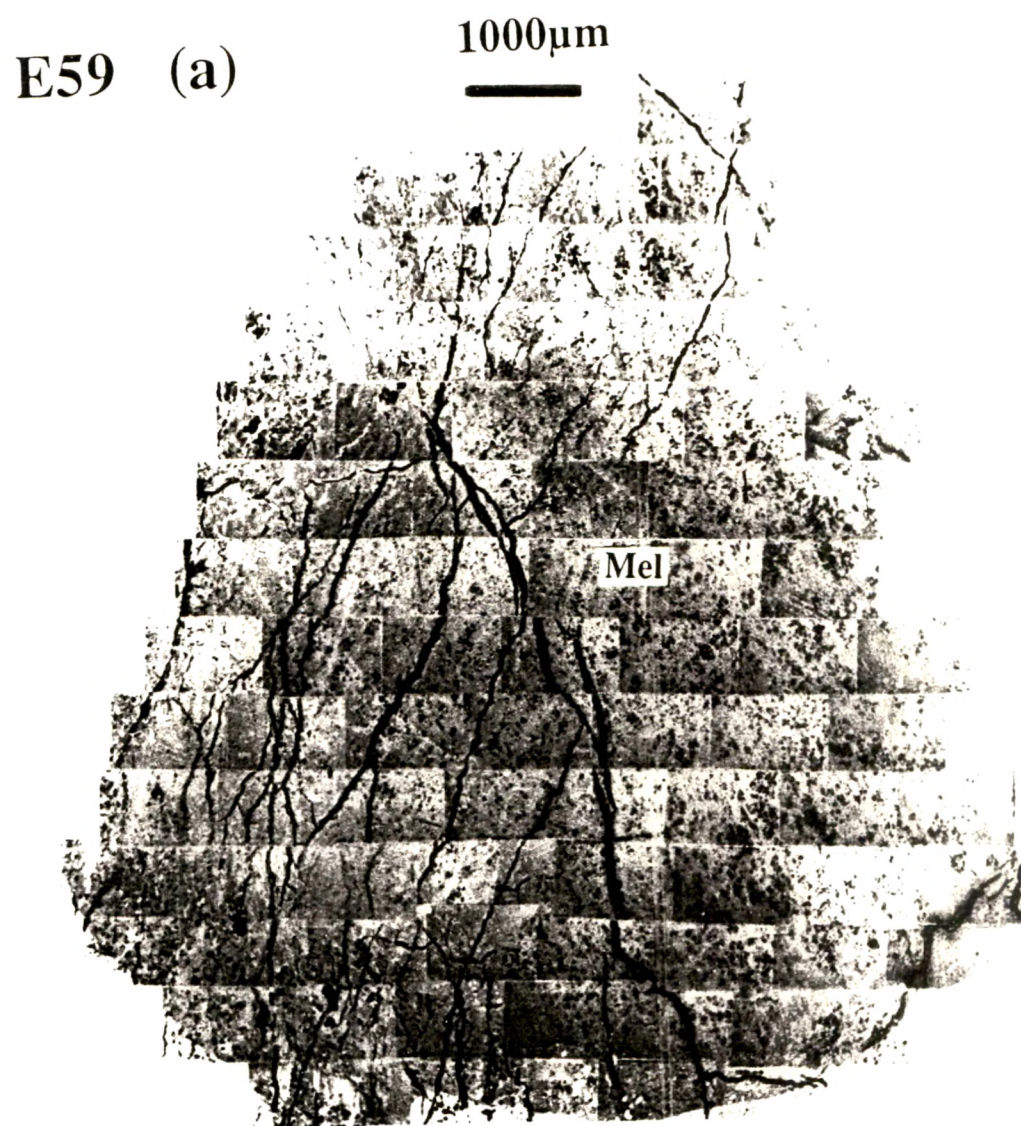


Fig.3.1

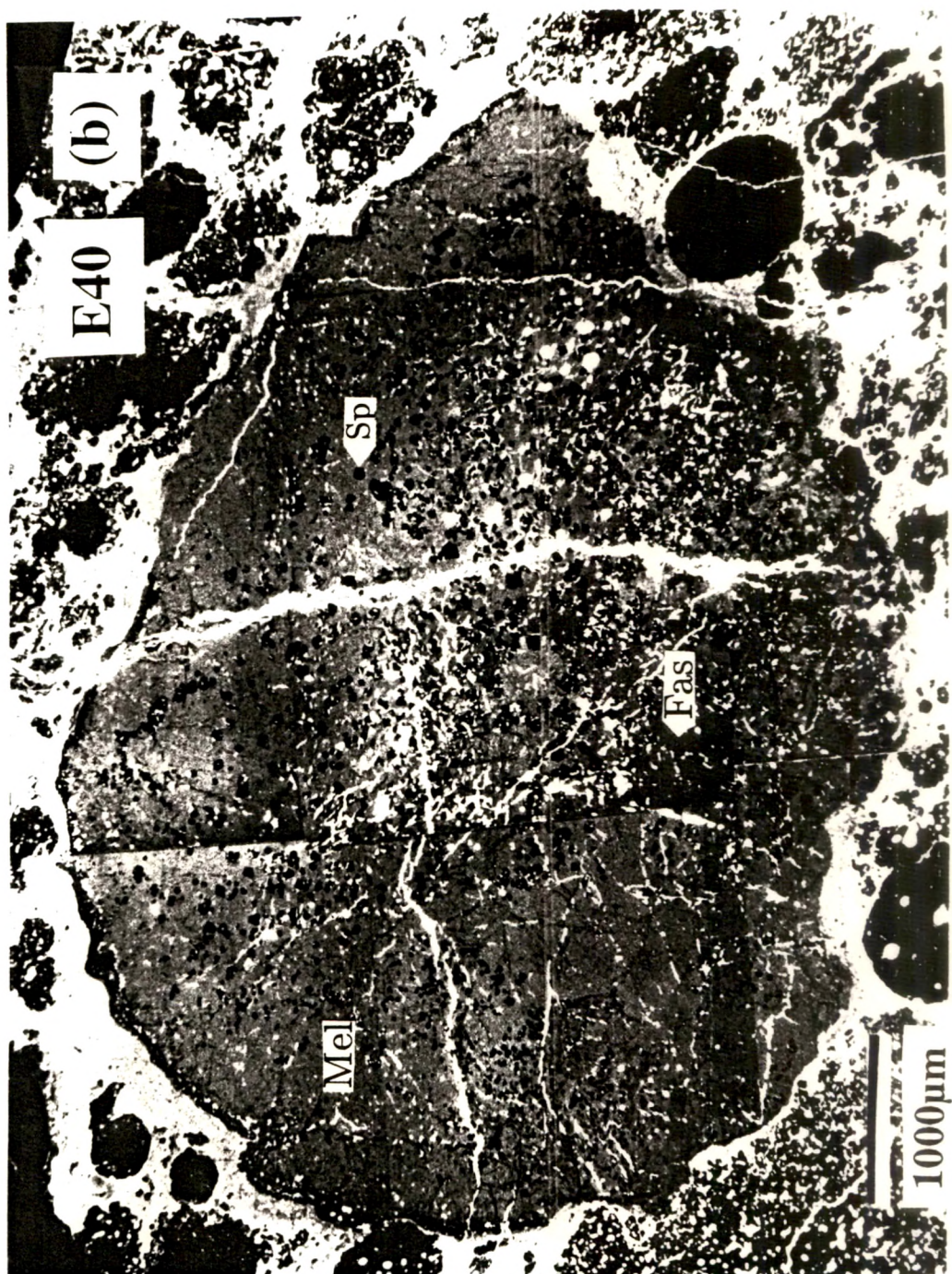


Fig.3.1 (Continued)

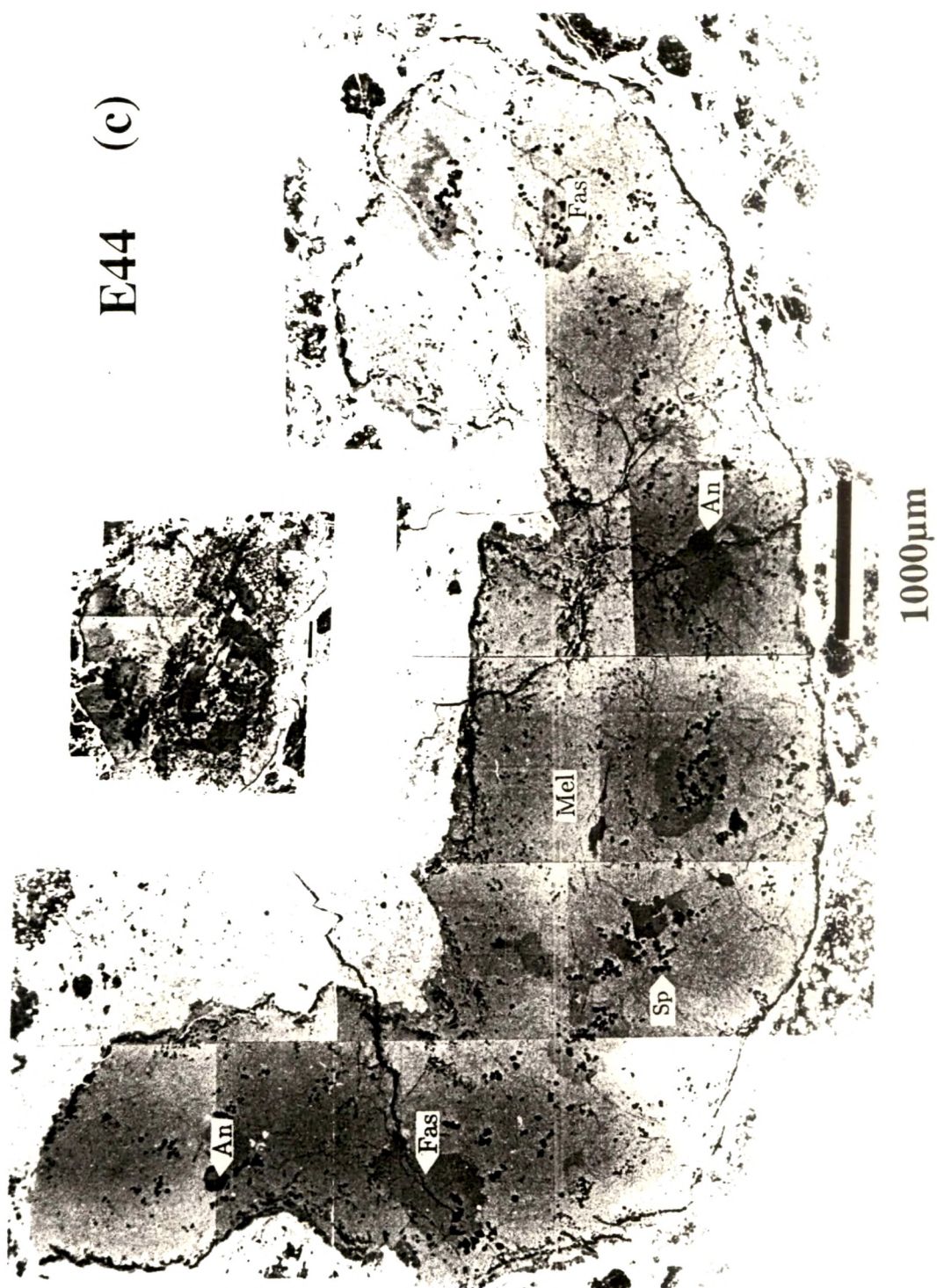


Fig.3.1 (Continued)

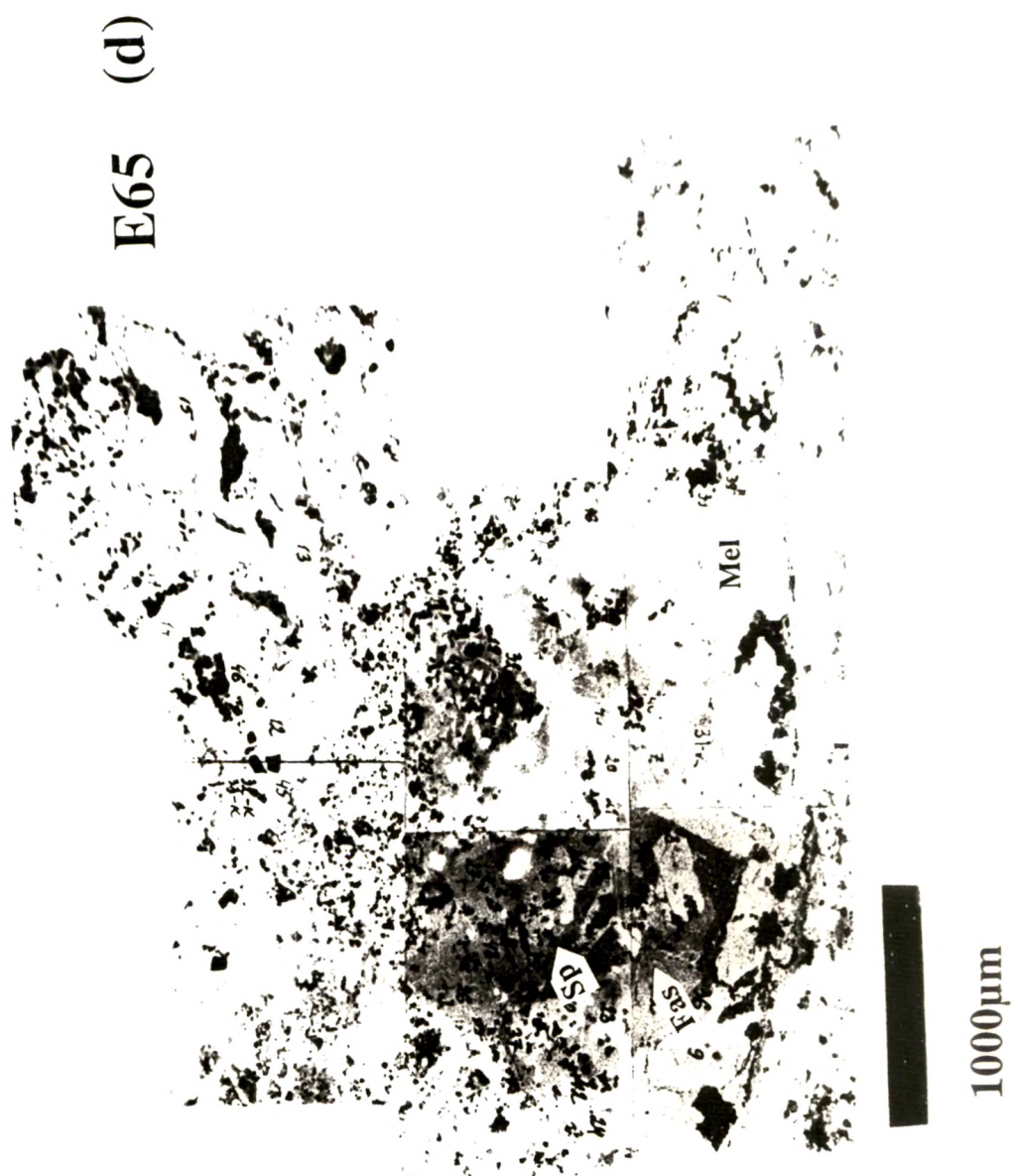


Fig.3.1 (Continued)



Fig.3.1 (Continued)

E36 (f)

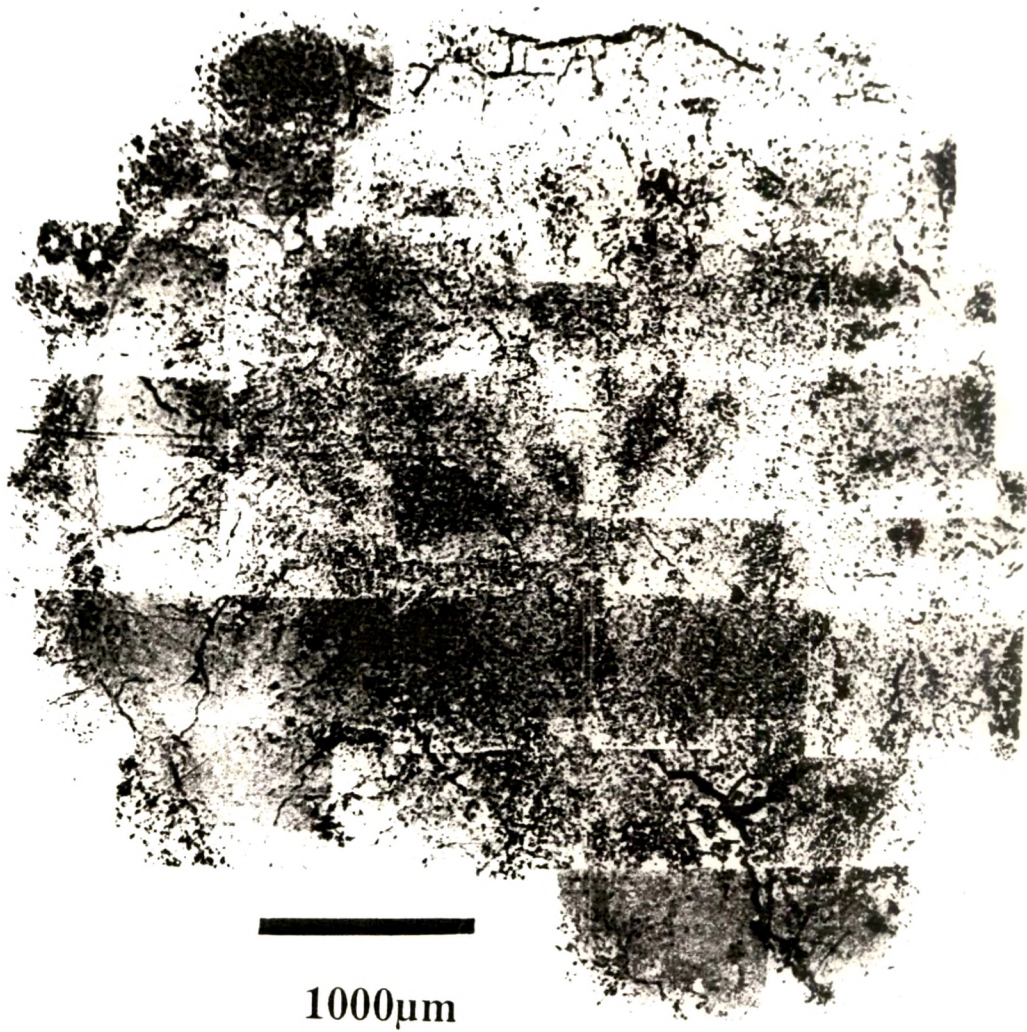


Fig.3.1 (Continued)



Fig.3.1 (Continued)

GR2 (h)



500μm

Fig.3.1 (Continued)

GR4 (i)



Fig.3.1 (Continued)

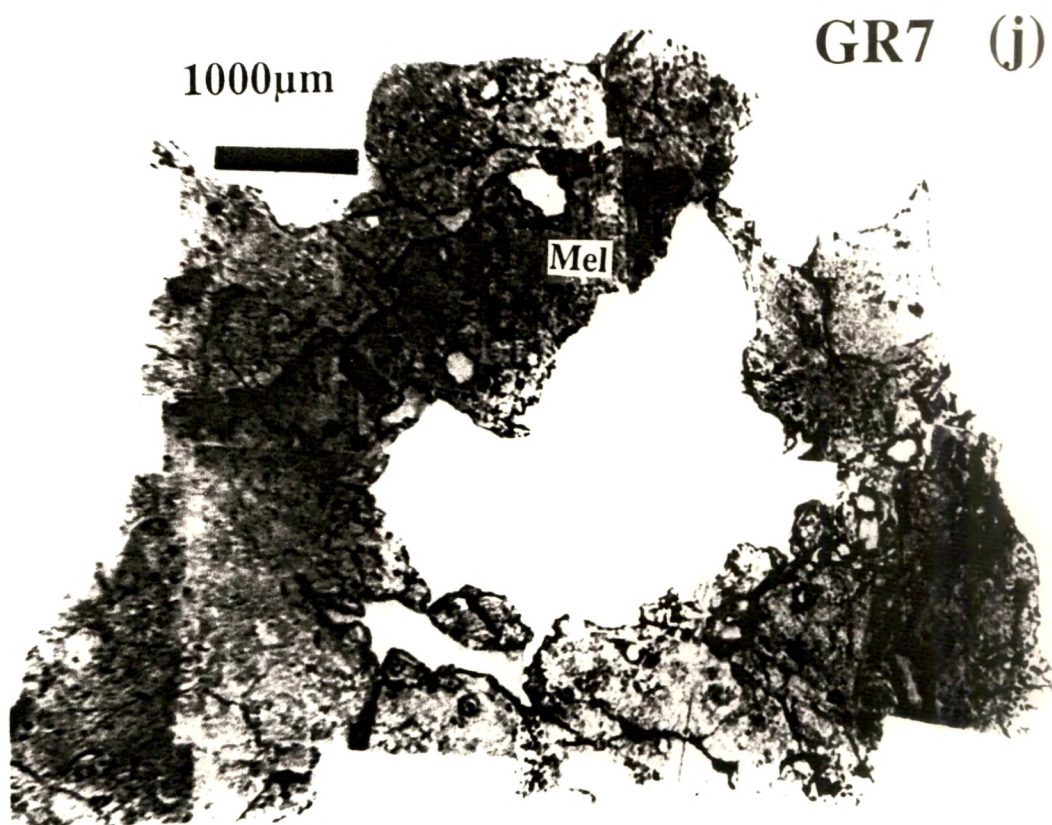


Figure 3.1: Optical photomicrograph of a polished section of Efremovka type A CAI E59, the dominant mineral phase is melilite. Backscattered electron photomicrographs of polished sections of the Efremovka type B1 CAIs E40 (b), E44 (c) and E64 (d). The E44 section analyzed represents a cut close to one of the edges of this CAI. A more representative cross section of E44 is shown as an inset in (c). The dominant mineral species are melilite, spinel and pyroxene can be easily identified. Anorthite present in E44 is marked. Backscattered electron photomicrograph of polished section of a Efremovka hibonite-rich CAI E50 (e). The dominant mineral phases are melilite, spinel and perovskite. Perovskite and hibonite rich zones are indicated. Optical photomicrograph and backscattered electron photomicrograph of polished sections of Efremovka type B2 CAIs E36 (f) and E60 (g). The dominant mineral phases are melilite and pyroxene. Optical photomicrographs of polished section of Grosnaja CAIs, type A GR2 (h), type C GR4 (i) and thin section of type B CAI GR7 (j). The dominant mineral phases are marked [Melilite = Mel, Pyroxene = Fas, Spinel = Sp, Hibonite = Hib, Anorthite = An].

Table 3.1: CAIs analyzed in this work

Petrographic type	Sample
Efremovka CAIs	
type A	E2 and E59
type B1	E40, E44 and E65
type B2	E36 and E60
hibonite-rich	E50
Grosnaja CAIs	
type A	GR4
type B	GR7
type C	GR2

Table 3.2: Composition of mineral phases in CAIs

Mineral	Composition
Primary Phases	
Corundum	Al_2O_3
Hibonite	$\text{CaAl}_{12}\text{O}_{19}$
Perovskite	CaTiO_3
Spinel	MgAl_2O_4
Fassaite	$\text{Ca}(\text{Mg}, \text{Ti}, \text{Al})(\text{Al}, \text{Si})_2\text{O}_6$
Melilite	$\text{Ca}_2\text{MgSi}_2\text{O}_7$ - $\text{Ca}_2\text{Al}_2\text{Si}_7$
Anorthite	$\text{CaAl}_2\text{Si}_2\text{O}_8$
Diopside	CaMgSiO_6
Secondary Phases	
Grossular	$\text{Ca}_3\text{Al}_2\text{Si}_3\text{O}_{12}$
Nepheline	NaAlSiO_4
Sodalite	$\text{Na}_8\text{Al}_6\text{Si}_6\text{O}_{24}\text{Cl}_2$
Calcite	CaCO_3

Table 3.3: Electron Microprobe Analysis of Melilite in Efremovka CAIs

	E40(B1)		E44(B1)		E65(B1)		E60(B2)
	mantle	core	mantle	core	mantle	core	
SiO ₂	29.83	38.59	26.66	38.55	30.17	35	42.06
TiO ₂	0.06	0.02	-	-	0.02	0.01	-
Al ₂ O ₃	23.79	10.85	29.01	10.80	25.14	17.09	4.76
Cr ₂ O ₃	-	-	-	-	-	-	0.18
V ₂ O ₃	-	-	-	-	-	-	0.11
CaO	41.17	40.89	41.43	40.41	39.94	40.68	39.31
MgO	4.18	9.81	2.78	10.16	4.96	7.84	13.09
FeO	0.03	0.02	0.01	-	0.03	0.16	0.28
MnO	-	-	0.09	0.02	-	-	-
Na ₂ O	0.02	0.10	0.01	0.05	0.07	0.19	0.14
K ₂ O	-	-	-	-	0.01	0.01	0.06
SUM	99.08	100.28	100	100	100.34	100.98	99.99

Note: "-" indicates no measurement

Table 3.4: Electron Microprobe Analysis of Pyroxene in Efremovka CAIs

	E65(B1)		E40(B1)		E44(B1)		E60(B2)	
	Low-Ti	High-Ti	Low-Ti	High-Ti	Low-Ti	High-Ti	Low-Ti	High-Ti
SiO ₂	45.39	39.75	42.23	37.41	44.68	35.17	52.24	33.99
TiO ₂	2.54	7.98	6.51	14.58	4.00	11.31	0.19	12.21
Al ₂ O ₃	16.67	20.80	16.32	17.82	13.67	21.24	3.08	22.56
Cr ₂ O ₃	0.05	0.06	0.10	0.06	0.03	-	-	-
V ₂ O ₃	-	-	0.07	0.26	0.02	0.74	-	0.68
CaO	25.78	24.95	25.47	24.10	24.99	24.52	22.65	23.39
MgO	11.43	8.96	9.87	7.41	12.50	7.08	18.95	7.05
FeO	0.54	0.05	0.05	0.32	-	0.13	0.81	-
MnO	0.02	0.01	-	-	0.03	-	0.08	0.02
Na ₂ O	0.06	-	-	0.03	0.08	-	-	0.07
K ₂ O	0.02	0.01	0.01	-	-	-	-	0.03
SUM	102.50	102.57	100.63	101.72	100	100	98	100

Note: "-" indicates no measurement

Table 3.5: Electron Microprobe Analyses of Mineral Phases in E50

	Melilite	Hibonite	Perovskite	Spinel
SiO ₂	25.25	0.00	0.68	0.00
TiO ₂	0.02	7.25	56.76	0.24
Al ₂ O ₃	31.94	79.81	1.09	69.63
FeO	0.08	0.00	0.04	0.58
MnO	0.00	0.00	0.11	0.00
MgO	2.33	4.73	0.05	28.99
CaO	40.24	7.92	41.09	0.17
Na ₂ O	0.00	0.23	0.15	0.40
K ₂ O	0.08	0.06	0.03	0.00
SUM	99.94	100.00	100.00	100.01

Table 3.6: Major element composition of mineral phases in Grosnaja CAIs

	GR2(Type C)				GR4 (Type A)				
	Anorthite	Pyroxene		Spinel	Garnet	Pyroxene	Melilite	Spinel	Garnet
		Core	Mantle						
SiO ₂	42.46	42.02	47.18	0.07	35.07	35.86	26.81	0.04	38.99
TiO ₂	0.08	5.16	2.50	0.38	0.01	9.55	0.03	0.35	0.01
Al ₂ O ₃	36.44	14.42	9.72	70.53	0.04	21.64	28.83	71.78	22.79
Cr ₂ O ₃	0.03	0.27	0.67	0.79	0.01	0.09	0.03	0.25	< 0.01
V ₂ O ₃	< 0.01	0.16	0.13	0.33	< 0.01	0.15	0.01	0.41	0.01
MgO	0.11	11.76	13.31	27.36	0.17	7.53	3.20	28.02	2.45
CaO	20.04	25.59	25.49	0.08	33.43	25.28	41.10	0.16	34.93
FeO	0.10	0.16	0.21	0.53	28.26	0.02	0.08	0.08	1.35
MnO	0.01	< 0.01	0.04	0.02	0.01	< 0.01	0.01	0.03	0.02
Na ₂ O	0.15	0.01	0.01	—	0.01	0.01	0.03	—	0.01
K ₂ O	0.01	< 0.01	< 0.01	—	0.01	< 0.01	< 0.01	—	< 0.01

Note: All values are based on averages of 3 to 15 individual analysis

Chapter 4

Results

In this chapter the results obtained from isotopic studies of eleven coarse-grained Ca-Al-Rich inclusions from Efremovka and Grosnaja meteorites by the ion microprobe are presented. Magnesium, potassium and calcium isotopic studies were carried out on these CAIs using the techniques and procedures described in Chapter 2. Mg-Al isotopic studies were carried out on all the CAIs [E2 and E59 (type A); E36 and E60 (type B2); E40, E44 and E65 (type B1); E50 (hibonite-rich); GR2 (type C); GR4 (type A); and GR7 (type B)]. The CAIs E44, E50 and E65 were analyzed for their potassium and calcium isotopic compositions.

4.1 Results from Mg-Al Isotopic Studies

Mg-Al isotopic studies were carried out to determine intrinsic Mg isotopic mass fractionation $F(\text{Mg})$ (Eq.2.2, Chapter 2) for the Efremovka CAIs, and non linear $\delta^{26}\text{Mg}$ excess (Eq.2.6, Chapter 2) and $^{27}\text{Al}/^{24}\text{Mg}$ values in all the CAIs.

The $F(\text{Mg})$ values were determined for the two major magnesium bearing phases, melilite and spinel, present in the peripheral and interior regions of several of the Efremovka CAIs. The measurements were carried out in a continuous run for individual CAI, and terrestrial standards were measured at regular intervals. Only in the case of E2 spinels in the rim were also analyzed. Further, a systematic study of spatial variation of $F(\text{Mg})$ within the CAIs were carried out in the case of E2 and E40. The results obtained from these

analyses are presented in Tables 4.1-4.4. The errors in $F(\text{Mg})$ values have been computed by taking into account the measurement uncertainties in $\Delta^{25}\text{Mg}$ for both the meteoritic phases and terrestrial standards. The $F(\text{Mg})$ values of spinels in some CAIs are slightly higher than melilite, however, it is not significant in view of the measurement uncertainties of $\sim 1.5\text{‰}/\text{amu}(2\sigma_m)$. This difference could partly be due to the fact that the terrestrial melilite standard used by us has a high Akermanite content [$\sim 36(65)\text{mole\%}$] compared to meteoritic melilite that spans a wide range of composition [$\sim 36(10-70)\text{mole\%}$].

The results (Tables 4.1 and 4.2) suggest significant differences in $F(\text{Mg})$ values between the peripheral and interior regions of the CAIs E2 and E40, and non-systematic spatial variation in $F(\text{Mg})$ values in E50. A detailed study was therefore carried out to determine the spatial variation in $F(\text{Mg})$ values for both melilite and spinel phases in E2 and E40 (Tables 4.3-4.4). In the case of E40 the studies were carried out along two nearly radial traverses one of which was close to an electron probe traverse that provided data on melilite composition. The melilite composition in E2 and E40 show similar trends with the near rim melilite being gehlenitic (more refractory, high Al/Mg) while melilite in the interior are akermanitic (less refractory, low Al/Mg). However, the $F(\text{Mg})$ values for melilite in these two CAIs show opposite trend. Melilite in the near rim region in E2 is enriched in the lighter isotopes [$F(\text{Mg}) \leq 0$] and those in the interior are enriched in the heavy isotopes; in E40 the trend is reverse with melilite in the near rim region enriched in the heavy isotopes and those in the interior have near normal Mg isotopic composition. Additionally, the $F(\text{Mg})$ values for all spinels in E40 do not match the melilite data. Some of the spinel grains near the rim and in the interior have higher $F(\text{Mg})$ values compared to those of melilite, much outside the limits of experimental uncertainties.

The magnesium isotopic mass fractionation in the CAI E2 was measured earlier by Fahey et al. (1987b). Even though the fractionation trend observed by us in this is similar to that reported by Fahey et al. (1987b), there are some differences in the absolute values. We obtain systematically lower $F(\text{Mg})$ values for the near-rim phases than Fahey et al. (1987b). Since the measurements were carried out on two different sections of E2, which is the largest

CAI in Efremovka measuring couple of cms across, these differences could be in part due to spatial dependence of the intensity of the process responsible for producing the observed intrinsic fractionation in this CAI. The data for the phases in the interior of this CAI showed a spread in F(Mg) values which agree with the range of values (7 to 11%) reported by Fahey et al. (1987b). We shall now consider the data pertaining to non-linear excess in ^{26}Mg in the CAIs from the Efremovka and Grosnaja meteorites.

If non-linear excess in ^{26}Mg ($\delta^{26}\text{Mg} > 0$, Eq.2.6, Chapter 2) is present in meteoritic phases, and if such an excess is of radiogenic origin, caused by the decay of the short-lived radionuclide ^{26}Al ($t_{1/2} \sim 0.7\text{Ma}$), the measured ^{26}Mg has two components and one can write :

$$\begin{aligned} \left(\frac{^{26}\text{Mg}}{^{24}\text{Mg}} \right)_m &= \left(\frac{^{26}\text{Mg}}{^{24}\text{Mg}} \right)_i + \left(\frac{^{26}\text{Mg}^*}{^{24}\text{Mg}} \right) \\ &= \left(\frac{^{26}\text{Mg}}{^{24}\text{Mg}} \right)_i + \left(\frac{^{26}\text{Al}}{^{27}\text{Al}} \right)_i \left(\frac{^{27}\text{Al}}{^{24}\text{Mg}} \right)_m \end{aligned} \quad (4.1)$$

where m stands for the measured isotopic ratio, i for the initial ratio at the time of formation of meteoritic phases (e.g. CAIs) and "*" represents the radiogenic component. If a CAI has different mineral phases with varying $^{27}\text{Al}/^{24}\text{Mg}$ values then Eq. 4.1 describes the evolution of the Mg-Al isotopic system. The intercept and slope of the best-fit line represent the initial $^{26}\text{Mg}/^{24}\text{Mg}$ and $^{26}\text{Al}/^{27}\text{Al}$ at the time of closure of the Mg-Al isotope system in the CAI. The procedure for obtaining a best-fit line to a set of data with errors in both coordinates have been given by York (1967, 1969), Williamson (1968) and Provost (1990). The intercept and slope of the Mg-Al evolution diagrams for different CAIs analyzed by us were determined by using the programs developed by Lugmair (1991) and Provost (1990). It should be noted here that secondary processes affecting the CAIs can lead to possible exchange of Mg between different phases within the CAI or between CAI and external phases/reservoir that can disturb the Mg-Al isotopic system and result in deviations from the above relation.

The fractionation corrected ^{26}Mg excess ($\delta^{26}\text{Mg}$) and the $^{27}\text{Al}/^{24}\text{Mg}$ values were

measured in all the Efremovka and Grosnaja CAIs, and the results are given in Tables 4.1-4.5. The $^{27}\text{Al}/^{24}\text{Mg}$ values were determined from the $^{27}\text{Al}^+ / ^{24}\text{Mg}^+$ values measured using the ion microprobe, and the Mg-Al yield factors [Table 2.2, Eq.2.7, Chapter2]. The different phases that have been analyzed are spinel, melilite, pyroxene, and anorthite. Hibonite was also analyzed in the case of E50. The $^{27}\text{Al}/^{24}\text{Mg}$ shows a wide variation in the analyzed phases, spinels and pyroxenes have the lowest values (≤ 3); melilites have intermediate values (1 to 50); and anorthites have the highest values (100 to 1000). The spread in the $^{27}\text{Al}/^{24}\text{Mg}$ values allow us to constrain the slope and the intercept of the Mg-Al evolution diagram for the different CAIs and obtain accurate values for initial magnesium and aluminum isotopic composition at the time of formation of CAIs. In the case of Grosnaja CAIs and some of the Efremovka CAIs (E36, E44, E59, E60 and E65) results pertaining to $\delta^{26}\text{Mg}$ and $^{27}\text{Al}/^{24}\text{Mg}$ values are only given as the measurements were made without the added precaution needed to obtain F(Mg) values. The Mg-Al evolution diagrams for the CAIs were obtained by combining the results presented in Tables 4.1-4.5 and these are shown in Figs.4.1a - 4.1k. Seven CAIs from Efremovka, E2 and E59 (type A), E36 and E60 (type B2), E40, and E65 (type B1), E50 (hibonite-rich), have well behaved Mg-Al isotope systematics with initial $^{26}\text{Al}/^{27}\text{Al}$ ranging from $(3.11 \times 10^{-5} \text{ to } 5.64) \times 10^{-5}$. The correlation in case of CAI E36 is not as good and although the data suggest the presence of radiogenic ^{26}Mg with an initial aluminium isotopic ratio close to the values obtained for the other Efremovka CAIs, we cannot completely rule out the possibility of some disturbances in the magnesium isotopic systematics in this CAI. The CAI E60 (type B2) shows an approximately well behaved systematics with an initial ratio of $(3.11 \pm 0.33) \times 10^{-5}$, although individual anorthite data points show a scatter, and yield $^{26}\text{Al}/^{27}\text{Al}$ ranging from $(1.86 \text{ to } 3.75) \times 10^{-5}$. The CAI E44 (type B1) shows a clear sign of disturbance in its Mg-Al isotopic systematics with data for melilite and anorthite showing completely different trends. If we consider the melilite and anorthite data separately, and use spinel and pyroxene as common members, they yield initial $^{26}\text{Al}/^{27}\text{Al}$ value of $(6.7 \pm 2.2) \times 10^{-5}$ (melilite) and $(4.6 \pm 1.1) \times 10^{-6}$ (anorthite) respectively. In the case of Grosnaja CAIs only GR2 (type C) yields a well behaved Mg-Al evolution diagram. However, the initial

$^{26}\text{Al}/^{27}\text{Al}$ value $[(3.14 \pm 0.49) \times 10^{-6}]$, is much lower than the values obtained for the Efremovka CAIs. In the case of GR4 (type A) and GR7 (type B), the data suggest extreme disturbance in the Mg-Al systematics and absence of any correlation between ^{26}Mg excess and $^{27}\text{Al}/^{24}\text{Mg}$ values. The initial $^{26}\text{Mg}/^{24}\text{Mg}$ at the time of formation of the CAIs are near normal within experimental uncertainties except in E60 which shows a 2‰ excess in the $^{26}\text{Mg}/^{24}\text{Mg}$ ratio above the solar system reference value.

Table 4.1: Mg-Al Data

Phase	F(Mg) $\pm 2\sigma_m$	$\delta^{26}\text{Mg}$ $\pm 2\sigma_m$	$^{27}\text{Al}/^{24}\text{Mg}$ $\pm 2\sigma_m$
E2(Type A)			
Spinel*	-2.6 ± 1.5	-1.3 ± 2.2	2.6
Spinel†	6.8 ± 1.5	0.4 ± 1.7	2.5
Melilite*	0.1 ± 1.6	8.1 ± 2.2	22.6 ± 0.7
Melilite*	-2.9 ± 1.2	7.4 ± 4.7	25.7 ± 0.3
Melilite†	3.5 ± 1.4	3.5 ± 2.1	8.5 ± 0.9
Melilite†	7.2 ± 1.7	1.5 ± 2.5	7.9
E40(Type B1)			
Spinel*	4.2 ± 1.6	2.4 ± 2.1	2.6
Spinel†	1.9 ± 2.0	1.0 ± 2.7	2.5
Melilite*	3.3 ± 1.3	6.7 ± 1.6	13.9 ± 0.7
Melilite*	4.8 ± 1.6	5.5 ± 2.6	18.9 ± 0.2
Melilite†	0.3 ± 1.3	1.9 ± 1.7	5.8
E44(Type B1)			
Spinel†	3.2 ± 2.2	3.0 ± 3.4	2.5
Spinel†	3.7 ± 2.1	2.3 ± 3.2	2.5
Melilite†	3.7 ± 1.4	3.2 ± 1.9	3.0
Melilite*	3.8 ± 1.4	3.4 ± 2.2	10.5 ± 0.1
E65(Type B1)			
Spinel	4.7 ± 1.5	2.5 ± 2.0	2.4
Spinel	4.6 ± 1.5	2.4 ± 1.8	2.5
Melilite	2.8 ± 1.3	3.2 ± 2.7	5.8
Melilite	2.7 ± 1.4	2.5 ± 2.9	6.1
E60(Type B2)			
Melilite*	-1.3 ± 1.6	2.0 ± 2.5	1.5
Melilite†	0.5 ± 1.4	-0.1 ± 2.2	0.4
Melilite†	-0.2 ± 1.5	2.8 ± 2.1	1.1
Spinel	1.6 ± 1.4	2.2 ± 1.5	2.5
E36 (Type B2)			
Melilite*	2.6 ± 1.3	3.97 ± 1.92	13.08 ± 0.28
Melilite†	4.7 ± 1.7	3.70 ± 2.34	21.52 ± 0.80
E59 (Type A)			
Melilite*	4.6 ± 1.4	3.75 ± 2.08	16.7 ± 0.2
Melilite†	3.8 ± 0.9	6.57 ± 3.10	15.9 ± 0.2

Note: F(Mg) and $\delta^{26}\text{Mg}$ are in permil/amu and permil
Errors less than 0.1 are not shown

*Near Rim

† Interior

Table 4.2: Mg-Al Data

Zone	F(Mg) $\pm 2\sigma_m$	$\delta^{26}\text{Mg}$ $\pm 2\sigma_m$	$(^{27}\text{Al}/^{24}\text{Mg})$ $\pm 2\sigma_m$
E50(Multizoned Hibonite-Rich)			
Melilite			
Near Rim	2.11 ± 1.73	4.57 ± 2.72	21.37 ± 0.11
Near Rim	-6.61 ± 2.34	19.02 ± 4.42	23.69 ± 0.06
Me + Sp	8.01 ± 1.76	5.37 ± 3.22	19.69 ± 0.11
Interior (Me + Per)	0.97 ± 1.98	12.76 ± 3.98	32.56 ± 3.36
Interior (Me + Per)	5.50 ± 2.45	7.56 ± 4.46	23.86 ± 0.09
Interior (Me + Per)	5.00 ± 2.15	4.58 ± 4.04	18.86 ± 0.15
Interior (Me + Per)	2.26 ± 1.85	11.37 ± 3.38	24.25 ± 0.28
Interior (Me + Per)	0.50 ± 1.84	4.30 ± 2.74	19.62 ± 0.37
Hibonite Rich	3.46 ± 2.70	14.38 ± 4.44	50.60 ± 0.22
Spinel			
Near Rim	1.06 ± 1.59	0.24 ± 2.22	2.59 ± 0.27
Me + Sp	9.20 ± 1.26	1.17 ± 1.67	2.60 ± 0.01
Me + Sp	8.30 ± 1.34	-0.42 ± 1.99	2.62 ± 0.01
Interior (Me + Per)	0.95 ± 1.50	1.41 ± 2.38	2.70 ± 0.03
Hibonite			
Hibonite Rich	-	7.08 ± 2.20	17.94 ± 0.03
Hibonite Rich	-	5.49 ± 2.38	15.16 ± 0.07

Note: F(Mg) and $\delta^{26}\text{Mg}$ are in permil/amu and permil
 Errors less than 0.1 are not shown

Table 4.3: Mg-Al Data

Position*	F(Mg)	$\delta^{26}\text{Mg}$	$^{27}\text{Al}/^{24}\text{Mg}^\dagger$
μm	$\pm 2\sigma_m$	$\pm 2\sigma_m$	$\pm 2\sigma_m$
E2(Type A) [§]			
Melilite Traverse			
20	0.1 ± 1.6	8.1 ± 2.2	22.6 ± 0.7
30	-2.8 ± 1.2	9.9 ± 3.5	25.7 ± 0.3
50	-0.3 ± 1.5	6.9 ± 2.1	15.7 ± 0.1
60	0.5 ± 1.4	6.5 ± 2.3	10.4 ± 1.2
150	2.5 ± 1.3	4.5 ± 1.4	8.7
320	3.7 ± 1.4	3.5 ± 2.1	9.36
350	3.5 ± 1.4	3.5 ± 2.1	8.5 ± 0.9
550	2.8 ± 1.3	3.4 ± 1.8	7.5 ± 0.1
800	3.2 ± 1.4	2.5 ± 2.0	9.7 ± 0.3
1000	7.2 ± 1.7	1.5 ± 2.5	7.9
1250	6.5 ± 1.8	6.1 ± 2.5	17.2 ± 0.2
1500	9.5 ± 2.0	0.7 ± 3.7	10.6
Spinel			
Rim	-1.2 ± 1.6	0.9 ± 1.7	2.6
Rim	-0.6 ± 1.4	2.4 ± 2.6	2.5
20	-2.6 ± 1.2	-1.3 ± 2.2	2.6
600	6.8 ± 1.5	0.4 ± 1.7	2.5
750	9.0 ± 1.2	0.6 ± 2.0	2.7
1250	6.6 ± 1.6	1.2 ± 2.5	2.5

Note :F(Mg) and $\delta^{26}\text{Mg}$ are in permil/amu and permil respectively.

*Distance from the inner boundary of the rim.

[†]Errors less than 0.1 are not shown.

[§]Data for this inclusion given in Table 4.1 are also included here.

Table 4.4: Mg-Al Data

Position*	F(Mg)	$\delta^{26}\text{Mg}$	$^{27}\text{Al}/^{24}\text{Mg}^\dagger$
μm	$\pm 2\sigma_m$	$\pm 2\sigma_m$	$\pm 2\sigma_m$
E40(Type B1)\$			
Melilite Traverse			
50	4.2 ± 2.2	6.5 ± 4.2	21.0 ± 0.2
60	3.3 ± 1.3	6.7 ± 1.6	13.9 ± 0.7
80	4.8 ± 1.6	3.0 ± 2.1	14.2 ± 0.1
120	5.4 ± 2.4	0.7 ± 2.6	12.0 ± 0.2
150	4.4 ± 1.6	5.5 ± 2.5	18.9 ± 0.2
170	2.9 ± 1.3	5.9 ± 3.4	16.2 ± 0.2
230	2.4 ± 1.7	6.1 ± 3.6	18.3 ± 0.1
300	3.3 ± 1.9	4.9 ± 2.6	12.9 ± 0.1
550	3.8 ± 1.8	3.2 ± 2.8	11.4 ± 0.1
1050	0.9 ± 2.1	5.5 ± 3.4	6.8 ± 0.1
1550	0.3 ± 1.3	1.9 ± 1.7	5.8
2550	0.5 ± 1.6	3.4 ± 3.0	3.8
Spinel Traverse			
50	4.2 ± 1.6	2.4 ± 2.1	2.6
170	5.5 ± 2.1	1.1 ± 3.2	2.7
370	2.9 ± 1.6	1.2 ± 2.0	2.7
500	5.6 ± 2.0	-0.5 ± 2.7	2.6
650	4.9 ± 1.7	0.0 ± 2.8	2.6
720	3.5 ± 1.9	2.3 ± 2.6	2.6
1250	2.6 ± 1.5	1.0 ± 2.3	2.4
1300	3.3 ± 1.5	1.2 ± 2.2	2.4
1900	2.5 ± 1.9	2.9 ± 3.0	2.5
2450	1.9 ± 2.1	1.0 ± 2.7	2.5
2520	2.3 ± 1.8	2.2 ± 2.8	2.5
2555	1.9 ± 2.0	2.7 ± 3.2	2.5
2570	2.3 ± 1.7	0.1 ± 2.6	2.4
2590	3.8 ± 1.8	1.1 ± 2.7	2.7
3000	2.2 ± 1.5	3.5 ± 2.6	2.5

Note :F(Mg) and $\delta^{26}\text{Mg}$ are in permil/amu and permil respectively.

*Distance from the inner boundary of the rim.

†Errors less than 0.1 are not shown.

\$Data for this inclusion given in Table 4.1 are also included here.

Table 4.5: Mg-Al DATA

Phase	$\delta^{26}\text{Mg}^*$ $\pm 2\sigma_m$	$^{27}\text{Al}/^{24}\text{Mg}^\dagger$ $\pm 2\sigma_m$
E36(Type B2)		
Melilite 1	3.27 ± 1.97	12.38 ± 0.20
Melilite 2	1.20 ± 2.40	8.52 ± 0.10
Melilite 3	-1.61 ± 0.87	3.50 ± 0.01
Melilite 4	3.47 ± 1.60	11.28 ± 0.36
Melilite 5	2.08 ± 1.02	4.96 ± 0.28
Melilite 6	3.22 ± 1.60	6.04 ± 0.16
Melilite 7	1.55 ± 2.22	2.00 ± 0.06
Melilite 8	1.92 ± 2.00	17.33 ± 0.60
Fassaite 1	-0.92 ± 2.16	1.72 ± 0.02
E40(Type B1)		
Fassaite 1	3.0 ± 2.5	2.0
Fassaite 2	3.1 ± 1.8	1.9
Fassaite 3	0.7 ± 2.5	1.5
E44(Type B1)		
Spinel 1	-0.1 ± 1.4	2.5
Spinel 2	-0.1 ± 1.9	2.5
Spinel 3	0.4 ± 2.1	2.6
Fassaite 1	0.2 ± 4.0	2.4
Fassaite 2	1.6 ± 2.8	2.5
Fassaite 3	3.0 ± 3.6	3.4
Fassaite 4	-1.2 ± 3.5	2.6
Melilite 1	5.1 ± 2.0	9.4 ± 0.3
Melilite 2	5.4 ± 3.6	14.1
Melilite 3	3.1 ± 2.7	8.8 ± 0.2
Melilite 4	7.2 ± 3.6	11.9 ± 0.1
Melilite 5	1.5 ± 2.8	4.7
Melilite 6	1.3 ± 3.2	6.0
Melilite 7	6.1 ± 3.2	10.2 ± 0.1
Melilite 8	4.9 ± 3.4	12.7
Anorthite 1	10.9 ± 9.7	301.4 ± 33.2
Anorthite 2	25.0 ± 7.7	710.9 ± 38.4
Anorthite 3	9.8 ± 5.6	226.4 ± 12.7
Anorthite 4	8.4 ± 6.5	369.9 ± 37.9
Anorthite 5	11.6 ± 7.2	292.5 ± 46.1

Table 4.5 (Continued)

Phase	$\delta^{26}\text{Mg}^*$ $\pm 2\sigma_m$	$^{27}\text{Al}/^{24}\text{Mg}^\dagger$ $\pm 2\sigma_m$
E59(Type A)		
Melilite 1	7.38 ± 2.24	21.9 ± 0.2
Melilite 2	6.03 ± 2.40	18.1 ± 0.2
Melilite 3	3.24 ± 2.20	12.1 ± 0.2
Melilite 5	8.04 ± 4.60	23.7 ± 0.2
Melilite 6	8.44 ± 2.92	34.0 ± 0.2
E60(Type B2)		
Spinel	2.2 ± 1.5	2.5
Melilite 1	3.6 ± 2.0	0.7
Melilite 2	1.0 ± 2.4	0.7
Melilite 3	2.2 ± 1.7	1.2
Anorthite 1	10.0 ± 2.7	60.8 ± 1.1
Anorthite 2	10.6 ± 2.0	40.3 ± 1.1
Anorthite 3	44.3 ± 4.4	158.1 ± 14.5
E65(Type B1)		
Spinel 1	-2.9 ± 2.3	2.7
Spinel 2	-1.1 ± 2.8	2.4 ± 0.3
Spinel 3	-1.6 ± 2.4	2.6
Spinel 4	-0.1 ± 2.7	2.5
Spinel 5	2.5 ± 3.0	2.6 ± 0.3
Spinel 6	-0.9 ± 2.4	2.5
Spinel 7	2.3 ± 1.6	2.5
Fassaite 1	0.7 ± 3.6	1.4
Fassaite 2	-0.1 ± 4.1	2.0
Fassaite 3	0.3 ± 2.7	1.4
Melilite 1	2.7 ± 1.2	6.6
Melilite 2	2.8 ± 1.3	2.9 ± 0.3
Melilite 3	1.8 ± 2.2	3.7
Melilite 4	1.7 ± 2.9	4.8
Melilite 5	4.4 ± 1.8	13.7 ± 0.1
Anorthite 1	48.8 ± 3.4	162.3 ± 10.2
Anorthite 2	42.7 ± 4.1	136.4 ± 8.6
Anorthite 3	26.1 ± 3.1	104.4 ± 6.6

* $\delta^{26}\text{Mg}$ is in permil.[†]Errors less than 0.1 are not shown.

Table 4.5 (Continued)

Phase	$\delta^{26}\text{Mg}^*$ $\pm 2\sigma_m$	$(^{27}\text{Al}/^{24}\text{Mg})$ $\pm 2\sigma_m$
GR4 (Type A)		
Melilite 1	3.4 ± 2.2	7.4 ± 0.04
Melilite 2	3.3 ± 1.8	6.1 ± 0.05
Melilite 3	7.3 ± 3.6	11.1 ± 0.15
Melilite 4	1.3 ± 3.3	8.8 ± 0.04
Melilite 5	3.4 ± 3.7	12.2 ± 0.04
Melilite 6	2.0 ± 3.4	12.1 ± 0.13
Melilite 7	-0.9 ± 2.6	5.0 ± 0.13
Melilite 8	2.0 ± 3.8	27.5 ± 0.40
Melilite 9	0.3 ± 2.9	10.9 ± 0.05
Melilite 10	3.0 ± 2.9	14.6 ± 0.60
Spinel 1	3.2 ± 2.4	2.5 ± 0.003
GR7 (Type B)		
Melilite 1	0.36 ± 1.54	1.44 ± 0.006
Melilite 2	4.32 ± 2.32	1.92 ± 0.012
Melilite 3	1.94 ± 2.08	3.55 ± 0.013
Melilite 4	3.98 ± 2.26	4.16 ± 0.033
Melilite 5	2.51 ± 3.02	3.35 ± 0.008
Melilite 6	-0.85 ± 1.99	3.21 ± 0.007
Melilite 7	1.45 ± 2.54	9.44 ± 0.398
Melilite 8	2.38 ± 1.80	5.44 ± 0.027
Melilite 9	4.51 ± 2.56	15.31 ± 0.51
Melilite 10	3.88 ± 2.14	13.76 ± 0.61
GR2 (Type C)		
Anorthite 1	12.6 ± 4.7	360.1 ± 30.1
Anorthite 2	8.3 ± 2.4	354.8 ± 11.0
Anorthite 3	6.7 ± 5.1	317.1 ± 2.6
Anorthite 4	8.4 ± 4.7	321.5 ± 3.5
Anorthite 5	8.8 ± 5.1	647.4 ± 64.1
Anorthite 6	7.6 ± 0.7	318.7 ± 2.08
Fassaite 1	0.1 ± 2.3	2.0 ± 0.003
Fassaite 2	0.6 ± 2.1	0.8 ± 0.001
Fassaite 3	0.1 ± 2.3	0.7 ± 0.001
Fassaite 4	1.0 ± 2.8	2.1 ± 0.004
Fassaite 5	2.2 ± 3.0	7.2 ± 0.004
Fassaite 6	0.4 ± 1.7	2.0 ± 0.002

 $\delta^{26}\text{Mg}$ is in permil

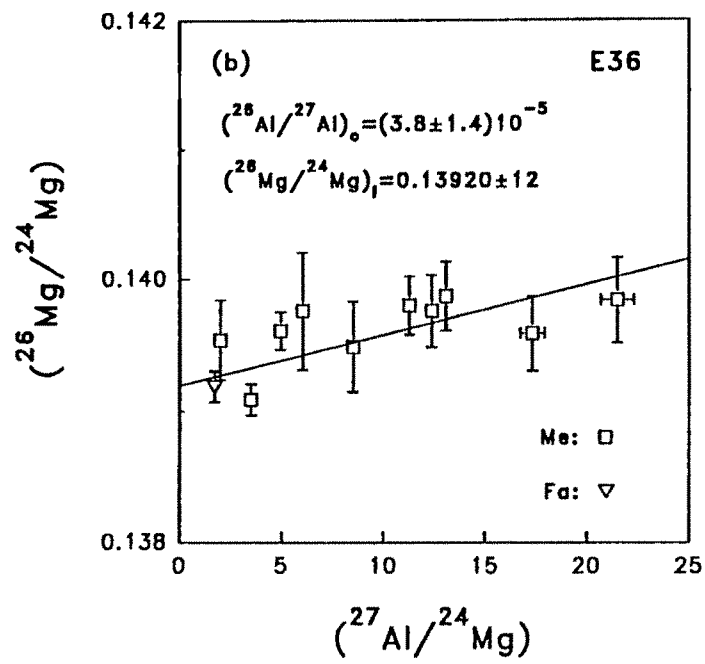
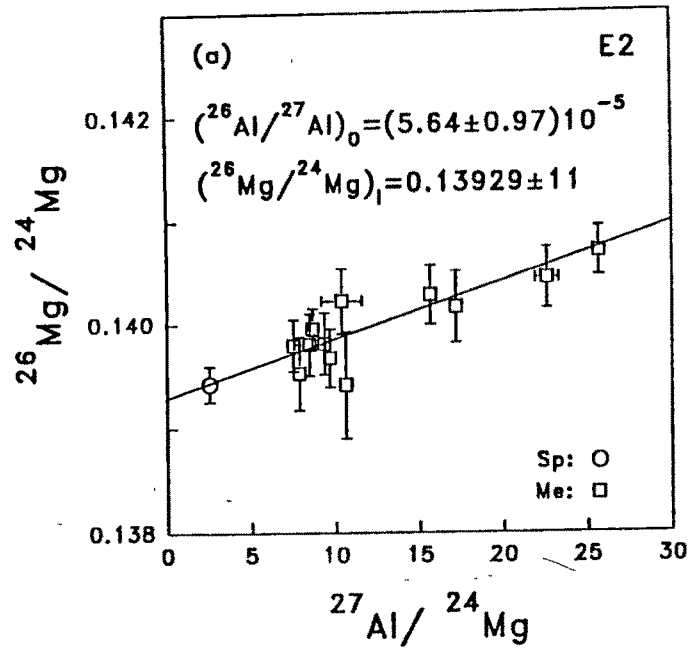


Fig.4.1

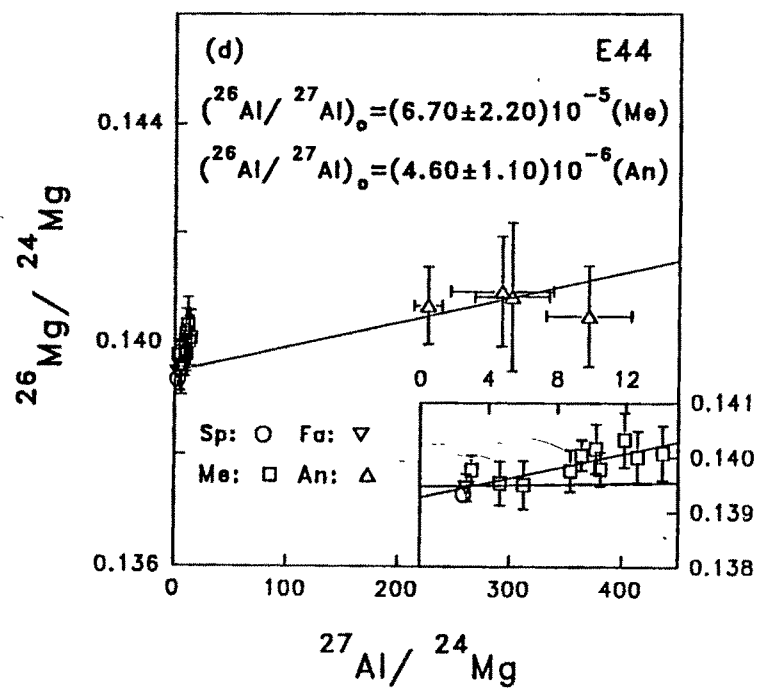
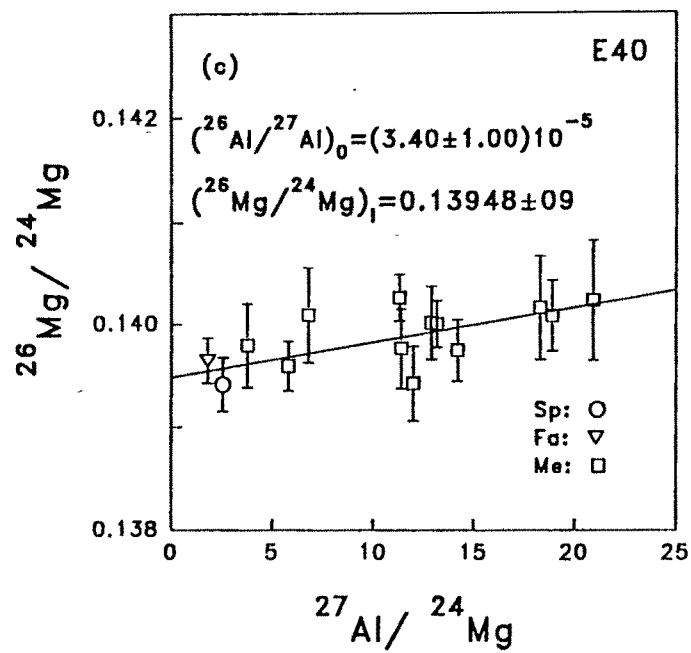


Fig.4.1 (Continued)

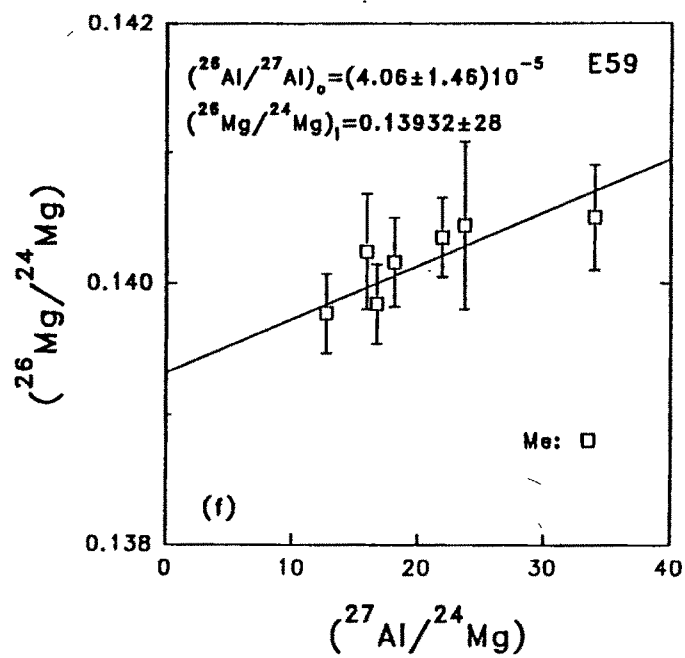
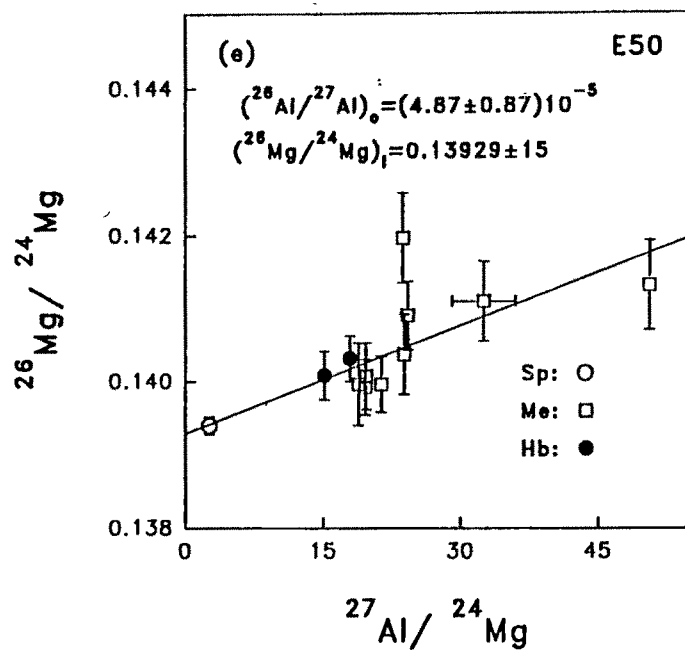


Fig.4.1 (Continued)

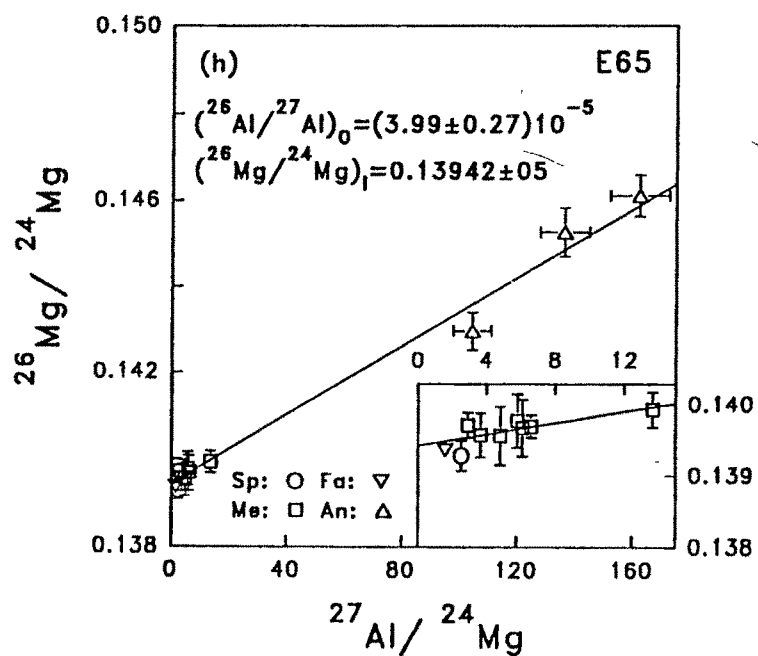
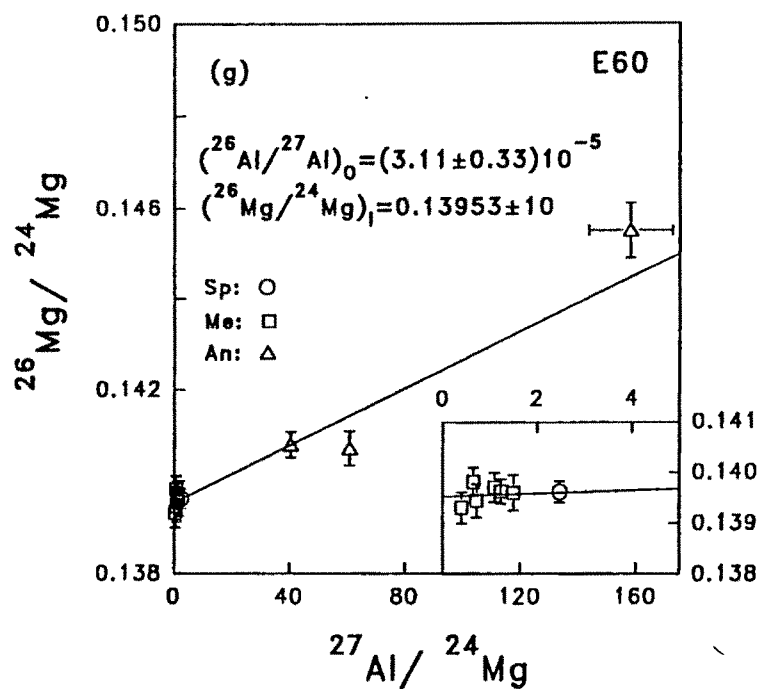


Fig.4.1 (Continued)

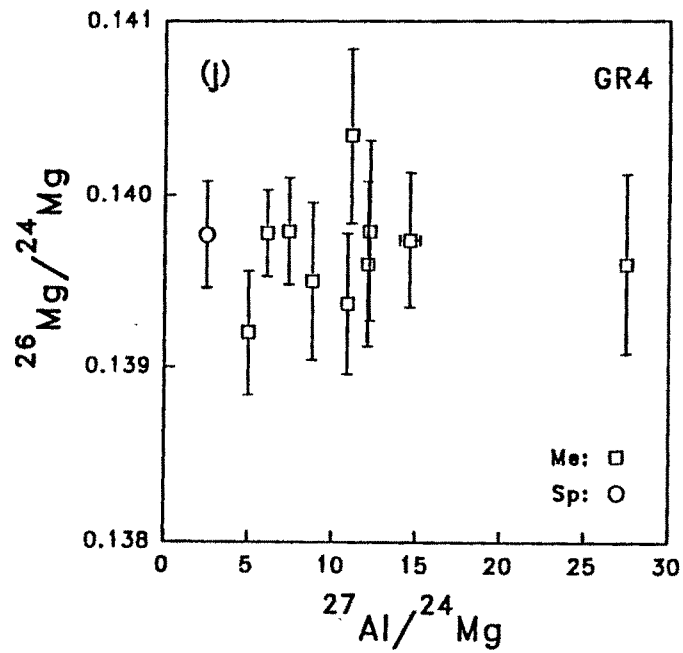
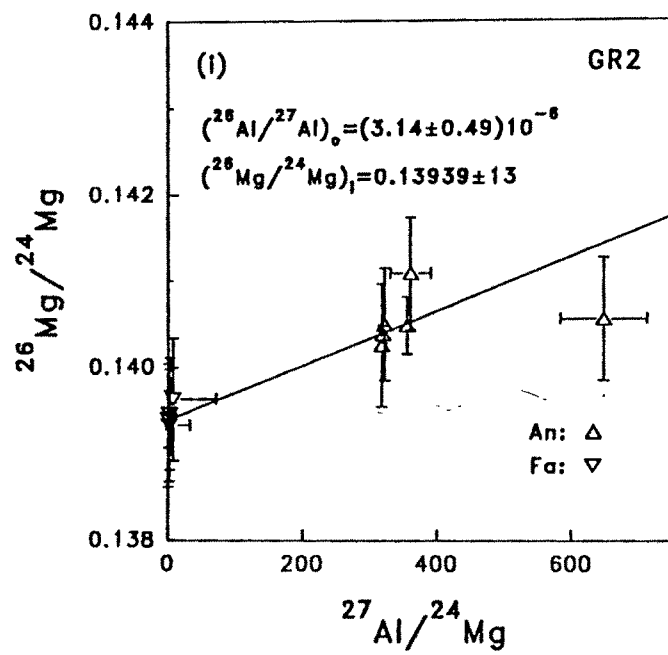


Fig.4.1 (Continued)

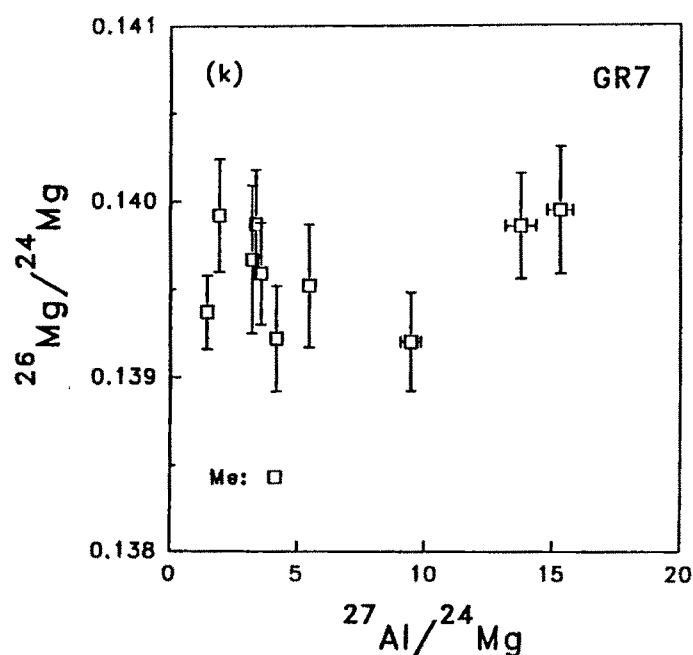


Figure 4.1: Mg-Al evolution diagram for the Efremovka CAIs E2 (type A), E36 (type B2), E40 (type B1), E44 (type B1), E50 (hibonite-rich), E59 (type A), E60 (type B2), E65 (type B1) and the Grosnaja CAI GR2 (type C), are shown in figures (a) to (i) respectively. In the case of Grosnaja CAIs GR4 (type A) and GR7 (type B) only the data have been plotted in fig(j) and fig(k) respectively. The abbreviation used for the different mineral phases that have been indicated in the figures are: Sp= spinel, Me=melilite, Fa=fassaite, An=anorthite, and Hb=hibonite. The initial $^{26}\text{Mg}/^{24}\text{Mg}$ and $^{26}\text{Al}/^{27}\text{Al}$ values for individual CAIs are also given in each figure. The two isochrons for E44 are drawn through melilite and anorthite data points assuming fassaites and spinels as common members in each case. Errors are $2\sigma_m$.

4.2 Results from K-Ca Isotopic Studies

Several of the Efremovka CAIs have been analyzed for their potassium and calcium isotopic composition with a view to look for the possible presence of the short-lived radionuclide ^{41}Ca at the time of formation of the CAIs. Previous attempts in this direction (Stegmann and Specht 1983) were not successful but there was a hint in the data of Hutcheon et al. (1984) for the presence of ^{41}Ca in the early solar system. We shall discuss some of the difficulties in carrying out such studies before presenting the results.

The short-lived radionuclide ^{41}Ca ($t_{1/2} \sim 0.1\text{Ma}$) decays to ^{41}K . If ^{41}Ca was present in the early solar system and was incorporated live into the CAIs at the time of their formation then we would observe an excess in the measured $^{41}\text{K}/^{39}\text{K}$ values in them, above the reference value of 0.072, and the measured $^{41}\text{K}/^{39}\text{K}$ will have two components :

$$\begin{aligned} \left(\frac{^{41}\text{K}}{^{39}\text{K}}\right)_m &= \left(\frac{^{41}\text{K}}{^{39}\text{K}}\right)_i + \left(\frac{^{41}\text{K}^*}{^{39}\text{K}}\right) \\ &= \left(\frac{^{41}\text{K}}{^{39}\text{K}}\right)_i + \left(\frac{^{41}\text{Ca}}{^{40}\text{Ca}}\right)_i \left(\frac{^{40}\text{Ca}}{^{39}\text{K}}\right)_m \end{aligned} \quad (4.2)$$

where i represents the initial ratio, m refers to the measured ratio and * represents the radiogenic component. As in the case of Mg-Al system, and the above relation (Eq. 4.2) represents the evolution of K-Ca isotopic system in the CAI. The intercept and slope of the best-fit line represented by (Eq.4.2) gives the initial $^{41}\text{K}/^{39}\text{K}$ and $^{41}\text{Ca}/^{40}\text{Ca}$ values at the time of closure of the K-Ca isotope system in the CAI. When Ca is present it is not possible to resolve ^{40}K from ^{40}Ca interference. Thus, although potassium consists of three isotopes (39, 40 and 41) it has to be treated as a two isotope system. *Therefore unlike the case of magnesium, it is not possible to determine the fractionation corrected residual for ^{41}K (i.e. $\delta^{41}\text{K}$).* The normal K isotopic composition measured for terrestrial minerals with Ca/K ratios ranging from 10^{-3} to $\sim 3 \times 10^6$ (Tables 2.5 and 4.6) suggest that the isotopic mass fractionation in the case of potassium isotopes must be small (\leq a few permil/amu). It

may be noted that instrumental mass fractionation generally favours the lighter isotopes and as such it will tend to suppress the signal at ^{41}K relative to ^{39}K . On the other hand, since the coarse-grained CAIs are derived from evaporative residues, one may expect an enrichment of the heavy isotopes (^{41}K relative to ^{39}K). However, in general the magnitude of instrumental mass fractionation far exceed intrinsic mass fractionation and we have neglected any possible effect of isotopic mass fractionation in analyzing the K isotopic data.

The isotopic analyses were carried out by cycling the magnet through the masses ^{39}K , ^{41}K , ^{40}CaH , ^{42}Ca , [$^{43}\text{Ca} - \Delta\text{M}$; $\Delta\text{M} = (43/41)(^{40}\text{CaH} - ^{41}\text{K})$], and ^{43}Ca . Each individual analysis consisted of 10-12 blocks of 5-6 cycles each. Ions from a restricted area of the sample surface (10 μm) were accepted during isotopic analysis by limiting the size of the field aperture to avoid contributions from the neighbouring phases and possible surface contamination from outside the sputtered spot. Proper care was taken during sample preparation to remove any K deposited on the sample surface while polishing. This was achieved by slowly heating the epoxy mounted samples in ultra-pure water (filtered through MilliporeTM Milli-Q Plus system) for a period of one to two hours. A pre-burn of the sample surface was conducted for ~ 30 minutes so that Ca/K reaches a steady value. Hibonite, perovskite and pyroxene with high Ca and low K content are ideally suited for K isotopic studies, while melilite and anorthite have Ca/K values $< 10^5$ and are found to be unsuitable for such studies.

Perovskites in E50, and pyroxenes in E65 and E44 were analyzed for their potassium and calcium isotopic composition. E50 and E65 have well behaved Mg-Al systematics with initial $^{26}\text{Al}/^{27}\text{Al}$ close to the canonical value of 5×10^{-5} . Even though the disturbed Mg-Al isotopic systematics in E44 suggest Mg exchange between melilite and anorthite in this CAI, the pyroxenes appear to be undisturbed with no petrographic evidence of secondary alteration. The results obtained in the present study are given in Table 4.6. The $^{40}\text{Ca}/^{39}\text{K}$ values were computed by using the measured ion ratios and the relative yield factor of 3.2 (Table 2.4, Chapter2) favouring K. The perovskite grains from E50 have lower Ca/K values compared to the terrestrial perovskite. This is probably because of contribution

from neighbouring melilite. Analyses of hibonite grains from E50 were not attempted for similar reasons. The $^{41}\text{K}/^{39}\text{K}$ values (Table 4.6) have been corrected for contribution to the ^{41}K signal from i) unresolvable ($^{40}\text{Ca}^{42}\text{Ca}$)⁺⁺ interference, and ii) contribution from the tail of the ^{40}CaH peak (see section 2.3.3, Chapter2). The typical signal at mass ^{41}K ranges from 0.3-0.8(c/s). The hydride contribution estimated from the count rate at ($^{43}\text{Ca} - \Delta\text{M}$) was found to be very small and in general it was less than the counting system background. The ($^{40}\text{Ca}^{42}\text{Ca}$)⁺⁺ correction is proportional to the measured ($^{40}\text{Ca}^+ / ^{39}\text{K}^+$) value in the sample and the magnitude of this correction ranges from a few percent to $\sim 70\%$ of the measured ($^{41}\text{K}^+ / ^{39}\text{K}^+$) values.

It can be seen from Fig.5.7 that the meteoritic phases with high Ca/K ($\geq 3 \times 10^5$) show clear evidence of excess ^{41}K ; with the measured $^{41}\text{K}/^{39}\text{K}$ values much above the reference value of 0.072. The large errors in the $^{41}\text{K}/^{39}\text{K}$ ratios are due to poor counting statistics at mass 41 and sometimes at mass 39 which are typically of the order of $\leq 4\%$ (at 1σ level), and the error associated with doubly charged calcium interference (see Table 4.6 footnote). The excess signal at mass 41, after all the corrections, ranges from 0.05 to 0.12(c/s), which is much above the dynamic background of the counting system, ≤ 0.01 (c/s). This excess accounts for ~ 10 -25% of the measured count rates at this mass. The slope of the best fit correlation line between $^{41}\text{K}/^{39}\text{K}$ and $^{40}\text{Ca}/^{39}\text{K}$ is $(1.6 \pm 0.3) \times 10^{-8}$ which represents the value of initial ($^{41}\text{Ca}/^{40}\text{Ca}$) at the time of formation of Efremovka CAIs. The intercept has a value (0.07134 ± 0.00085) which is close to the reference value of 0.072. We shall consider the plausible causes for excess ^{41}K in Efremovka CAIs and its implications towards early solar system processes in the next chapter.

Table 4.6: K-Ca Data

Sample	$^{40}\text{Ca}/^{39}\text{K}^\dagger$ $\pm 2\sigma_m$	$^{41}\text{K}/^{39}\text{K}^\dagger$ $\pm 2\sigma_m$
Terrestrial Minerals		
Microcline*	$\sim 10^{-3}$	0.07187 ± 0.0001
Anorthositic Glass ** (An-Mg-5)	8.6×10^3	0.07107 ± 0.0013
Pyroxene 1** (Ti-PX-1)	2.1×10^4	0.07301 ± 0.0012
Pyroxene 2** (CAI-PX-1)	3×10^6	0.06999 ± 0.0064
Perovskite [®]	$\sim 4 \times 10^6$	0.06475 ± 0.0091
Efremovka CAIs		
E50		
Perovskite 1	$(1.69 \pm 0.01) \times 10^5$	0.07476 ± 0.0022
Perovskite 2	$(5.95 \pm 0.01) \times 10^4$	0.06992 ± 0.0020
Perovskite 3	$(1.36 \pm 0.01) \times 10^5$	0.07365 ± 0.0020
E65		
Pyroxene 1	$(7.30 \pm 0.81) \times 10^4$	0.07399 ± 0.0017
Pyroxene 2	$(2.67 \pm 0.29) \times 10^5$	0.07782 ± 0.0044
Pyroxene 3	$(5.87 \pm 0.85) \times 10^4$	0.07176 ± 0.0018
Pyroxene 4	$(9.73 \pm 1.33) \times 10^4$	0.07122 ± 0.0020
Pyroxene 5	$(1.75 \pm 0.28) \times 10^5$	0.07441 ± 0.0028
Pyroxene 6	$(1.52 \pm 0.42) \times 10^5$	0.07646 ± 0.0039
Pyroxene 7	$(9.34 \pm 0.54) \times 10^5$	0.08390 ± 0.0085
Pyroxene 8	$(9.87 \pm 0.95) \times 10^5$	0.09311 ± 0.0107
Pyroxene 9	$(5.94 \pm 0.66) \times 10^5$	0.08303 ± 0.0088
Pyroxene 10	$(1.28 \pm 0.06) \times 10^6$	0.09738 ± 0.0100
Pyroxene 11	$(3.55 \pm 0.30) \times 10^6$	0.08934 ± 0.0426
Pyroxene 12	$(2.18 \pm 0.11) \times 10^6$	0.09851 ± 0.0218
Pyroxene 13	$(1.15 \pm 0.07) \times 10^6$	0.08862 ± 0.0131
Pyroxene 14	$(1.05 \pm 0.08) \times 10^6$	0.08874 ± 0.0081
Pyroxene 15	$(8.92 \pm 0.62) \times 10^6$	0.13293 ± 0.0628
Pyroxene 16	$(2.68 \pm 0.39) \times 10^7$	0.48472 ± 0.3050
E44		
Pyroxene 1	$(2.84 \pm 0.39) \times 10^6$	0.15437 ± 0.0398
Pyroxene 2	$(2.44 \pm 0.14) \times 10^6$	0.13015 ± 0.0103

Table 4.6(Continued)

* US National Museum Standard (USNM 143966).

**Samples prepared at Caltech (Courtesy I. Hutcheon).

@Sample obtained from Vernadsky Institute, Moscow.

†The ($^{40}\text{Ca}/^{39}\text{K}$) values for *terrestrial perovskite and meteoritic phases* were obtained from ion microprobe data using an ion yield of 3.2, favouring K over Ca during sputtering. The yield factor is based on terrestrial pyroxene with high Ca/K.

‡Values are corrected for ($^{40}\text{Ca}^{42}\text{Ca}$)⁺⁺ interference. The value for [$^{40}\text{Ca}^{43}\text{Ca}$]⁺⁺/ $^{43}\text{Ca}^+$ ratio for pyroxene and perovskite are $(2.64 \pm 0.09) \times 10^{-5}$ and $(2.79 \pm 0.04) \times 10^{-5}$ respectively. The magnitude of ($^{40}\text{Ca}^{42}\text{Ca}$)⁺⁺ correction is given by:

$$[\text{Ca}^{43}\text{Ca}]^{++}/^{43}\text{Ca}^+ \times (^{42}\text{Ca}^+ / ^{40}\text{Ca}^+) \times (^{40}\text{Ca}^+ / ^{39}\text{K}^+)$$

where ($^{40}\text{Ca}^+ / ^{42}\text{Ca}^+$) = 151.02

Chapter 5

Discussion

In this chapter we consider the results obtained from isotopic studies of CAIs from the Efremovka and Grosnaja meteorites along with other available data from these CAIs to understand the processes leading to their formation, as well as time scales for certain early solar system processes and solar-stellar relationship. The primary emphasis during isotopic analyses of CAIs was to look for possible departures in the measured isotopic ratios from the normal solar system (reference) values. Such departures, if present, can serve as extremely useful tracers to probe the above aspects.

The discussion presented in this chapter is divided into five subsections.

- (i) Processes affecting the formation of CAIs,
- (ii) Relict spinels and nebular environment for the formation of CAIs,
- (iii) Mg-Al isotopic systematics and isotopic heterogeneity in the nebula,
- (iv) ^{41}Ca in the early solar system,
- (v) Extinct radionuclides and time scales for early solar system processes.

5.1 Processes Affecting the Formation of CAIs

Studies of isotope mass fractionation in CAIs allows one to delineate the nature of their source material and the principle processes leading to their formation. For example, positive mass fractionation in magnesium isotopes [$F(\text{Mg}) > 0$] would imply evaporative residue as the source material for CAIs as such residues are expected to be enriched in heavy isotopes. Conversely, mass fractionation favouring the lighter isotopes [$F(\text{Mg}) < 0$] in CAI would suggest their formation by condensation from a gas depleted in heavy isotopes.

Both melilite and spinel phases in the Efremovka coarse-grained CAIs analyzed in this work are generally enriched in their heavy isotopes i.e. $F(\text{Mg}) > 0$ (see Tables 4.1-4.4; Fig. 5.1). Even though there is an apparent trend for a higher $F(\text{Mg})$ value for spinel compared to melilite (e.g. E65, E44), we do not consider this difference to be significant in view of the measurement uncertainties in $F(\text{Mg})$ [typically $\sim 1.5\%/amu$ ($2\sigma_m$)]. Positive mass fractionation is clearly evident in five (E36, E44, E50, E59, E65) of the CAIs analyzed. In the case of E2 and E40, $F(\text{Mg})$ values for melilite and spinel show certain systematic spatial variation. In E2 a few data points for rim spinel and near-rim phases do show $F(\text{Mg}) \leq 0$, however, the $F(\text{Mg})$ values for melilite in the inclusion interior are positive. In the case of E40, the interior melilites have near normal or slightly above normal Mg isotopic composition, but the values are much higher for melilites and spinels near the rim as well as many spinel grains in the interior. The $F(\text{Mg})$ values in the multizoned hibonite-rich inclusion E50 show non-systematic spatial variations, but both melilite and spinel are generally enriched in the heavier isotopes: the $F(\text{Mg})$ values in the melilite-perovskite zone are near normal, in the melilite-spinel zone both melilite and spinel have high $F(\text{Mg})$ values, and in the inclusion interior, melilite in both the hibonite-rich zone and in areas where it is in association with perovskite have $F(\text{Mg}) \geq 0$. Although the values for the type B2 inclusion E60 are near normal, there is a hint in the data for a positive $F(\text{Mg})$ value. The general trend for positive $F(\text{Mg})$ values for the Efremovka coarse-grained CAIs suggest evaporative residue as the source material for these objects. This is in accord with what one generally expects for coarse-grained refractory inclusions based on earlier work on CAIs

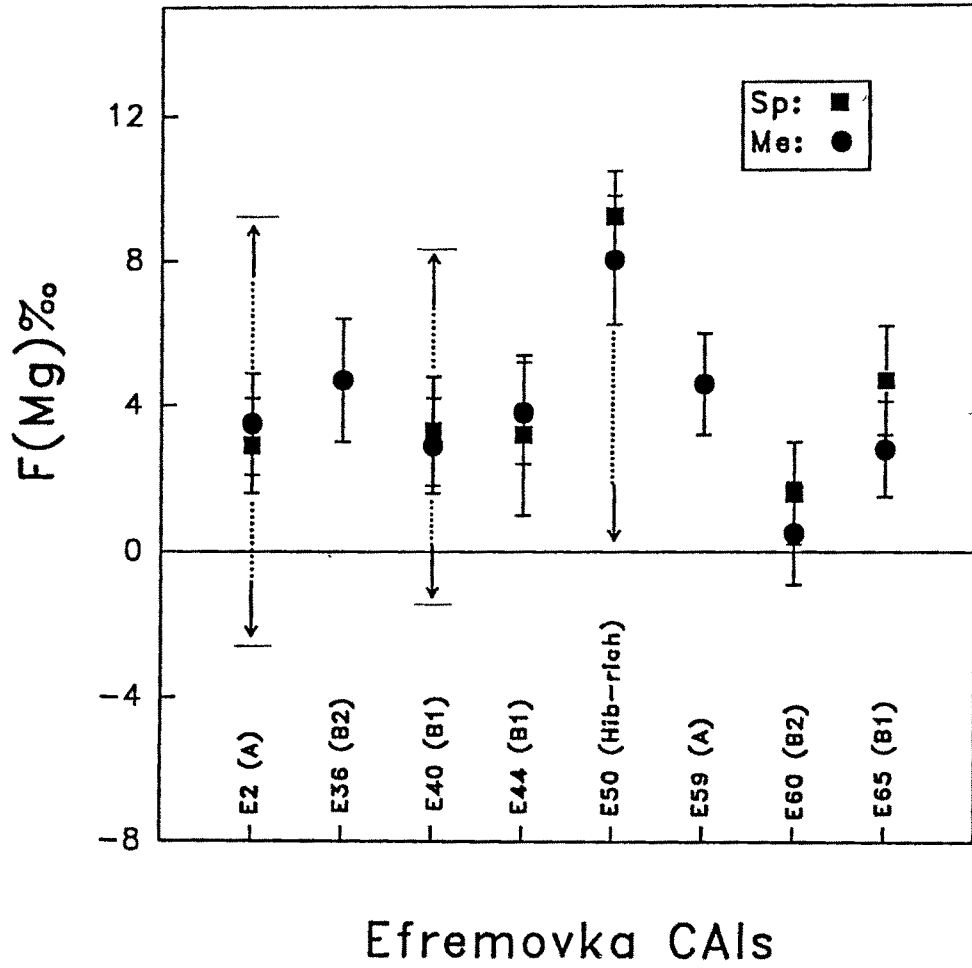


Figure 5.1: The intrinsic mass fractionation $F(\text{Mg})$ in the melilite (Me) and spinel (Sp) phases of the Efremovka CAIs analyzed in this study are shown. In the case of E2, E40, and E50 the range of $F(\text{Mg})$ values is indicated by the arrow marks. Note that within experimental uncertainty melilite and spinel have similar $F(\text{Mg})$ values. In the case of E36 and E59 $F(\text{Mg})$ values were measured only for melilite.

from other meteorites (Esat and Taylor, 1984; Clayton et al., 1988; MacPherson et al., 1988). There is no hint in the data for extreme magnesium isotope mass fractionation, and none of the Efremovka inclusions studied in this work can be classified as so called FUN inclusion, characterized by high $F(\text{Mg})$ values, typically $>10\%$ (Wasserburg et al. 1977, Brigham 1990).

The results obtained for the spatial variation in $F(\text{Mg})$ in the Efremovka CAIs (Tables 4.1 and 4.4) suggest a significant and systematic difference in $F(\text{Mg})$ values between peripheral and interior phases only in E2 and E40.

The spatial variation in $F(\text{Mg})$ for these two CAIs [E2 and E40] showed extremely contrasting trends (Figs. 5.2-5.3). Such trends could result from either isotopic exchange between distinct reservoirs or specific process(es) affecting these inclusions during their formation and evolution. The $F(\text{Mg})$ trend seen by us in E2, where $F(\text{Mg})$ value increases from the near rim region to the inclusion interior agree with the results reported previously by Fahey et al. (1987b). The observed variation cannot be produced by an external thermal event affecting this inclusion during its formation. Fahey et al. (1987b) suggested that the $F(\text{Mg})$ trend seen in E2 can be approximated by a diffusion profile although the exact nature of the process leading to the observed trend cannot be determined. Diffusional exchange of magnesium between an isotopically normal and an isotopically heavy reservoir, the latter representing the parent material of E2, could be one of the possible mechanisms that can be proposed to explain the fractionation trend seen in this inclusion.

In contrast to E2, the fractionation trend in E40 (Fig. 5.3), with higher $F(\text{Mg})$ values for melilite near the inclusion boundary compared to that in the inclusion interior, is unique in the sense that this trend is seen for the first time in a normal (non-FUN) refractory inclusion. Before attempting to explain this trend in terms of physical processes affecting this inclusion, we note that the melilite near the rim of E40 is gehlenitic (high Al/Mg ; more refractory) and it is akermanitic (low Al/Mg ; less refractory) in the interior (Fig. 5.3). We now consider several plausible scenarios that can explain either or both the isotopic and petrographic data. These include:

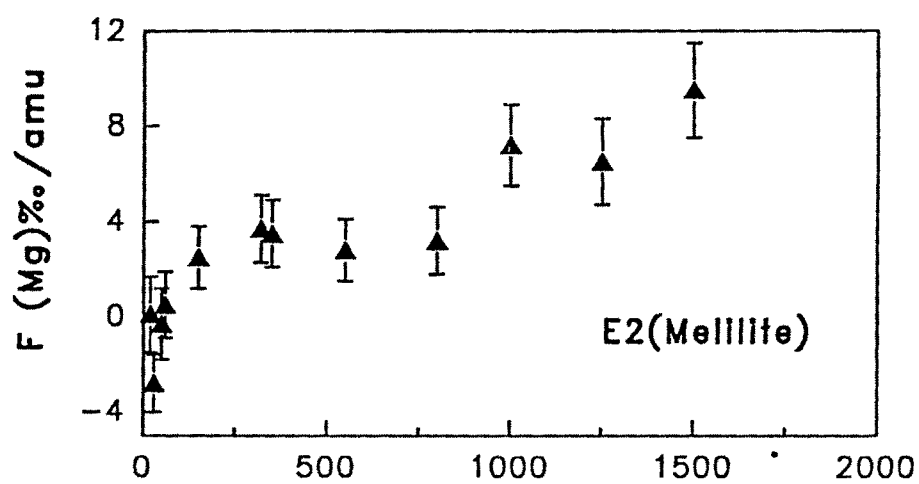


Figure 5.2: Magnesium isotopic mass fractionation in melilite from compact type A Efremovka CAI E2. $F(\text{Mg})$ values have been plotted as function of distance from the inner edge of the rim.

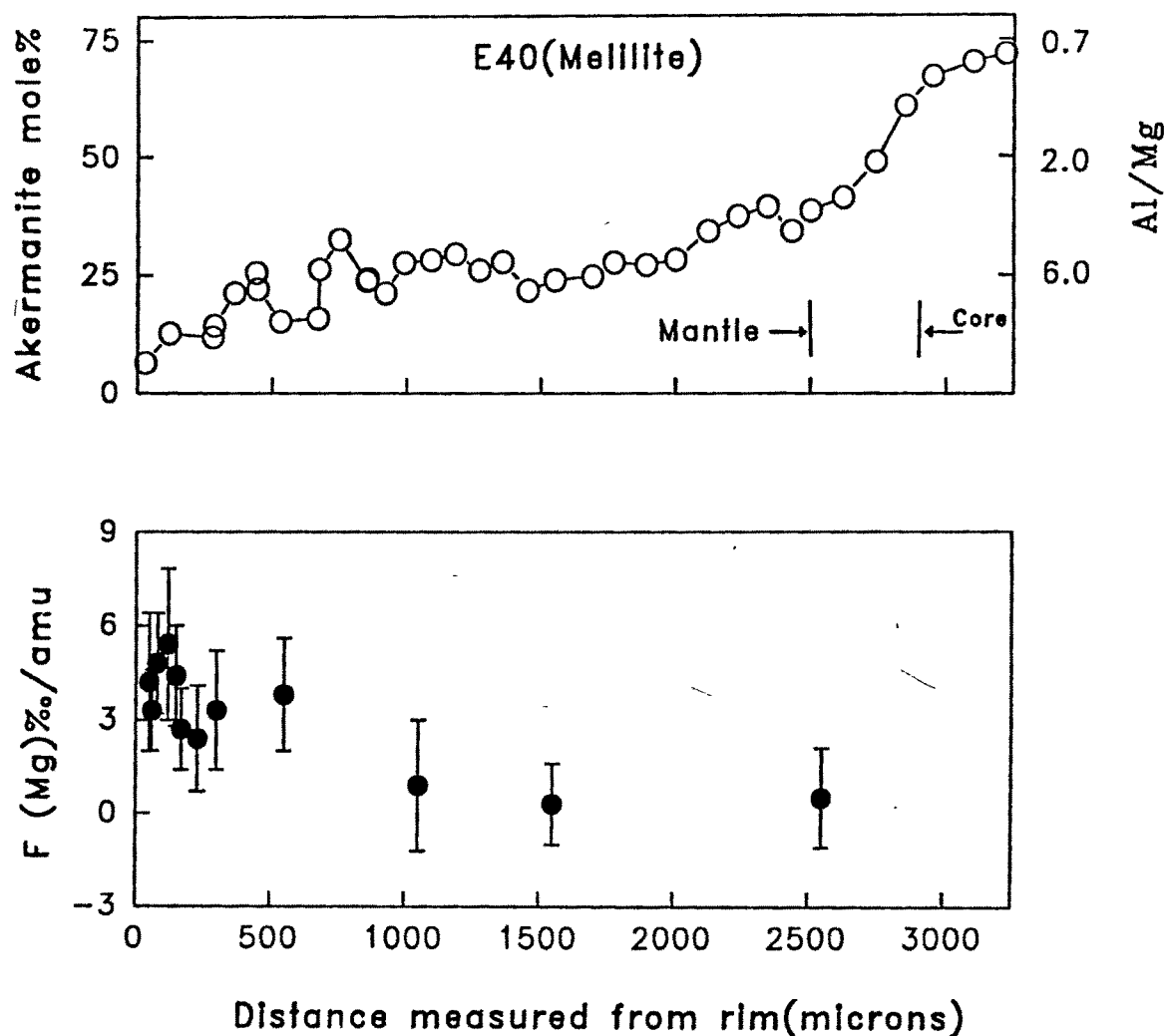


Figure 5.3: Electron probe data for akermanite content in melilite along a nearly radial traverse in type B1 Efremovka CAI E40. Ion microprobe data for magnesium isotopic mass fractionation in melilite close to this traverse is also shown. The akermanite content and F(Mg) values show an inverse correlation. The approximate extent of the mantle melilite and the beginning of the core region are indicated.

- (i) isotopic exchange between parent melt of E40 and an external reservoir of appropriate composition,
- (ii) evaporation of Mg from E40 following its crystallization,
- (iii) evaporation of Mg from the parent melt of E40 prior to its crystallization.

If the trend is due to isotopic exchange, we need a positively fractionated external reservoir with $F(\text{Mg}) \geq 4\text{-}6\text{‰}$ exchanging magnesium isotopes with a reservoir of normal isotopic composition, representing the parent material of E40. Even though a positively fractionated external magnesium isotopic reservoir is a difficult proposition, we cannot completely rule out such a scenario. Alternatively, one can also postulate that E40 evolved from a melt characterized by high $F(\text{Mg})$ that reequilibrated with an isotopically normal reservoir following the crystallization of melilite and spinel near the inclusion boundary. However, such a scenario appears ad-hoc as melilite crystallization in CAIs is a very quick processes (Wark and Lovering 1982, Stolper and Paque 1986), and there may not be enough time for reequilibration following the crystallization of melilite near the boundary, and prior to crystallization of melilite in the interior.

If the observed fractionation trend in E40 is due to a thermal event, e.g. processes (ii) or (iii) above, we need a heating episode during the formation of this inclusion that resulted in loss of magnesium from its boundary region. The most obvious process that could be responsible for this is a volatilization event affecting this inclusion. Since the petrographic features of E40, (the rounded shape, coarse grained texture and mineralogy) suggest its formation via melt crystallization, the volatilization event could have affected either the parent melt of E40 or the inclusion proper following its crystallization. However, experimental studies have shown that evaporation from solid can lead to positive mass fractionation in Mg isotopes only within the first few tens of micron of the surface (Wang et al. 1991). The observed fractionation effect in E40 (high $F(\text{Mg})$ values), on the other hand, persists up to a few hundred microns from the inclusion boundary. Therefore, evaporation from solid as a cause for the observed fractionation trend in E40 may be ruled out.

Finally, if we consider evaporation from the parent melt of E40, the observed increase in $F(\text{Mg})$ values near the surface as well as the lower akermanitic content ($\text{\AA k}10\text{-}15$) in this region, can be explained by considering a loss of $\leq 25\%$ Mg from a melt with a composition similar to the mantle region of E40 [$\text{\AA k}(25\text{-}35)\%$]. This follows from the experimental data obtained by Davis et al. (1990) who have measured the magnitude of isotopic fractionation in O, Mg and Si during evaporation of a melt of forsteritic composition. We would like to note that fractional crystallization from the parent melt of E40 could have led to the observed range of melilite composition in this inclusion. Therefore, it is *a priori* not necessary to invoke volatilization loss to explain the variation in the melilite composition near the boundary region of this inclusion. However, it is interesting to note that the proposed volatilization event with a loss of $\leq 25\%$ Mg from the boundary region can in fact lead to the progressive decrease of the Akermanitic content in the near rim region (Fig. 5.3) if the initial composition was similar to that of the mantle ($\text{\AA k}25\text{-}30\%$). The volatilization event leading to the observed magnesium isotope mass fractionation trend in E40 should also result in correlated oxygen and silicon isotope mass fractionations (Davis et al. 1990). The expected O and Si isotope mass fractionations are $\leq 4\text{\textperthousand}/\text{amu}$ and $\leq 2.5\text{\textperthousand}/\text{amu}$ respectively. Unfortunately, there are experimental difficulties in the measurement of oxygen isotopic ratios of insulating solids by the ion microprobe, and high instrumental mass fractionation for silicon in melilite ($\sim 50\text{\textperthousand}/\text{amu}$) does not allow for a precise determination of the variation of $F(\text{Si})$ in E40 melilite. The absence of Ca-aluminate in E40, which is expected during intense evaporation of melilite [$\text{\AA k}(50)$] (Hashimoto, 1991), qualitatively suggests that the degree of evaporation in E40 was not extremely intense. There are however other Efremovka CAIs (e.g., E66a) where an association of gehlenite, perovskite, and Ca-aluminates is seen in their boundary regions. This perhaps resulted from a more intense evaporation process than in the case of E40. Since the proposed volatilization event affecting the parent melt of E40 can explain both the isotopic and compositional variation in melilite, we consider this to be a more plausible process compared to the isotopic exchange scenarios discussed earlier.

It is difficult to establish whether the proposed volatilization event was itself responsible for the formation of E40 or whether it was a secondary event that affected the parent

melt of E40 produced in a separate thermal event. However, the duration of the volatilization event has to be necessarily short so that the compositional gradient generated by it is not obliterated by melt diffusion. Clayton et al. (1984) and Davis et al. (1991) have proposed similar scenarios for explaining the nearly sympathetic petrographic and isotopic data for two forsterite-bearing FUN inclusions. *Although possible correlation between isotopic and petrographic data in CAIs have been conjectured before this is the first instance in which sympathetic behaviour has been seen in a normal (non-FUN) refractory inclusion.* This observation substantiates the role of volatilization and melt crystallization as important CAI forming processes.

5.2 Relict Spinel and Nebular Environment for the Formation of CAIs

The CAI E40 has texture and mineralogy that suggests its crystallization from a melt and the two dominant mineral phases in this inclusion, melilite and spinel, are expected to be in isotopic equilibrium. The spinels in this inclusion show some groupings in size; the spinels near the boundary are generally small (10-20 μ m) compared to those in the inclusion interior (\sim 20-60 μ m), and some spinels in the pyroxene rich core are close to 100 μ m in size (Fig. 5.4). The F(Mg) values for different spinel groups provided a surprise. We found that the spatial variation in F(Mg) for spinel is not exactly similar to melilite. This can be seen in Fig. 5.5 where we show the data for magnesium isotope mass fractionation in both melilite and spinel across a couple of nearly radial traverses in this inclusion. The F(Mg) values for spinels near the boundary are generally high and similar to the melilite values, whereas the spinels in the inclusion interior show a spread in their F(Mg) values in contrast to melilite, whose F(Mg) values suggest near normal magnesium isotopic composition. The basic results that are evident in the data shown in Fig. 5.5 are:

- (i) small and medium sized spinels near the inclusion periphery have high F(Mg) that are similar and at times higher than melilite,

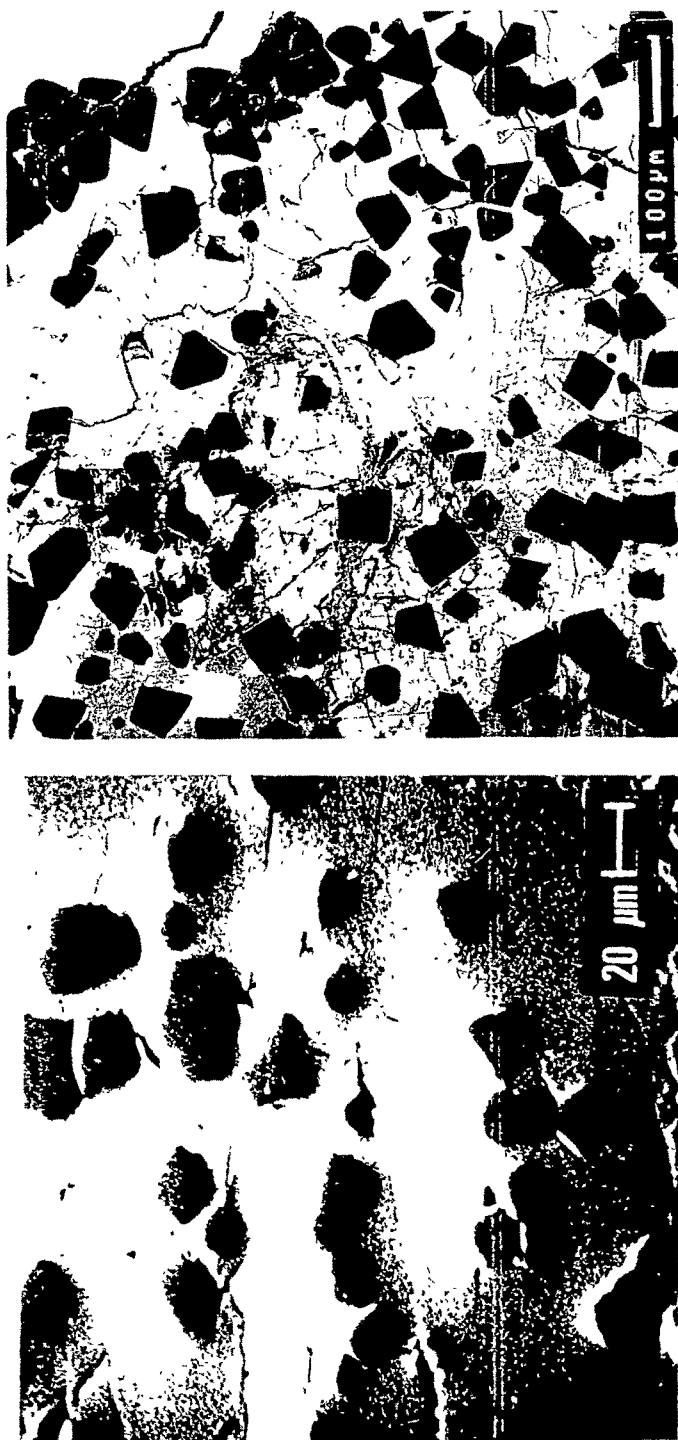


Figure 5.4: Photomicrographs of spinels from the boundary and interior regions of E40 showing clear size groupings. Scale bars are 20 and 100 μm respectively.

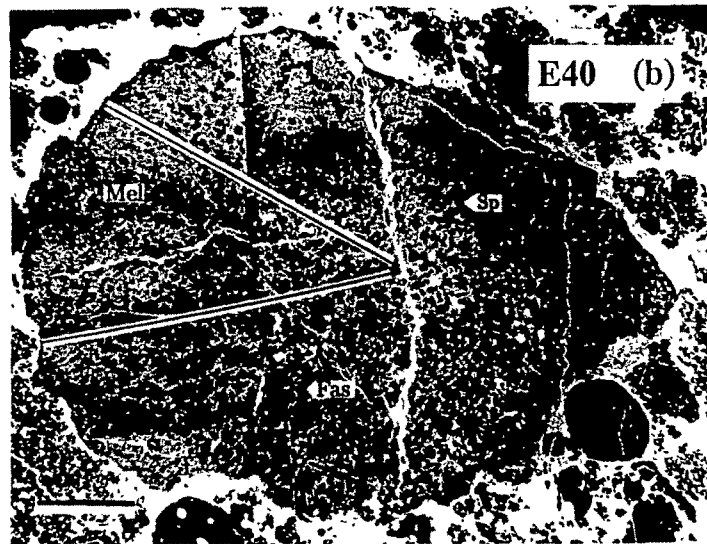
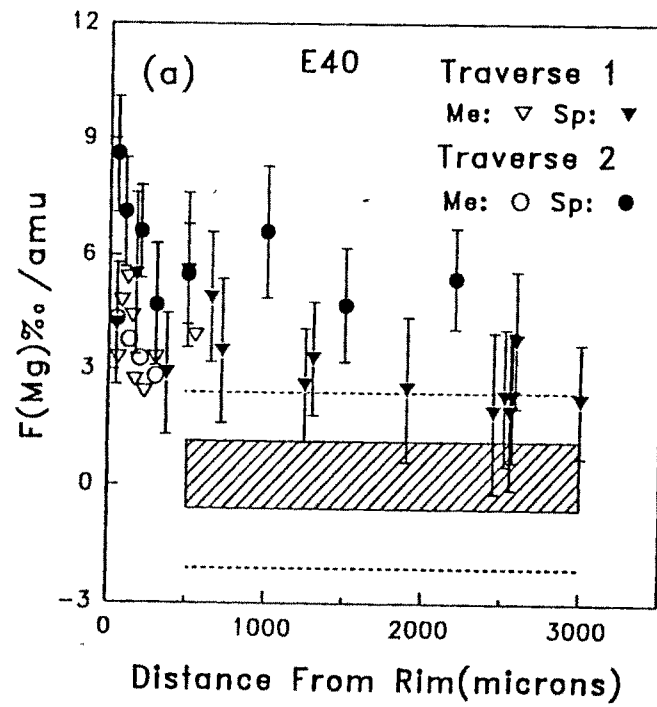


Figure 5.5: Magnesium isotopic mass fractionation in melilite and spinel (Fig.a) from Efremovka CAI E40 measured along two radial traverses (Fig.b). The measured range of melilite fractionation for the interior melilite ($\geq 500\mu\text{m}$) falls within the shaded area and the dotted line encompasses the extreme error limits of individual measurements in melilite.

- (ii) medium sized spinels in the inclusion interior have both low and high F(Mg) values; the lower F(Mg) values match those of melilite in the interior,
- (iii) large spinels in the core region have F(Mg) values similar to melilite in the interior.

The spinels with low F(Mg) in the inclusion interior may be considered to be in isotopic equilibrium with the melilite. However, the presence of spinels with F(Mg) values much greater than that for melilite in the inclusion interior was unexpected. One can consider two possible explanations for this observation:

- (i) movement of spinels with high F(Mg) values, initially present near the peripheral (near rim) region, into the inclusion interior during the crystallization of this CAI.
- (ii) the spinel grains with high F(Mg) are relict or extraneous to the inclusion.

We shall now consider these two possibilities. Laboratory based simulation experiments on the formation of CAIs similar to E40 (i.e. Type B1) were carried out by Wark and Lovering (1982). These experiments have led to the idea of movement of spinels from the periphery into the interior during crystallization of CAI resulting in spinel rich core, that are commonly observed in type B1 CAIs. In this scenario small spinel grains crystallize near the inclusion boundary about 20°C prior to melilite crystallization. However, once melilite starts crystallizing, they grow rapidly and push some of the spinel grains into the interior. These spinel grains continue to grow in the interior of the CAI and get trapped in late crystallizing phases. Since both melilite and spinel near the boundary of the inclusion E40 have high F(Mg), due to the volatilization event experienced by the parent melt of this CAI (Sec. 5.1), the presence of spinels with high F(Mg) values in the interior may be due to movement of boundary spinels as proposed by Wark and Lovering (1982). However, if this was the case, the small boundary spinels that were pushed into the interior would grow as they moved inward. Therefore, one would expect the spinel grains in the interior to have a core with high F(Mg) and a peripheral region with lower value of F(Mg) similar to that for melilite in the interior. However, we could not find such a difference in the F(Mg) values

for the edge and center of spinel grains in the interior, and such differences, if present, are definitely smaller than our measurement uncertainties ($\pm 1.5\text{‰}$ /amu). Therefore the spinel redistribution hypothesis can be ruled out as an explanation for the discordance in the isotopic data between melilite and spinel.

The other possibility that can readily explain the discordant F(Mg) data for spinel and melilite in E40 is that the spinels with distinctly different and high F(Mg) values compared to the melilite are extraneous to this inclusion and represent relict spinels. These spinels were present in the parent melt of E40 and retained their identity due to incomplete melting and lack of isotopic equilibration. We believe that some of the small and medium-sized spinels in the interior of E40 with F(Mg) values outside the melilite envelope are relict. Some of the small spinels near the boundary (e.g. first spinel data point) may also represent relict phases. It is difficult to make any specific comment about the relative abundance of relict spinels because of their random occurrence and possible sampling bias. While a good fraction of the small spinels could be relict, the fraction is much smaller for the medium sized spinels and none of the core spinels analyzed can be termed as relict. The relict spinels could have been present in the parent material of E40 or they were incorporated into the parent melt of E40 prior to its crystallization. In both the scenarios spinel grains can escape complete melting if the melt was spinel saturated (Ulyanov, 1991). The possible presence of relict phases in coarse-grained CAIs was suggested by Stolper (1982) and Stolper and Paque (1986) on the basis of results obtained from laboratory experiments aimed at understanding the crystallization sequence in these objects. Attempts to identify relict grains from studies of trace elements in coexisting mineral phases in CAIs have met only with limited success (e.g., Kuehner et al., 1989; Simon et al., 1991). Isotopic data, that are suggestive of the presence of relict phases in early solar system objects, are also rare and there are only a couple of observations that include those of Zinner et al. (1991), who argued for an extraneous origin of a magnesiowustite-metal fremdling in a CAI from Vigarano, and of Sheng et al. (1991a) who identified relict spinels in plagioclase-olivine-inclusions (POIs) from several carbonaceous chondrites. This study provides the first evidence for the presence of relict grain representing a major constituent phase of CAI. The implications

of the observation for the thermal evolutionary history of E40 in particular and CAIs in general are discussed below.

The observed isotopic disequilibrium between spinel and melilite in E40 suggest lack of isotopic exchange between the relict spinels and the parent melt of E40. This allows us to place limits on the cooling rate during crystallization of E40 if we have the following inputs:

- (i) Magnesium self diffusion constant in spinel in contact with Mg rich melt at high temperature,
- (ii) Initial temperature of the parent melt of type B1 CAIs to which E40 belongs.

Laboratory based simulation experiments have been conducted by Sheng et al. (1991b) to determine the Mg self diffusion constant in solid spinel in contact with a melt of composition similar to plagioclase-olivine inclusions. They observed that the self diffusion constant varies as a function of temperature and can be approximated by the Arrhenius Relation :

$$D = D_0 \exp(-E/RT) \quad (5.1)$$

where D is the diffusion constant, D_0 is the pre-exponential factor, R is the gas constant, T is the temperature and E is the activation energy. The values of D_0 for spinel and melt obtained by Sheng et al. (1991b) are 74.6 cm^2 and 7791 cm^2 respectively, while the activation energies (E) are $\sim 384 \text{ kJ}$ and $\sim 343 \text{ kJ}$ respectively. The initial melt temperature for type B1 CAI like E40 is expected to be between 1400°C to 1500°C . These values were inferred by Stolper and Paque (1986) who carried out simulation experiments designed to reproduce petrographic features of Type B inclusions starting with a melt of $\text{CaO-Al}_2\text{O}_3\text{-MgO-SiO}_2$ in appropriate proportions.

Based on these two sets of inputs viz. self diffusion constant of Mg in spinel and initial temperature of the parent melt of CAI like E40, one can obtain a relation between cooling

rate and spinel size demanding complete isotopic homogenization of the spinel with the melt. This relation given by Kaiser and Wasserburg (1983) can be written as:

$$(d/2)^2 = \frac{RT_o^2 D(T_o)}{r_o E} \quad (5.2)$$

where d is the minimum grain size (diameter) of spinel that will undergo isotopic homogenization with the melt, R is the gas constant, T_o is the initial temperature of the melt, $D(T_o)$ is the diffusion constant at the initial temperature, r_o is the cooling rate ($^{\circ}\text{C/hr}$) and E is the activation energy. Since the relict spinels in E40 are possibly present in two distinct size groups, we calculate cooling rates considering two limiting sizes of spinels $10\mu\text{m}$ and $60\mu\text{m}$. The calculated cooling rates range from 70°C/hr to 2°C/hr for an initial melt temperature of 1400°C , and from 370°C/hr to 10°C/hr for an initial melt temperature of 1500°C . These values are in fact lower limits as they are based on the time required for complete isotopic homogenization. Although the lower bounds of the cooling rates overlap with the cooling rates deduced from textural and mineralogical studies of CAIs (Wark and Lovering, 1982; MacPherson et al., 1984; Stolper and Paque, 1986), the upper bounds are probably closer to the true cooling rates as the higher rates are compatible with the lack of a detectable spatial gradient of $F(\text{Mg})$ in the larger spinel grains. A recent study of trace element distributions in melilite from type B1 CAIs (Davis et al., 1992) also suggests that the true cooling rates of CAIs are probably closer to the upper bound set by petrographic and textural studies ($\gg 2^{\circ}\text{C/hr}$).

The implications of the cooling rates of the parent melts of CAIs on their formation environment in the nebula was considered in detail by MacPherson et al. (1984). They noted that the cooling rate deduced from petrographic observation ($< 50^{\circ}\text{C/hr}$) are orders of magnitude higher than the cooling rate for the solar nebula as a whole ($10^{-5^{\circ}\text{K/hr}}$), but, are much lower than that for a radiating droplet in a low density solar nebula ($\sim 10^5^{\circ}\text{C/hr}$). Theoretical estimate of cooling rate of a liquid droplet in a low density solar nebula ($P \leq 10^{-3}$) (Tschuiyama et al., 1980 and Macpherson et al., 1984) can be made by the equation:

primitive meteorites could have formed in localized hot-spots relaxes the requirement of an uniformly hot solar nebula, with initial temperature exceeding the melting/condensation temperatures of the refractory phases, in the region of their formation. A low temperature nebula will also be in conformity with standard models for the solar nebula (e.g., Wood and Morfill, 1988). The presence of localized hot and dense microenvironments in the nebula is a pointer towards efficient gas-dust fractionation needed to explain the relatively oxidizing environment in which refractory objects like CAIs and POIs and perhaps chondrules have formed (Anders, 1985). The localized heat source cannot be identified unambiguously even though several possibilities have been suggested; these include lightening (Whipple 1966, Cameron 1966), intense flares from the protosun (Herbig 1978) and probably frictional heating due to gas drag (Wood 1983, 1984).

5.3 Mg-Al Isotopic Systematics and Isotopic Heterogeneity in the Nebula

The presence of the short-lived nuclide ^{26}Al in early solar system objects (CAIs) has been demonstrated conclusively by many workers (Lee et al. 1976, and references in Wasserburg 1985, MacPherson et al., 1988). Studies in different types of CAIs from carbonaceous meteorites belonging to CV and CO groups and individual refractory grains like corundum and hibonite from CM meteorites (Fahey et al. 1987a, Ireland et al. 1990, Virag et al. 1991) have been carried out to obtain information on the initial distribution of ^{26}Al in the solar nebula at the time of formation of these refractory phases. The importance of studying this aspect arises from the following reasons:

- (i) if the distribution of ^{26}Al in the nebula is homogeneous it may be used as a chronometer for early solar system processes.
- (ii) ^{26}Al is a potential heat source for melting and differentiation of meteorite parent bodies.

$$\frac{dT}{dt} = \frac{3\epsilon\sigma}{r\rho \left(C_P + \frac{\Delta H_C}{\Delta T_C} \right)} [T^4 - T_o^4] \quad (5.3)$$

where T and T_o are the absolute temperatures of the liquid and surrounding medium, ϵ is the emissivity, taken to be 0.8 (Carslaw and Jaeger, 1959), σ is the Stefan-Boltzman constant ($5.7 \times 10^{-12} \text{Jcm}^{-2}\text{sec}^{-1}\text{K}^{-4}$), ρ is the density which is $\sim 2.8 \text{gm/cm}^3$ (Bottinga and Weill, 1970), r is the radius ($\sim 0.25 \text{cm}$), C_P is the specific heat ($\sim 1.5 \text{J/gm}^\circ\text{K}^{-1}$; Carmichael et al., 1977), ΔH_C is the latent heat of crystallization ($\sim 550 \text{J/gm}$), and ΔT_C is the temperature interval over which the liquid crystallizes ($\sim 350^\circ\text{K}$; MacPherson et al. 1984). Since we have considered 1400°C (1673°K) and 1500°C (1773°K) as the initial melt temperature of type B1 CAIs like E40, we calculate the cooling rates when the ambient gas temperature T_o is comparable to these two temperatures. When the initial melt temperature is 1773°K and T_o is equal to 1772°K and 1763°K the cooling rates are $\sim 515^\circ\text{C/hr}$ and 5070°C/hr respectively. Similarly when initial melt temperature is 1673°K and when T_o is equal to 1672°K and 1663°K the cooling rates are $\sim 428^\circ\text{C/hr}$ and $\sim 4250^\circ\text{C/hr}$. These calculations show that if the ambient temperature of the nebula is only 1°K less than the liquid droplet the theoretically estimated cooling rates are comparable to the upper limits obtained by our isotopic data. However theoretical models of solar system formation predict temperatures of $< 1000^\circ\text{K}$ in the region of meteorite formation (Wood and Morfill 1988). Even though some theoretical estimate of higher nebular temperature has been made (Boss, 1993), they are still much below the required value of $> 1600^\circ\text{K}$. Thus a low pressure, low temperature environment cannot satisfy the constraint on cooling rates deduced from the observed data in CAIs. One is therefore constrained to invoke localized hot and dense regions in the nebula that will allow for both partial melting of solids and cooling rates appropriate for the formation of CAIs. Sheng et al. (1991a) have made such a suggestion for the formation of most of the refractory objects in the early history of the solar system, by extending their arguments based on the observation of relict spinels in plagioclase-olivine inclusions (POIs), a class of less refractory objects from carbonaceous chondrites that have probably formed at a later time than the CAIs. The possibility that the refractory objects/phases found in

If the distribution of ^{26}Al is homogeneous it can also be used to pinpoint the astrophysical site(s) which could have contributed ^{26}Al to the solar nebula. In this section we discuss the Mg-Al isotopic data for the Efremovka and Grosnaja CAIs to address the above questions. The presence of excess ^{26}Mg in refractory phases resulting from *in situ* decay of ^{26}Al should satisfy the following relation between measured $^{26}\text{Mg}/^{24}\text{Mg}$ in the phases and the initial value of ($^{26}\text{Al}/^{27}\text{Al}$) at the time of their formation:

$$\left(\frac{^{26}\text{Mg}}{^{24}\text{Mg}}\right)_m = \left(\frac{^{26}\text{Mg}}{^{24}\text{Mg}}\right)_i + \left(\frac{^{26}\text{Al}}{^{27}\text{Al}}\right)_i \left(\frac{^{27}\text{Al}}{^{24}\text{Mg}}\right)_m \quad (5.4)$$

The CAIs from Efremovka show well behaved Mg-Al systematics (Fig.4.1) except in E44 where one can see discordance in Mg-Al isotopic data for two different mineral phases [melilite and anorthite] (Fig.4.1d). A minor disturbance can be discerned in the anorthite data for the inclusion E60 (Fig.4.1g) where individual anorthite data yield a range of initial $^{26}\text{Al}/^{27}\text{Al}$ values. Amongst the Grosnaja CAIs only GR2 (Fig.4.1i) has a well behaved systematics but with much lower initial ($^{26}\text{Al}/^{27}\text{Al}$) than the Efremovka CAIs. *The presence of ^{26}Mg excess and its correlation with ($^{27}\text{Al}/^{24}\text{Mg}$) in most of the Efremovka CAIs and in the Grosnaja CAI GR2 confirm the presence of live ^{26}Al in the region of solar nebula where these CAIs formed.*

An important observation that can be made from our data is the fact that the initial ($^{26}\text{Al}/^{27}\text{Al}$) in all but one of the Efremovka inclusions is close to the canonical value of 5×10^{-5} (Fig. 5.6) seen primarily in unaltered type B1 CAIs from CV and CO chondrites [MacPherson et al 1988 and Clayton et al. 1988 and references therein]. The Efremovka CAIs analyzed by us represent four major petrographic types (A, B1, B2, and hibonite rich) and none of them have any distinct signatures of major secondary petrographic alteration. On the other hand, all the Grosnaja CAIs representing three petrographic types [A, B and C (anorthite rich)] have distinct signatures of secondary petrographic alteration [presence of calcite, garnet, Na-rich plagioclase etc] and are characterized by disturbed Mg-Al systematics and/or much lower initial $^{26}\text{Al}/^{27}\text{Al}$ values (0 to 6×10^{-6}). A similar

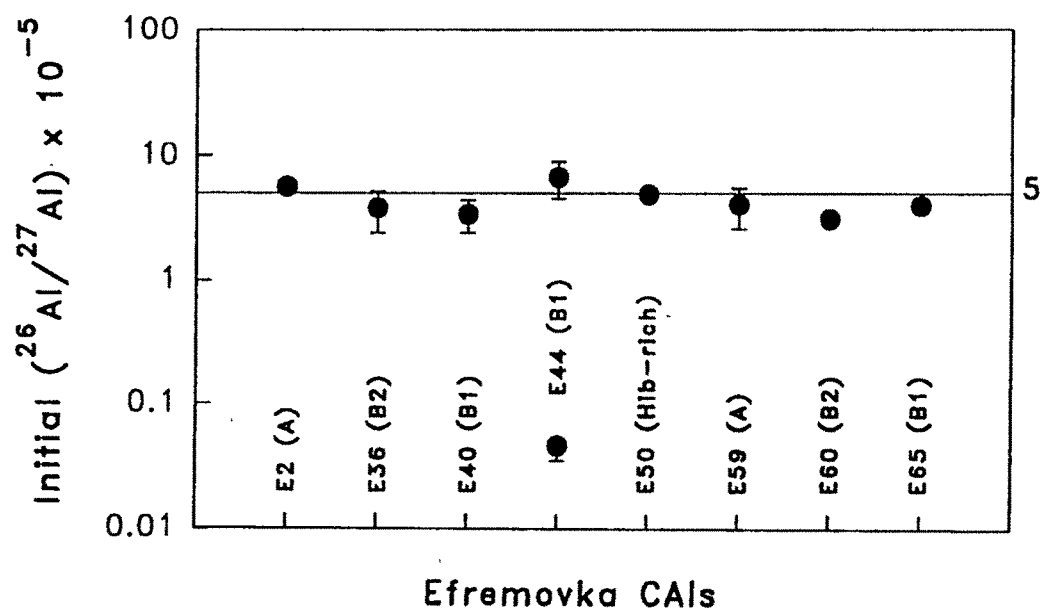


Figure 5.6: Initial $^{26}\text{Al}/^{27}\text{Al}$ in eight Efremovka CAIs analyzed for their magnesium isotopic systematics. The analyzed CAIs represent four petrographic types (A, B1, B2 and hibonite-rich).

situation holds for CAIs studied in earlier work (Macpherson et al., 1988 and references therein) with initial ($^{26}\text{Al}/^{27}\text{Al}$) varying over a wide range from 0 to 5×10^{-5} . Till date more than 500 inclusions and/or refractory phases have been analyzed from carbonaceous chondrites for their Mg isotopic composition and the main observations are :

- (i) a good number of type B1 inclusions show well behaved Mg-Al isochron with initial ($^{26}\text{Al}/^{27}\text{Al}$) close to 5×10^{-5} often referred to as the canonical value,
- (ii) in general type B2 and type A inclusions either have disturbed Mg-Al systematics or have much lower initial ($^{26}\text{Al}/^{27}\text{Al}$) ratio with few exceptions,
- (iii) hibonite-rich inclusions from CM meteorites that have large Ti and Ca isotopic anomalies have initial ($^{26}\text{Al}/^{27}\text{Al}$) that are one or two orders of magnitude lower than the canonical value, and more often devoid of excess ^{26}Mg ; on the other hand hibonites with initial Al isotopic composition close to the canonical value do not show large Ti and Ca isotopic anomaly,
- (iv) Corundum grains fall into distinct groups with different initial Al isotopic composition, the highest being close to the canonical value.

The observed variation in initial $^{26}\text{Al}/^{27}\text{Al}$ ratio in CAIs and refractory phases in different meteorites may be attributed to one or more of the following:

- (i) differences in the time of formation of CAIs and the refractory phases (assuming an uniform distribution of ^{26}Al in the nebula)
- (ii) heterogeneous distribution of ^{26}Al in the solar nebula
- (iii) secondary alteration of some of the objects leading to disturbances in the Mg-Al isotopic systematics.

If the variations are simply ascribed to time assuming an uniform distribution of ^{26}Al in the solar nebula with initial $^{26}\text{Al}/^{27}\text{Al}$ close to the canonical value it would imply a

large time interval ($> 5\text{Ma}$) between the formation of type B1 inclusions and other types of inclusions and some of the refractory phases in CM meteorites. This is a difficult proposition as hibonites found in CM chondrite are more refractory than the phases seen in type B1 CAIs, and they also have much larger Ti/Ca isotopic anomalies than in the case of type B1 CAIs and were either contemporaneous or formed prior to the CAIs. These considerations have led many researchers to propose extreme heterogeneity in the distribution of ^{26}Al in the solar nebula as the cause for the observed variation in the initial $^{26}\text{Al}/^{27}\text{Al}$ seen in refractory phases and CAIs from carbonaceous chondrites. Even though, the fact that bulk of the CAIs analyzed to date have signatures of secondary alteration in low temperature environment which can potentially disturb the Mg-Al systematics leading to low or near absence of ^{26}Al in these objects was noted, it was not emphasized to be the main cause for the observed variations.

The most important feature of the results obtained from this study suggest that the canonical value of 5×10^{-5} for the initial ($^{26}\text{Al}/^{27}\text{Al}$) ratio is not restricted to type B1 CAIs alone. This allows us to generalize upon our results. On the basis of Efremovka data one can question the validity of extreme spatial heterogeneity in the distribution of ^{26}Al in the solar nebula in the region of formation of Efremovka CAIs. Data obtained in this study suggest that all the Efremovka CAIs have most probably sampled the same ^{26}Al reservoir and the variation seen in E60 and E44 may be attributed to secondary processes. In fact the presence of nepheline in E60 indicates possible presence of secondary processes affecting the anorthites. The initial Mg isotopic ratio in E60 which is 2‰ above the reference value is also suggestive of secondary event leading to reequilibration of Mg isotopic systematics in the CAI. The discordant data for melilite and anorthite in E44 is exactly what one expects if there was an exchange of Mg between these two phases with contrasting Al/Mg ratios. Podošek et al., (1991) proposed such a scenario to explain the observed Mg-Al systematics in several Allende CAIs that have disturbed record of secondary alteration, and suggested that secondary processes leading to exchange/reequilibration of Mg isotopes is the main cause for the observed disturbances in Mg-Al systematics seen in petrographically altered CAIs. The Efremovka data, therefore, do not support the idea of an extreme spatial

inhomogeneity of ^{26}Al in the solar nebula. However, we cannot rule out the possibility that there can be more than one distinct reservoir of ^{26}Al in the nebula, particularly in light of the data for hibonite and corundum from CM meteorites. Virag et al., (1991) have in fact suggested the presence of three distinct ^{26}Al reservoir, two of them with initial ($^{26}\text{Al}/^{27}\text{Al}$) $\sim 5 \times 10^{-5}$ and $\sim 2 \times 10^{-6}$ and a third one without ^{26}Al to explain the Mg-Al isotopic systematics in Murchison corundum grains. Although, these grains may have probably sampled a restricted area of the solar nebula, this observation coupled with Efremovka data suggest probable presence of specific zones/reservoirs in the nebula with distinct ($^{26}\text{Al}/^{27}\text{Al}$) isotopic composition.

In the light of isotopic homogeneity of ^{26}Al proposed above for the region in the nebula where the Efremovka CAIs have formed, we shall consider the spatial extent of such homogeneity in comparison to the nebular distribution of ^{16}O and ^{50}Ti , two stable isotopes with anomalous (enriched) abundances in many refractory phases. Oxygen is one of the major elements in the solar system. Isotopic composition of O has been studied extensively in CAIs, chondrules, meteorites, and lunar and terrestrial samples (Clayton 1978, 1993 and references therein). Oxygen has three isotopes (16, 17 and 18) and isotopic ratios are normalized with respect to ^{16}O which is the most abundant isotope, and the isotopic data of oxygen is expressed as deviation ($\delta^{17}\text{O}$ and $\delta^{18}\text{O}$) from the reference value (standard mean ocean water). On the three isotope plot of $\delta^{17}\text{O}$ vs $\delta^{18}\text{O}$ the oxygen isotopic data from different samples are expected to lie on a fractionation line with slope equal to half. However, oxygen isotopic data for refractory phases in CAIs fall on a line with slope ~ 1 (Clayton et al., 1973; Clayton 1978, 1993 and references therein). The individual phases in CAIs show a great variation in oxygen isotopic composition. Certain phases like spinel show a maximum enrichment in ^{16}O ($\delta^{17}\text{O} \sim -40\text{‰}$) and phases like melilite have almost normal isotopic composition. The internal variations have been interpreted as having originated from secondary exchange of O with an external gaseous reservoir. The most ^{16}O rich mineral exchanged the least with this external reservoir whereas the least ^{16}O rich phase experienced maximum exchange, probably due to greater diffusion rates of oxygen (Muehlenbachs and Kushiro 1974 and Hayashi and Muehlenbachs 1984). The

oxygen isotopic data in CAIs can be attributed to the presence of two reservoirs, one (dust) enriched in ^{16}O and another (gas) depleted in ^{16}O and the mixing of these two reservoirs generated the line with slope ~ 1 (Clayton et al. 1985). If one considers the oxygen isotopic data for bulk meteorites and terrestrial and lunar samples they fall on different lines with slope half. The fact that for large ($\gg \text{km}$) objects the oxygen isotopic data do not fall on a single fractionation line indicates a planetary scale heterogeneity in oxygen. On the other hand Ti isotopic anomalies particularly enrichment and at times depletion in the neutron rich isotopes (^{49}Ti and ^{50}Ti) seen in hibonite grains from CM meteorites, show a random scatter in their absolute magnitude. Fahey et al., (1985, 1987a) and Zinner et al., (1986b), suggested that these random variations arise from plausible heterogeneous distribution of the carriers of these anomalies viz. interstellar dust grains in the nebula at a very small scale length. It is interesting to note that Ti-rich phases like pyroxene in type B1 CAIs from CV meteorites have nearly normal Ti isotopic composition. Thus it seems that Ti isotopic variations occur at a spatial scale length that is much smaller than that of ^{26}Al which in turn is perhaps smaller than planetary scale length in the variation of oxygen isotopic distribution in the nebula.

5.4 ^{41}Ca In The Early Solar System

The studies of potassium isotopic composition in Efremovka CAIs, results of which were presented in the previous chapter (Table 4.6) was intended to look for the presence of the short-lived radionuclide ^{41}Ca ($\tau \sim 0.15\text{Ma}$) in the early solar system. The unaltered Efremovka CAIs with initial ($^{26}\text{Al}/^{27}\text{Al}$) close to the canonical value of 5×10^{-5} and containing phases like pyroxene and perovskite with high Ca/K are ideal to look for possible presence of ^{41}Ca in the solar nebula at the time of formation of these CAIs. Previous attempts in this direction (Stegmann and Specht 1983, Hutcheon et al. 1984) using CAIs from Allende and Leoville were not very successful although the data of Hutcheon et al., (1984) provided a hint for the presence of ^{41}Ca in a couple of Allende CAIs with an upper limit of $(8 \pm 3) \times 10^{-9}$ for the initial ($^{41}\text{Ca}/^{40}\text{Ca}$) at the time of their formation. If

^{41}K excess resulting from ^{41}Ca decay is present in refractory phases of CAI one can write the following relation for K-Ca systematics:

$$\left(\frac{^{41}\text{K}}{^{39}\text{K}}\right)_m = \left(\frac{^{41}\text{K}}{^{39}\text{K}}\right)_i + \left(\frac{^{41}\text{Ca}}{^{40}\text{Ca}}\right)_i \left(\frac{^{40}\text{Ca}}{^{39}\text{K}}\right)_m \quad (5.5)$$

The results obtained in the present study, shown in Fig. 5.7, clearly demonstrates that presence of excess ^{41}K in the analyzed phases, particularly those with $\text{Ca}/\text{K} > 3 \times 10^5$. A very good correlation between ^{41}K and the ^{40}Ca content of the analyzed phases has also been observed. The best fit line through the data points yields an initial $(^{41}\text{K}/^{39}\text{K})$ close to the reference value of 0.072 and has a slope of $(1.6 \pm 0.3) \times 10^{-8}$. Even though the Ca/K value for most of the data points lie in the region of $(0.3 \text{ to } 3) \times 10^6$, the correlation holds true even for phases with extreme Ca/K ratio of 2×10^7 . The value of the slope of the correlation line obtained by us is higher than the value $[8 \pm 3] \times 10^{-9}$ reported by Hutcheon et al. (1984). However, a majority of the data points (4 out of 6) with high $^{40}\text{Ca}/^{39}\text{K}$ ($> 5 \times 10^5$) reported by Hutcheon et al. (1984) suggest a higher value for the slope that is closer to the value obtained by us.

We, therefore, believe that the excess ^{41}K signal seen by us in the Efremovka CAIs are real and consider the possible causes for this excess. The observed ^{41}K excess in the Efremovka CAIs can result from any one of the following reasons:

- (i) production of ^{41}Ca by secondary neutrons during cosmic ray exposure of the Efremovka meteorite resulting from (n, γ) reaction with ^{40}Ca present in the CAIs and its subsequent decay,
- (ii) ^{41}K locked in refractory stardust that are part of the initial components of the solar nebula from which the CAIs are formed,
- (iii) presence of the short-lived radionuclide ^{41}Ca in the early solar system that was incorporated 'live' into the CAIs during their formation and its *in situ* decay.

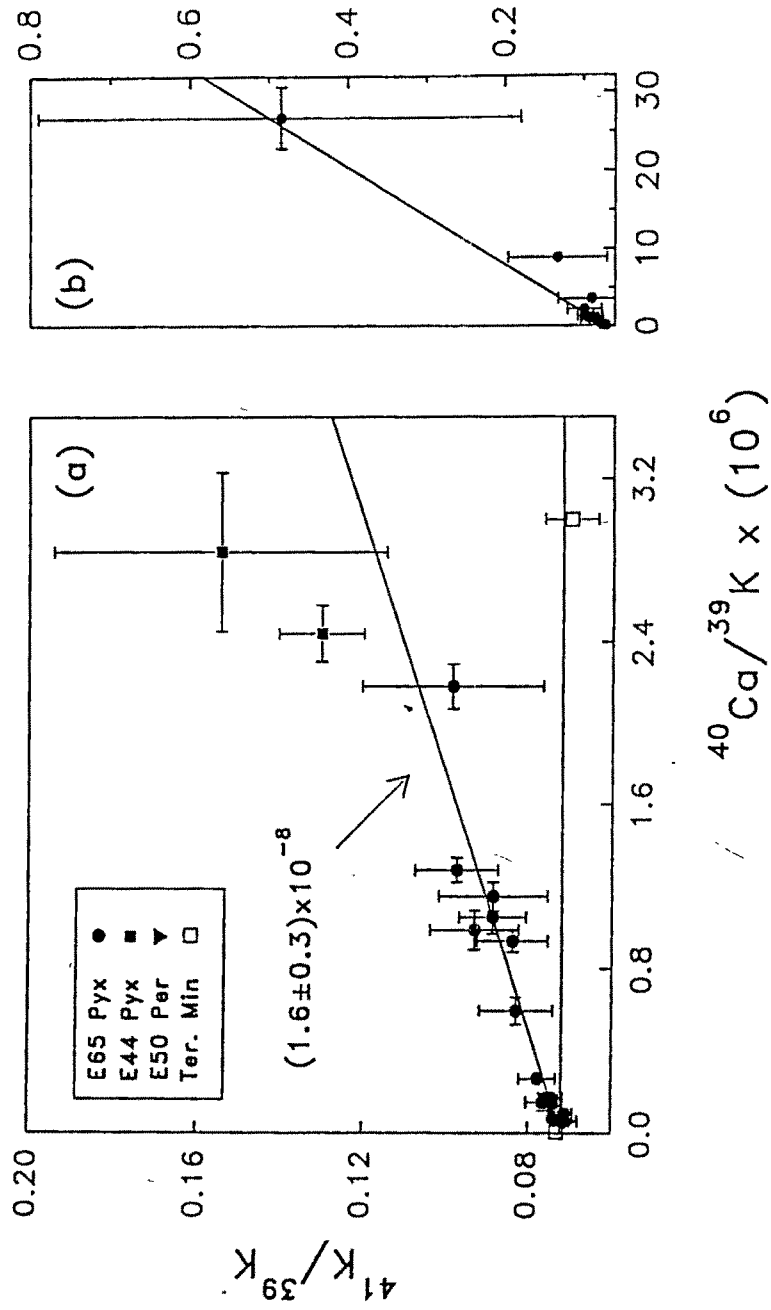


Figure 5.7: Plot of measured potassium isotope ratios as a function of $^{40}\text{Ca}/^{39}\text{K}$ for refractory perovskite(Per) and pyroxene(Pyx) phases in CAIs E50, E44 and E65. For clarity, phases with $\text{Ca}/\text{K} \leq 3.5 \times 10^6$ are shown in Fig(a), while all data points are shown in Fig(b). The open symbols represent data for terrestrial pyroxene, the horizontal line represents the reference potassium isotope ratio (0.072) and the slope of the best fit line is $(1.6 \pm 0.3) \times 10^{-8}$.

As already noted an important observation in this study is the extremely good correlation of excess ^{41}K with ^{40}Ca contents of the analyzed phases. The observed correlation between excess ^{41}K and ^{40}Ca is a natural expectation if the excess ^{41}K is either due to cosmic ray induced effect or due to the presence of ^{41}Ca in the early solar system. On the other hand, such a correlation is difficult to explain in the 'fossil' hypothesis.

If the excess ^{41}K is due to cosmogenic production of ^{41}Ca , the secondary neutron fluence experienced by the Efremovka meteorite should be sufficient to account for the $^{41}\text{Ca}/^{40}\text{Ca}$ ratio of $(1.6 \pm 0.3) \times 10^{-8}$ which represents the slope of the correlation line in Fig. 5.7. With a thermal neutron cross section of 440mb for the $^{40}\text{Ca}(n,\gamma)^{41}\text{Ca}$ (Mughabghab et al., 1981) reaction, a thermal neutron fluence of $\sim 3 \times 10^{16}$ is necessary to explain the observed ratio. Although no direct estimate of the thermal neutron fluence experienced by the Efremovka samples is available a reasonable estimate can be made by comparing it with Allende, as both of them belong to the same meteorite type (CV3). The expected secondary fluence in a meteorite depends mainly on three parameters: the cosmic ray exposure duration, the pre-atmospheric size and the chemical composition of the meteorite. The preatmospheric size is an important parameter as the production of secondary neutrons within the meteorite increases with shielding depth and reaches a maximum at a shielding depth of $\sim 100\text{-}150\text{gmcm}^{-2}$. The noble gas data for the Efremovka meteorite (Mazor et al., 1970) suggest a cosmic ray exposure age of $\sim 10\text{Ma}$ for this meteorite which is twice that for the Allende (Fireman and Gobel 1970). However, the pre-atmospheric size of Efremovka, with a recovered mass of $\sim 21\text{Kg}$, is likely be much smaller than that of Allende for which the recovered mass exceeds 2000Kg. A fairly reliable estimate of the neutron fluence experienced by Allende has been made by Gobel et al., (1982) based on studies of the neutron produced isotope ^{36}Ar (from ^{36}Cl). The inferred values are a few times 10^{14}cm^{-2} (up to 10^{15}cm^{-2}). Even if we consider the higher value of neutron fluence estimated for Allende and the factor of two higher exposure age of Efremovka compared to Allende, the neutron fluence experienced by Efremovka cannot exceed a few times 10^{15}cm^{-2} in view of its smaller pre-atmospheric size. This fluence is an order of magnitude less than that required to explain the observed ^{41}K excess in the Efremovka CAIs. Therefore, the

possibility that the observed ^{41}K excess is due to production by secondary neutrons during the cosmic ray exposure of the Efremovka meteorite in the interplanetary space can be ruled out.

The possibility that 'fossil' records of extinct nuclide decay products may be found in primitive meteorite was proposed by Clayton (1977, 1982, 1986). He has also suggested specifically that ^{41}K of 'fossil' origin could be present in refractory inclusions of primitive meteorites, which would enhance the $^{41}\text{K}/^{39}\text{K}$ ratio in these objects above the normal solar system value (Clayton 1977). In this model the refractory condensates (stardust) formed in stellar environment (e.g. supernova envelope) will be enriched in their refractory element concentrations (e.g. Ca) compared to the volatile (e.g. K) and as such they will have high Ca/K ratio and also excess ^{41}K from ^{41}Ca decay. Since these stellar condensates are expected to be an important component of the solar nebula they will find their way into the CAIs that are considered to be some of the first solids to form in the solar system via processes invoking condensation, evaporation, and/or melting/recrystallization. These CAIs can therefore inherit excess ^{41}K from the stellar condensates. The magnitude of ^{41}K excess in the CAI will depend upon several parameters including the initial elemental fractionation in the stellar environment during the formation of the stellar condensates and the degree of enrichment of stellar condensates, relative to normal solar system matter, in the parent material from which the CAIs are formed. While this scenario has its own appeal, it does not readily explain the correlation between excess ^{41}K and ^{40}Ca content seen in our data. One may attempt to explain this correlation by considering mixing of two components during the formation of the CAIs with one of the components having both high (Ca/K) ratio and large ^{41}K excess and the other with lower ratio and normal potassium isotopic composition (Clayton, 1993). Such a scenario appears *ad hoc* and there are quite a few free parameters, particularly fractionation factors, whose values cannot be easily constrained. The data presented by us suggest an enrichment in the $^{41}\text{K}/^{39}\text{K}$ ratio by a factor of six in the pyroxene with the highest Ca/K value. Thus in the 'fossil' model, the stellar condensates must be characterized by values that are much higher than this enrichment factor, a proposition difficult to accommodate. It may also be noted that

Clayton (1977) predicted an enhancement of only 0.25% for the $^{41}\text{K}/^{39}\text{K}$ value in CAI based on this model. Thus it is extremely unlikely that the observed ^{41}K excess could be of 'fossil' origin. The presence of a small component of 'fossil' ^{41}K in the CAIs however cannot be ruled out unequivocally.

The ^{41}K excess in the Efremovka CAIs and its correlation with ^{40}Ca can therefore be best explained by considering the presence of live ^{41}Ca in the early solar system at the time of formation of the Efremovka CAIs. Because of the short half-life of ^{41}Ca , the observation of ^{41}K excess in early solar system objects puts some stringent constraint on the time interval between the last nucleosynthetic input to the solar nebula and the formation of some of the first solar system solids (CAIs). We shall consider these time scales based on ^{26}Al and ^{41}Ca data in Efremovka CAIs in the following section.

5.5 Extinct Radionuclides and Time Scales for Early Solar System Process

The presence of short-lived nuclei decay product in CAI allow us to constrain the time interval between the last injection of nucleosynthetic matter to the solar nebula and the formation of these objects. The strictest lower limit on this time interval is provided by the observation of radionuclide with the shortest meanlife. Prior to this study ^{26}Al ($\tau \sim 1.1\text{Ma}$) was the shortest lived radionuclide whose presence in the early solar system was conclusively established. The present study showed that ^{41}Ca with a six times shorter meanlife ($\sim 0.15\text{Ma}$) than ^{26}Al was also present in the early solar system. As a first approximation we assume that that all the solar system Al, Mg, Ca and K was injected during the last nucleosynthetic event prior to the isolation of the nebula. The time interval ' Δ ' between injection of this matter [containing ^{26}Al and ^{41}Ca] into the solar nebula and formation of CAIs is given by the relation:

$$\Delta = -\frac{1}{\lambda} \cdot \ln \left[\frac{M}{P} \right] \quad (5.6)$$

where M is the measured ratio, P is the production ratio and λ is the radioactive decay constant for the particular nuclide. Before we apply the above relation to evaluate Δ we consider the production ratios of ($^{26}\text{Al}/^{27}\text{Al}$) and ($^{41}\text{Ca}/^{40}\text{Ca}$) in the various astrophysical sites. A discussion on the plausible nucleosynthetic sites for ^{26}Al is given by Clayton and Leising (1987); these are:

- (i) explosive nucleosynthesis in supernova where $P \sim 10^{-3}$ (Truran and Cameron 1978, Woosley and Weaver 1980),
- (ii) hydrostatic carbon burning in massive stars $P \sim 10^{-3}$ (Arnett and Wefel 1978),
- (iii) high temperature hydrogen burning in nova and asymptotic giant branch stars where $P \sim 0.1$ to 1 (Hillebrandt and Theileman 1982, Cameron 1985, and Wasserburg et al. 1994).

While the production ratio of ($^{26}\text{Al}/^{27}\text{Al}$) vary over a wide range the situation in case of ^{41}K which is believed to be produced as its radioactive progenitor ^{41}Ca is simpler. The nucleosynthetic processes that have been considered for production of ^{41}Ca are:

- (i) explosive oxygen burning: $P \sim 1.5 \times 10^{-3}$ (Woosley et al. 1973),
- (ii) explosive silicon burning: $P \sim 10^{-3}$ (Bodansky et al. 1968).

The production ratio of ($^{41}\text{Ca}/^{40}\text{Ca}$) can also be estimated by considering the solar system abundance of K and Ca isotopes. Since ^{41}Ca is the radioactive progenitor of ^{41}K , the production ratio is $\sim 4 \times 10^{-3}$. If we consider equal production of the odd mass nuclides ^{41}Ca and ^{43}Ca we get a production value of 1.3×10^{-3} . The production ratio for ^{41}Ca is thus much more tightly constrained than ^{26}Al and ranges from $[1 \text{ to } 4] \times 10^{-3}$.

Based on the above production ratios (P) for ^{26}Al and the measured ratio (M) of 5×10^{-5} in CAIs the estimated time interval Δ varies from 3 to 10 Ma. In the case of ^{41}Ca , the value for Δ is <1.5 Ma for a measured ratio of 1.6×10^{-8} . If we assume that the injection of ^{26}Al

and ^{41}Ca into the solar nebula had taken place contemporaneously we can use data for both ^{26}Al and ^{41}Ca and get a value of Δ by using the relation:

$$\Delta = -\frac{1}{\lambda_i - \lambda_j} \cdot \ln \left[\frac{M_i}{P_i} \cdot \frac{P_j}{M_j} \right] \quad (5.7)$$

where P_i and P_j refer to production ratios, M_i and M_j refer to measured ratios in CAIs, and λ_i and λ_j refer to the decay constants of the two short-lived radionuclides. For the range of above mentioned production ratios for ^{26}Al and ^{41}Ca , Efremovka CAIs yield Δ value in the range of 0.6 to 2Ma.

However, these values are upper limits as the above relation does not take into account the dilution of the freshly injected matter with pre-existing nebular matter of normal composition. There is no simple way of rigorously estimating this dilution factor. One can only make an order of magnitude calculation based upon the short lived radioisotope ^{129}I ($\tau \sim 23\text{Ma}$). The production processes of iodine isotopes are well understood, and the production ratio of $^{129}\text{I}/^{127}\text{I}$ is of the order of unity. The measured initial value of $^{129}\text{I}/^{127}\text{I}$ in meteoritic phases is $\sim 10^{-4}$. If the decrease in the initial ratio from its value at production is ascribed to free decay interval ' Δ ' then the time interval is ~ 200 Ma. However, the presence of ^{26}Al and ^{41}Ca in CAIs show that free decay interval is only a few million years, which is negligible compared to the meanlife of ^{129}I . Therefore, one can postulate a dilution factor of $\sim 10^4$ to explain the measured initial $^{129}\text{I}/^{127}\text{I}$ ratio. One must however note that ^{129}I has a meanlife much greater than that of ^{26}Al and ^{41}Ca and therefore, it could have been produced over a much longer time scale in different stellar sites/sources and these individual contributions cannot be easily decoupled. Further, there is no *a priori* way of predicting whether all short-lived nuclei were introduced into the solar nebula from the same source(s) and got diluted to the same extent. Wasserburg et al., (1994) have recently proposed a similar dilution factor by considering data for various short-lived nuclides in the early solar system and assuming a common source (AGB star) for their origin. A nebular dilution factor of $\sim 10^4$ combined with the measured and production ratios of ^{41}Ca

in Efremovka CAIs yield a time interval Δ of $< 1\text{Ma}$. Even though the uncertainty in the proper choice of $^{26}\text{Al}/^{27}\text{Al}$ makes it difficult to exactly obtain this time scale, the required production rate that will yield a time scale compatible with that obtained from ^{41}Ca is 0.15 which is within the range predicted for different stellar sites. The ^{41}Ca data predicts the strictest lower limit for the time interval between the injection of freshly synthesized nucleosynthetic matter to the solar nebula and formation of CAIs. The time scale obtained from ^{41}Ca is also consistent with the recent observation of ^{60}Fe in differentiated meteorites (Shukolyukov and Lugmair 1993a, b) which suggest that the time interval between the isolation of the nebula and the formation of large ($\gg \text{km-sized}$) objects and their subsequent heating, melting and recrystallization is $< 10\text{Ma}$.

Chapter 6

Summary and Conclusions

The primary aim of this thesis was to analyze pristine CAIs from primitive meteorites to understand the formation and evolution of these early solar system objects and to delineate the time scales of early solar system processes. CAIs from the carbonaceous chondrite Efremovka, representing different petrographic types, that have not undergone major secondary alteration, were selected for this study. These CAIs have been analyzed for their Mg, K and Ca isotope compositions. In addition, several CAIs from the Grosnaja meteorite with distinct signatures of secondary petrographic alterations were also analyzed to assess the effect of secondary alterations on Mg-Al isotopic systematics. The isotopic studies were carried out using the techniques of secondary ion mass spectrometry. A brief summary of the work carried out and the important results and conclusions obtained are given below.

The Efremovka CAIs studied in this work encompass all the major petrographic types (A, B1, B2 and hibonite-rich) which allow us to generalize upon our results. Since these studies were carried out on a newly acquired ion microprobe, the instrument was thoroughly tested for its suitability for high mass resolution isotopic studies of Mg, K, Ca and Ti by analyzing terrestrial analogs of the meteoritic phases. Extensive tests were carried out to ensure that conditions necessary for reproducible and high-precision isotopic measurements are adequately met by the instrument. Measurement of terrestrial standards as well as isotopically doped silicate glasses gave good results with a precision of 2‰ ($2\sigma_m$) for

magnesium isotopic analysis even on samples with low Mg content (few hundred ppm). Reliable measurements of isotopic compositions of other elements (e.g. Ca and Ti) that require extremely high mass resolution ($M/\Delta M \sim 10,000$) could also be performed with high precision.

Magnesium isotopic studies of Efremovka CAIs belonging to different petrographic types revealed well-behaved isotopic systematics. This confirms their pristine nature as inferred from earlier trace element as well as petrographic studies which showed the near absence of secondary alteration products in these inclusions. The isotopic data provided new information on the nebular sites and processes responsible for the formation of the CAIs, and also on the distribution of ^{26}Al in the solar nebula. These are:

- (i) Sympathetic behaviour of isotopic and petrographic data, seen for the first time in a non-FUN refractory inclusion (E40), substantiates the role of volatilization as an important CAI forming process. A short duration volatilization event, affecting the parent melt of this CAI, can best explain the observed correlation between isotopic and petrographic data in this Efremovka CAI.
- (ii) The presence of relict spinel was inferred from the observed isotopic disequilibrium in coexisting spinel and melilite in an once-molten Efremovka CAI. This facilitates finer constraints on the cooling rate of the parent melt of this inclusion. The deduced cooling rates range from few degrees to few hundred degrees per hour depending on the initial temperature of the source melt (1400 to 1500°C). Such cooling rates are not viable in the low pressure nebular environment. Further, the predicted temperatures of $< 1000^\circ\text{K}$ in the meteorite forming zone ($\sim 3\text{AU}$), in the standard model of solar nebula, point towards localized hot and dense regions, that allow for both partial melting of refractory precursors of CAIs and appropriate cooling rate, as the most plausible site for CAI formation. This also suggests an efficient gas-dust fractionation mechanism operating in the nebula.
- (iii) All the Efremovka CAIs and one of the Grosnaja CAIs are characterized by the pres-

ence of excess ^{26}Mg which correlates well with ^{27}Al , confirming the presence of live ^{26}Al in the nebula at the time of formation of these CAIs. The values for the initial aluminium and magnesium isotopic ratios at the time of formation of the different Efremovka CAIs can be explained if we consider a relatively uniform source reservoir characterized by a normal magnesium isotopic composition and an initial $^{26}\text{Al}/^{27}\text{Al}$ close to the canonical value of 5×10^{-5} . The disturbed isotopic systematics, seen in one of the Efremovka CAIs, can be understood in terms of partial reequilibration involving isotopic exchange between two mineral phases with contrasting Al/Mg ratios. The observed extreme variation in initial $^{26}\text{Al}/^{27}\text{Al}$ in the Grosnaja CAIs can be attributed to post-formation processes affecting these CAIs. Our data, therefore, suggest a relatively homogeneous distribution of ^{26}Al in the region of CAI formation. We do not favour the view of an extremely heterogeneous distribution of ^{26}Al in the solar nebula, proposed to explain the large variation $^{26}\text{Al}/^{27}\text{Al}$ seen in many CAIs. As most of these CAIs also show clear signatures of secondary alteration, these variations most probably reflect late stage disturbances in Mg isotopic systematics due to secondary processes affecting these CAIs. If we consider all the isotopic data in totality it is however difficult to rule out the presence of more than one distinct reservoir of ^{26}Al in the solar nebula.

- (iv) The K-Ca isotopic studies of Efremovka CAIs have indicated definite presence of ^{41}K excess in them which correlates well with ^{40}Ca content of the analyzed phases. Several possibilities like neutron induced reaction during cosmic ray exposure of the Efremovka meteorite, contribution from 'fossil' ^{41}K locked in stellar condensates that can find their way into the CAIs, and the presence of 'live' ^{41}Ca in the early solar system were considered. The last alternative can best explain our observations. Our data yield an initial $^{41}\text{Ca}/^{40}\text{Ca}$ ratio of $(1.6 \pm 0.3) \times 10^{-8}$ at the time of formation of Efremovka CAIs. ^{41}Ca can now be added to the list of extinct radionuclides that were present in the early solar system.
- (v) The presence of short-lived radionuclides ^{26}Al and ^{41}Ca allows us to put strong

constraint on the time interval between the cessation of nucleosynthetic input to the solar nebula and the formation of solar system objects. Our data suggest this time interval to be $< 1\text{Ma}$. Such a short time interval is also consistent with the recent observation of excess ^{60}Ni (resulting from decay of ^{60}Fe [meanlife $\sim 2\text{Ma}$]) in differentiated meteorites that suggests the formation of large ($\gg \text{Km}$ -sized) objects in the early solar system and their subsequent melting, cooling and recrystallization within a short span of $< 10\text{Ma}$.

6.1 Scope for Future Work

The work presented in this thesis represents the first detailed study of pristine CAIs from the Efremovka carbonaceous chondrite. The study was conducted to explore the possibility of a better understanding of the processes in the formative stages of the solar system. The Efremovka CAIs have lived up to the promise of their primeval nature. The results summarized in the preceding pages are very encouraging and attest to the utility of carrying out detailed study of such CAIs.

The petrographic and isotopic studies of Efremovka CAIs have allowed us to identify important CAI forming process like volatilization. Similar studies of CAIs from the carbonaceous chondrites Vigarano and Leoville that are also free from major secondary alteration effects will be useful in this regard. Laboratory based simulation experiments have indicated the formation of Ca-aluminates during intense evaporation of melilite. Such phases are not present in any of Efremovka CAIs analyzed in this work although they are present in some other Efremovka CAIs (e.g., E66). Detailed studies of such CAIs may further improve our understanding and quantification of processes like volatilization during the formation of CAIs.

The advantages of isotopic studies in identifying relict phases have been clearly demonstrated in this study. Relict grains can probably go a long way in indentifying precursors of not only CAIs but also of chondrules. In fact a very recent report on obser-

vation of relict spinel in chondrules (Misawa and Fujita 1994) suggests CAIs as one of the precursor component of chondrules. The constraints on nebular environment for CAI formation, obtained from this study, should be cross checked by studying other CAIs. These may provide us with finer details of nebular environment (e.g. extent of gas-dust fractionation, temperature and density) which can improve our understanding of the state of the solar nebula. The nature and cause for the localized heat source is not well understood and needs further study.

Mg-Al isotopic systematics of Efremovka CAIs negate the idea of an extremely heterogeneous distribution of ^{26}Al in the solar nebula. Although the sample set consisted of the major petrographic types, type C and fine-grained inclusions did not form a part of this study. Isotopic studies of such inclusions from other meteorites are few in number. A study of petrographically unaltered type C and fine-grained inclusions from Efremovka will probably complete the picture. Further studies of CAIs from CV and CM meteorites may probably allow us to identify if there were more than one distinct reservoir of ^{26}Al and their spatial extent. Proper identification of the causes for the presence of distinct reservoirs of ^{26}Al will enhance our understanding of mixing scale lengths of dust and gas in the evolutionary epoch of the solar nebula or vice versa.

The story of ^{41}Ca has just begun, and it is necessary to study a large number of CAIs to establish its presence on a firm footing. The important Ca-rich phases e.g. hibonite and perovskite, which are less abundant in CAIs from CV meteorites but more abundant in CM meteorites, could not be studied in detail in this work. These phases are probably better candidates than pyroxenes for such studies. Enstatite chondrites which have formed in a reducing environment have an important phase, oldhamite (CaS), this may also be suitable for K-Ca isotopic studies.

The list of possible short-lived radionuclides whose presence in the early solar system has been established is far from complete. Although the presence of ^{60}Fe has been established in differentiated meteorites, its presence in CAIs or chondrules is yet to be confirmed experimentally due to the lack of Fe-rich Ni-poor phases in these objects. If the secondary

alteration processes affecting the CAIs took place rather early in the history of the solar system the Fe-rich altered phases in CAIs (e.g. hedenbergite, garnet, hercynite) may be good candidates for such studies. In addition, one can also analyze Fe-rich olivine grains in chondrules. Presence of ^{99}Tc ($t_{1/2} \sim 0.2\text{Ma}$) and ^{36}Cl ($t_{1/2} \sim 0.3\text{Ma}$) which decay to ^{99}Ru and ^{36}Ar respectively, is yet to be conclusively established. A hint for the presence of ^{99}Tc in the early solar system was reported by Yin et al. (1992) in the Marlinga meteorite. Since ^{99}Tc and ^{36}Cl have halflives more than twice that of ^{41}Ca they should have been present in the early solar system at the time of CAI formation. The presence of ^{99}Tc in AGB stars undergoing thermal pulsations is well established. Therefore, excess ^{99}Ru due to ^{99}Tc decay in primitive objects will provide strong experimental evidence in favour of the recent proposal that a single AGB star was a major contributor of several short-lived radionuclides to the solar nebula (Wasserburg et al., 1994). Further, it would be interesting to investigate the production rates of ^{41}Ca and ^{36}Cl in AGB stars. Another important question is whether the contribution of short-lived radionuclides to the solar nebula was from a single source or multiple sources over a long period of time. The currently available data on ^{26}Al and ^{60}Fe favour a single injection (Wasserburg et al. 1994). Presence of ^{41}Ca , and ^{99}Tc and ^{36}Cl (if proven) will provide rigorous constraint in this regard. While both thermal ionization mass spectrometer and ion microprobe will play significant role in our future endeavour to understand the formation and early evolution of the solar system, higher resolution ion microprobe than presently available will probably be best suited for further studies of refractory microphases from primitive meteorites.

References

- Anders E. (1985) Chondrites in the solar nebula: A review. *Meteoritics* 20, 601-602.
- Armstrong J. T., Huneke J. C., Shaw H. F., Finnerty T. A., and Wasserburg G. J. (1982) Standard $\text{CaAl}_2\text{Si}_2\text{O}_8$ glasses with various Mg isotopic compositions for ion microprobe characterization. In *Microbeam Analysis - 1982* (ed. K. F. J. Heinrich), pp. 205-209. San Francisco Press.
- Armstrong J. T., Hutcheon I. D., and Wasserburg G. J. (1984) Disturbed Mg isotopic systematics in Allende CAI. *Lunar Planet. Sci.* XV, 15-16.
- Arnett D. and Wefel J. P. (1978) ^{26}Al production from a stellar evolutionary sequence. *Astrophysical Journal (Lett.)* 224, L139-L142.
- Begemann F. (1980) Isotopic anomalies in meteorites. *Rept. Prog. Phys.* 43, 1309-1356.
- Bennighoven A., Rudenauer F. G., and Werner H. W. (1987) Secondary Ion Mass Spectrometry: Basic Concepts, Instrumental Aspects, Applications and Trends. John Wiley and Sons, New York.
- Bodansky D., Clayton D. D., and Fowler W. A. (1968) Nuclear quasi-equilibrium during silicon burning. *Astrophysical Journal (Suppl.)*, 16, 299-371.
- Boss A. P. (1993) Midplane temperatures in the solar nebula. *Lunar and Planet. Sci.* XXIV, 151-152.
- Bottinga Y., and Weill D. F. (1970) Densities of liquid silicate systems calculated from molar volumes of oxide components. *American J. of Science* 269, 169-182.
- Brigham C. A., Hutcheon I. D., Papanastassiou D. A., and Wasserburg G. J. (1988) Isotopic heterogeneity and correlated isotope fractionation in purple FUN inclusions. *Lunar Planet. Sci.* XIX, 132-133.
- Brigham C. A. (1990) Isotopic heterogeneity in Ca-Al-Rich meteoritic inclusions. Ph.D. dissertation, California Institute of Technology.
- Caillet C., Zinner E. K., and MacPherson G. J. (1991) Mg-Al isotopic study of a deformed and recrystallized Leoville type B refractory inclusion: Hot accretion into a cold matrix, and if so when? *Lunar Planet. Sci.* XXII, 167-168.
- Cameron A. G. W. (1966) The accumulation of chondritic material. *Earth Planet. Sci. Lett.* 1, 93-96.
- Cameron A. G. W. (1985) Formation and evolution of the primitive solar nebula In *Protostars and Planets II* (eds. E. H. Levy and M. S. Mathews), pp 1073-1099. University of Arizona Press, Tucson.

- Cameron A. G. W. (1993) Nucleosynthesis and star formation. In *Protostars and Planets III* (eds. E. H. Levy, J. I. Lunine and M. S. Mathews), pp 47-73. University of Arizona Press, Tucson.
- Carslaw H. S. and Jaeger J. C. (1959) *Conduction of Heat in Solids*. (2d ed.). Oxford Univ. Press, London.
- Carmichael I. S. E., Nicholls J., Spera F. J., Wood B. J., and Nelson S. A. (1977) High temperature properties of silicate liquids; Applications to the equilibration and ascent of basic magma. *Phil. Trans. Royal Soc. (London)* A286, 373-431.
- Catanzaro E. J., Murphy T. J., Garner E. L., and Shields W. R. (1966) Absolute isotopic abundance ratios and atomic weights of magnesium. *J. Res. Nat. Bur. Stand.* 70a, 453-458.
- Clayton D. D. (1977) Interstellar potassium and argon. *Earth Planet. Sci. Lett.* 36, 381-390.
- Clayton D. D. (1982) Cosmic chemical memory: A new Astronomy. *Quat. J. of Roy. Ast. Soc.* 23, 174-212.
- Clayton D. D. (1986) Interstellar fossil ^{26}Mg and its possible relationship to excess meteoritic ^{26}Mg . *Astrophysical Journal* 310, 490-498.
- Clayton D. D., and Leising M. D. (1987) ^{26}Al in the interstellar medium. *Phys. Rept.* 144, 1-50.
- Clayton D. D. (1993) (private communication).
- Clayton R. N., Mayeda T. K., and Grossman L. (1973) A component of primitive nuclear composition in carbonaceous chondrites. *Science* 182, 485-488.
- Clayton R. N. (1978) Isotopic anomalies in early solar system. *Ann. Rev. Nucl. Part. Sci.* 28, 501-522.
- Clayton R. N., MacPherson G. J., Hutcheon I. D., Davis A. M., Grossman L., Mayeda T. K., Molini-Velsko C., and Allen J. M. (1984) Two forsterite-bearing FUN inclusions in the Allende meteorite. *Geochim. Cosmochim. Acta* 48, 535-548.
- Clayton R. N., Mayeda T. K., Molini-Velsko C. A. (1985) Isotopic variations in solar system material: evaporation and condensation of silicates. In *Protostars and Planets II* (eds. D. C. Black and M. S. Mathews), pp 755-771, Univ. of Arizona Press, Tucson.
- Clayton R. N., Mayeda T. K., Palme H., and Laughlin J. (1986) Oxygen, silicon and magnesium isotopes in Leoville refractory inclusions and chondrules from Vigarano. *Lunar Planet. Sci.* XVII, 139-140.
- Clayton R. N., Hinton R. W., and Davis A. M. (1988) Isotopic variations in rock forming elements in meteorites. *Phil. Trans. Roy. Soc.(London)* A325, 483-501.
- Clayton R. N. (1993) Oxygen isotopes in meteorites. *Ann. Rev. Earth Planet. Sci.* 21,

115-149.

- Compston W. and Pidgeon R. T. (1986) Jack hills , evidence of more very old detrital zircons in Western Australia. *Nature* 321, 766-769.
- Davis A. M., and Hinton R. W. (1986) Magnesium and titanium isotopic compositions and trace element chemistry of refractory inclusions in the Ornans carbonaceous chondrite. *Lunar Planet. Sci.* XVII, 154-155.
- Davis A. M., Hashimoto A., Clayton R. N., and Mayeda T. K. (1990) Correlated isotopic mass fractionation of oxygen, magnesium and silicon in forsterite evaporation residues. *Nature* 347, 655-658.
- Davis A. M., MacPherson G. J., Clayton R. N., Mayeda T. K., Sylvestor P. J., Grossman L., Hinton R. W. and Laughlin J. R. (1991) Melt solidification and late-stage evaporation in the evolution of a FUN inclusion from the Vigarano C3V chondrite. *Geochim. Cosmochim. Acta* 55, 621-637.
- Davis A. M., Simon S. B., and Grossman L. (1992) Melilite composition trends during crystallization of Allende Type B1 refractory inclusion melts. *Lunar Planet. Sci.* XXIII, 281-282.
- Esat T. M., and Taylor S. R. (1984) Correlated REE and Mg anomalies in Allende Inclusions. *Lunar Planet. Sci.* XV, 252-253.
- Fahey A., Goswami J. N., McKeegan K. D., and Zinner E. (1985) Evidence for extreme Ti enrichment in primitive meteorites. *Ap. J. (Letters)* 296, L17-L20.
- Fahey A., Zinner E., and Kurat G. (1986) Anomalous Ca and Ti in a hercynite-hibonite inclusion from Lance. *Meteoritics* 21, 359-361.
- Fahey A., Goswami J. N., McKeegan K. D., and Zinner E. (1987a) Al, Pu, Ti, REE, and trace element abundances in hibonite grains from CM and CV meteorites. *Geochim. Cosmochim. Acta* 51, 329-350.
- Fahey A., Zinner E. K., Crozaz G., and Kornacki A. S. (1987b) Microdistribution of Mg isotopes and REE abundances in a Type A calcium- aluminium-rich inclusion from Efremovka. *Geochim. Cosmochim. Acta* 51, 3215-3229.
- Fireman E. L. and Gobel R. (1970) Argon-37 and Argon-39 in recently fallen meteorites and cosmic ray variations. *J. Geophys. Res.* 75, 2115-2124.
- Gnaser H. and Hutcheon I. D. (1987) Preferential emission of lighter isotopes in the initial stage of sputtering. *Surface Science* 195, 499-512.
- Gobel R., Begemann F., and Ott U. (1982) On neutron-induced and other noble gases in Allende inclusions. *Geochim. Cosmochim. Acta*, 46, 1777-1792.
- Goswami J. N., Srinivasan G., and Ulyanov A. A (1993) Grosnaja ABCs: Magnesium isotope composition. *Lunar Planet. Sci.* XXIV, 553-554.

- Grossman L. (1975) Petrography and mineral chemistry of Ca-rich inclusions in the Allende meteorite. *Geochim. Cosmochim. Acta* 39, 433-454.
- Grossman L. (1972) Condensation in the primitive solar nebula. *Geochim. Cosmochim. Acta* 36, 597-619.
- Grossman L. (1980) Refractory inclusions in the Allende meteorite. *Ann. Rev. Earth Planet. Sci.* 8, 559-608.
- Harper C. L. (1993) Isotopic astronomy from anomalies in meteorites: Recent advances and new frontiers. *J. Phys. G. (Nucl. Part. Phys.)* 19, 581-594.
- Hartmann D., Woosley S. E., and El. Eid, M. F., (1985) Nucleosynthesis in neutron-rich supernova ejecta. *Astrophysical Journal* 297, 837-845.
- Hashimoto A. (1991) Evaporation of melilite. *Meteoritics* 26, 344.
- Hayashi T. and Muehlenbachs K. (1984) Rapid oxygen diffusion in melilite and its relevance to meteorites. *EOS Trans. Amer. Geophys. Union* 65, 308.
- Herbig G. H. (1978) Some aspects of early stellar evolution that may be relevant to the origin of the solar system. In *The origin of the Solar System*, (eds. S. F. Dermott), pp.219-235. Wiley and Sons, New York.
- Hillebrandt W. and Thielemann F. K. (1982) Nucleosynthesis in novae a source of Ne-E, ^{26}Al ? *Astrophysical Journal* 255, 617-623.
- Hinton R. W., Davis A. M., and Scatena-Wachel D. E. (1987) Large negative Ti-50 anomalies in refractory inclusions from the Murchison carbonaceous chondrite - Evidence for incomplete mixing of neutron-rich supernova ejecta into the solar system. *Astrophysical Journal* 313, 420-428.
- Hinton R. W., Davis A. M., Scatena-Wachel D. E., Grossman L., and Draus R. J. (1988) A chemical and isotopic study of hibonite-rich refractory inclusions in primitive meteorites. *Geochim. Cosmochim. Acta* 52, 2573-2598.
- Huneke J. C., Armstrong J. T., and Wasserburg G. J. (1983) FUN with PANURGE: High mass resolution ion microprobe measurements of Mg in Allende inclusions. *Geochim. Cosmochim. Acta* 47, 1635-1650.
- Hutcheon I. D. (1982) Ion probe magnesium isotopic measurements of Allende inclusions. *Amer. Chem. Soc. Symp. Series* 176, 95-128.
- Hutcheon I. D., Armstrong J. T., and Wasserburg G. J. (1984) Excess ^{41}K in Allende CAI: A hint reexamined. *Meteoritics* 19, 243-244.
- Hutcheon I. D., Armstrong J. T., and Wasserburg G. J. (1986) Mg isotope studies of CAI in C3V chondrites. *Lunar Planet. Sci. XVII*, 372-373.
- Ireland T. R., Compston W., and Heydegger H. R. (1985) Titanium isotopic anomalies in hibonites from Murchison carbonaceous chondrite. *Geochim. Cosmochim. Acta* 49,

1989-1993.

- Ireland T. R., Compston W., and Esat T. M. (1986) Magnesium isotopic composition of olivine, spinel, and hibonite from the Murchison carbonaceous chondrite. *Geochim. Cosmochim. Acta* 50, 1413-1421.
- Ireland T. R. (1988) Correlated morphological, chemical and isotopic characteristics of hibonites from the Murchison carbonaceous chondrites. *Geochim. Cosmochim. Acta* 52, 2827-2839.
- Ireland T. R. (1990) Presolar isotopic and chemical signatures in hibonite-bearing refractory inclusions from the Murchison carbonaceous chondrite. *Geochim. Cosmochim. Acta* 54, 3219-3237.
- Jungck M. H. A., Shimamura T., and Lugmair G. W. (1984) Ca isotope variations in Allende. *Geochim. Cosmochim. Acta* 48, 2651-2658.
- Kaiser T., and Wasserburg G. J. (1983) The isotopic composition and concentration of Ag in iron meteorites and the origin of exotic silver. *Geochim. Cosmochim. Acta* 47, 43-48.
- Kornacki A. S., and Fegley B. Jr. (1984) Origin of spinel-rich chondrules and inclusions in carbonaceous and ordinary chondrites. *Proc. Lunar Planet. Sci. Conf. 14th*, B588-B596.
- Kuehner S. M., Davis A. M., and Grossman L. (1989) Identification of relict phases in a once-molten Allende inclusion. *Geophys. Res. Lett.* 16, 775-778.
- Lapareur M. (1980) Le micro-analyseur ionique de seconde generation Cameca, model 3F. *Rev. Tech. Thompson-CSF* 12, 225-265.
- Lee T., Papanastassiou D. A., and Wasserburg G. J. (1976) Demonstration of ^{26}Mg excess in Allende and evidence for ^{27}Al . *Geophys. Res. Lett.* 3, 109-112.
- Lee T., Papanastassiou D. A., and Wasserburg G. J. (1977) ^{26}Al in the early solar system: Fossil or fuel? *Astrophysical Journal Lett.* 211, L107-L110.
- Lee T. (1979) New isotopic clues to solar system formation. *Rev. Geophys Space Phys.* 17, 1591-1611.
- Lee T. (1988) Implications of isotopic anomalies for nucleosynthesis. In: *Meteorites and Early Solar System* (eds J. F. Kerridge and M. S. Mathews), pp 1063-1089. Arizona Univ. Press, Tucson.
- Lugmair G. W. (1991) (private communication).
- Macdougall J. D., and Goswami J. N. (1981) Windows to early solar system processes: Refractory inclusions in CV and CM chondrites. *Proc. Indian Acad. Sci. (Earth Planet. Sci.)* 50, 1-26.
- MacPherson G. J., and Grossman L. (1981) A once-molten, coarse grained, Ca-rich

- inclusion in Allende. *Earth Planet. Sci. Lett.* 52, 16-24.
- MacPherson G. J., Paque J., Stolper E., and Grossman L. (1984) The origin and significance of reverse zoning in melilite from Allende Type B inclusions. *J. Geol.* 92, 289-305.
- MacPherson G. J., Wark D. A., and Armstrong J. T. (1988) Primitive material surviving in chondrites: Refractory inclusions. In *Meteorites and the Early Solar System* (eds. J. F. Kerridge, and M. S. Matthews), pp. 746-807. Arizona Univ. Press, Tucson.
- Marvin U. B., Wood J. A., and Dickey J. S. Jr. (1970) Ca-Al-Rich phases in the Allende meteorite. *Earth Planet. Sci. Lett.* 7, 346-350.
- Mason B., and Taylor S. R. (1982) Inclusions in the Allende meteorite. *Smithsonian Contrib. Earth Sci.* 25.
- Mazor E. Heymann D., and Anders E. (1970) Noble gases in carbonaceous chondrites. *Geochim Cosmochim. Acta* 34, 781-824.
- McKeegan K. D., Walker R. M., and Zinner E. (1985) Ion microprobe isotopic measurement of individual interplanetary dust particle. *Geochim. Cosmochim. Acta* 49, 1971-1987.
- Molini-Velsko C. A. (1983) Isotopic composition of silicon in meteorites. Ph.D. dissertation, University of Chicago.
- Muehlenbachs K. and Kushiro I. (1974) Oxygen isotope exchange and equilibrium of silicates with CO₂ or O₂. *Carnegie Inst. of Washington Year Book* 73, 232-236.
- Mughabghab S. F., Divadeenam M., and Holden N. E. (1981) *Neutron Capture Cross Section Vol I*. Academic Press, New York.
- Nagasawa H., Blanchard D. P., Jacobs J. W., Brannon J. C., Philpotts J. A., and Onuma N. (1977) Trace element distribution in mineral separates of the Allende inclusions and their genetic implications. *Geochim. Cosmochim. Acta* 41, 1587-1600.
- Nazarov M. A., Ulyanov A. A., Korina M. I., and Kolesov G. M. (1982) Efremovka CAI's : Major and Trace Element Chemistry. *Lunar Planet. Sci.* XIII, 584-585.
- Nazarov M. A., Korina M. I., Ulyanov A. A., Kolesov G. M., and Sherbovsky E. Ya. (1984) Mineralogy, petrology and chemical composition of Ca and Al-rich inclusions of Efremovka meteorite. (In Russian) *Meteoritika* 43, 49-66.
- Niederer F. R., and Papanastassiou D. A. (1984) Ca isotopes in refractory inclusions. *Geochim. Cosmochim. Acta* 48, 1279-1294.
- Podosek F. A. (1978) Isotopic structures in solar system materials. *Ann. Rev. Astron. Astrophys* 16, 293-334.
- Podosek F. A., Zinner E. K., MacPherson J. G., Lundberg L. L., Brannon C. J., and Fahey A. J. (1991) Correlated study of initial Sr/ Sr and Al-Mg isotopic systematics and

- petrographic properties in a suite of refractory inclusions from the Allende meteorite. *Geochim. Cosmochim. Acta* 55, 1083-1110.
- Provost A. (1990) An improved diagram for isochron data. *Chemical Geology* 80, 85-99.
- Sears D. W. G. and Dodd R. T. (1988) Overview and classification of meteorites. In *Meteorites and the Early Solar System* (eds. J. F. Kerridge, and M. S. Matthews), pp. 3-31. Arizona Univ. Press, Tucson.
- Sheng Y. J., Hutcheon I. D., and Wasserburg G. J. (1991a) Origin of plagioclase-olivine inclusions in carbonaceous chondrites. *Geochim. Cosmochim. Acta* 55, 581-599.
- Sheng Y. J., Wasserburg G. J., and Hutcheon I. D. (1991b) Self-diffusion of magnesium in spinel and in equilibrium melts: constraints on flash heating of silicates. *Geochim. Cosmochim. Acta* 55, 2535-2546.
- Shukolyukov A. and Lugmair G. W. (1993a) Live Iron-60 in the early solar system. *Science*, 259, 1138-1142.
- Shukolyukov A. and Lugmair G. W. (1993b) ^{60}Fe in eucrites. *Earth Planet. Sci. Lett.* 119, 159-166.
- Simon S. B., Grossman L., and Davis A. M. (1991) Fassaite composition trends during crystallization of Allende Type B refractory inclusion melts. *Geochim. Cosmochim. Acta* 55, 2635-2655.
- Slodzian G., Chaintreau M. P., and Dennebouy R. C. (1987) Self regulated potential at insulating surfaces in presence of a strong electrostatic extraction field. *Proc. 11th Int. Conf. on X-ray optics and microanalysis (Canada)*.
- Stegmann W. and Specht S. (1983) Investigation of Mg and K isotopic abundances in Allende and Leoville Ca-Al-Rich Inclusions. *Meteoritics* 18, 402.
- Stolper E. (1982) Crystallization sequences of Ca-Al-rich inclusions from Allende: An experimental study. *Geochim. Cosmochim. Acta* 46, 2159-2180.
- Stolper E., and Paque J. (1986) Crystallization sequences of Ca-Al-rich inclusions from Allende: The effects of cooling rate and maximum temperature. *Geochim. Cosmochim. Acta* 50, 1785-1806.
- Thiemens M. H. (1988) Heterogeneity in the nebula: evidence from stable isotopes. In *Meteorites and Early Solar System* (eds. J. F. Kerridge, and M. S. Matthews), pp. 899-923. Arizona Univ. Press, Tucson.
- Tilton G. R. (1988) Age of the solar system. In *Meteorites and the Early Solar System* (eds. J. F. Kerridge, and M. S. Matthews), pp. 259-275. Arizona Univ. Press, Tucson.
- Truran J. W., and Cameron A. G. W. (1978) ^{26}Al production in explosive carbon burning. *Astrophysical Journal* 219, 226-229.
- Tsuchiyama A. , Nagahara H., and Kushiro I. (1980) Experimental reproduction of

- textures of chondrules. *Earth Planet. Sci. Lett.* 48, 155-165.
- Ulyanov A. A., Korina M. I., Nazarov M. A., and Sherbovsky E. Ya. (1982) Efremovka carbonaceous chondrite. *Lunar Planet. Sci.* XIII, 813-814.
- Ulyanov A. A. and Kolesov G. M. (1984) REE in CAIs of Efremovka chondrite. *Lunar Planet. Sci.* XV, 874-875.
- Ulyanov A. A., Ustinov V. I., Zagryazhskaya G. D., Gavrilov E. Ya., and Shukolyukov Yu. A. (1988) Oxygen isotope compositions of refractory inclusions of carbonaceous chondrites. *Geochemistry International* 25, No 3, 13-20.
- Ulyanov A. A. and Kononkova N. N. (1990) Mineralogy of metal rich refractory inclusions in the carbonaceous chondrite Efremovka. (In Russian) *Meteoritika* 49, 74-92.
- Ulyanov A. A. (1991) (private communication).
- Virag A., Zinner E., Amari S., and Anders E. (1991) An ion microprobe study of corundum in the Murchison meteorite: Implications for Al and O in the early solar system. *Geochim. Cosmochim. Acta* 54, 2045-2062.
- Wang J., Davis A. M., Hashimoto A., and Clayton R. N. (1991) The role of diffusion in the isotopic fractionation of magnesium during evaporation of forsterite. *Lunar Planet. Sci.* XXII, 1461-1462.
- Wark D. A. and Lovering J. F. (1977) Marker events in the early solar system: Evidence from rims on Ca-Al-rich inclusions in carbonaceous chondrites. *Proc. Lunar Sci. Conf.* 8, 95-112.
- Wark D. A. and Lovering J. F. (1982) The nature and origin of type B1 and B2 Ca-Al-rich inclusions in the Allende meteorite. *Geochim. Cosmochim. Acta* 46, 2581-2594.
- Wark D. A. (1987) Plagioclase-rich inclusions in carbonaceous chondrite meteorites: Liquid condensates? *Geochim. Cosmochim. Acta* 51, 221-242.
- Wasserburg G. J., Lee T., and Papanastassiou D. A. (1977) Correlated O and Mg isotopic anomalies in Allende inclusions: II Magnesium. *Geophys. Res. Lett.* 4, 299-302.
- Wasserburg G. J., Papanastassiou D. A., and Lee T. (1980) Isotopic heterogeneities in solar system. In *Early Solar System and Present Solar System* (ed. D. Lal) pp. 144-191. North Holland, Amsterdam.
- Wasserburg G. J. and Papanastassiou D. A. (1982) Some short-lived nuclides in the early solar system - A connection with the placental ISM. In *Essays in Nuclear Astrophysics* (eds. C. A. Barnes, D. D. Clayton, and D. N. Schramm), pp. 77-140. Cambridge Univ. Press.
- Wasserburg G. J. (1985) Short-lived nuclei in early solar system. In *Proto Stars and Planets II* (eds. D. C. Black and M. S. Matthews) pp 703-737. Arizona Univ. Press, Tucson.

- Wasserburg G. J., Busso M., Gallino R., and Raiteri C. M. (1994) Asymptotic Giant Branch Stars as a source of short-lived radioactive nuclei in the solar nebula. *Astrophysical Journal* 424, 412.
- Wetherill G. W. and Chapman C. R. (1988) Asteroids and meteorites. In *Meteorites and the Early Solar System* (eds. J. F. Kerridge and M. S. Matthews), pp. 35-67. Arizona Univ. Press, Tucson.
- Whipple F. L. (1966) Chondrules: Suggestions concerning their origin. *Science* 153, 54-56.
- Williamson J. H. (1968) Least square fitting of a straight line. *Canadian Jour. of Physics* 46, 1845-1847.
- Wood J. A. (1983) Formation of chondrules and CAIs from interstellar grains accreting to the solar nebula. Mem. Natl. Inst. Polar Res. Special Issue 30, 84-92.
- Wood J. A. (1984) On the formation of meteoritic chondrules by aerodynamic drag heating in the solar nebula. *Earth Planet. Sci. Lett.* 70, 11-26.
- Wood A. and Morfill G. E. (1988) A review of solar nebula models. In *Meteorites and the Early Solar System* (eds. J. F. Kerridge and M. S. Matthews), pp. 329-347. Arizona Univ. Press, Tucson.
- Woosley S. E., Arnett W. D., and Clayton D. D. (1973) The explosive burning of oxygen and silicon. *Astrophysical Journal (Supple.)* 231, 231-312.
- Woosely S. E. and Weaver T. A. (1980) Explosive neon burning and ^{26}Al gamma ray astronomy. *Astrophysical Journal* 238, 1017-1025.
- Yin Q., Jagoutz E., and Wanke H. (1992) Re-search for extinct ^{99}Tc and ^{98}Tc in the early Solar System. *Meteoritics* 27, 310.
- York D. (1967) The best isochron. *Earth Planet. Sci. Lett.* 2, 479-482.
- York D. (1969) Least-squares fitting of a straight line with correlated errors. *Earth Planet. Sci. Lett.* 5, 320-324.
- Zinner E., Fahey A. J., and McKeegan K. D. (1986a) Characterization of electron multipliers by charge distributions. In *Secondary Ion Mass Spectrometry (SIMS V)* (eds. A. Bennighoven, R. J. Colton, D. S. Simons, and H. W. Werner) pp 170-172. Springer Verlag, Berlin, Heidelberg, New York.
- Zinner E., Fahey A. J., Goswami J. N., Ireland T. R., and McKeegan K. D. (1986b) Large ^{48}Ca anomalies are associated with ^{50}Ti anomalies in Murchison and Murray hibonites. *Astrophysical Journal Lett.* 311, L103-L107.
- Zinner E. K., Caillet C., and El Goresy A. (1991) Evidence for extraneous origin of a magnesiowustite metal Fremdling from the Vigarano CV3 chondrite. *Earth Planet. Sci. Lett.* 102, 252-264.

List of Publications

- Goswami J. N., Srinivasan G., and Ulyanov A. A. (1991) Ion-Probe studies of Efremovka CGIs-I : Magnesium isotopic composition. *Lunar Planet. Sci.* XXII, 469-470.
- Goswami J. N., Shah V. G., and Srinivasan G. (1991) Isotopic studies by a secondary ion mass spectrometer: Parametric investigations. *Proc. 5th National Symp. on Mass Spec.* (Ahmedabad, India), Paper EPS-18/1-4.
- Goswami J. N., Srinivasan G., and Ulyanov A. A. (1991) Titanium, calcium and magnesium isotopic compositions in a hibonite-rich inclusion from Efremovka. *Meteoritics* 26, 339.
- Goswami J. N., Srinivasan G., and Ulyanov A. A. (1992) Isotopic disequilibrium in coexisting mineral phases in an Efremovka CGI : An ion probe study. *Lunar Planet. Sci.* XXIII, 431-432.
- Goswami J. N., Srinivasan G., and Ulyanov A. A. (1993) Grosnaja ABCs: Magnesium isotope composition. *Lunar Planet. Sci.* XXIV, 553-554.
- Srinivasan G., Ulyanov A. A., and Goswami J. N. (1993) Search for ^{41}K excess in Efremovka CAIs. *Meteoritics* 28, 442.
- Srinivasan G., Ulyanov A. A., and Goswami J. N. (1993) Time Scales for the Formation of Early Solar System Objects. *Proc. 6th National Symposium on Mass Spectrometry* (Dehradun, India), Paper EPS-24/489-491.
- Goswami J. N., Srinivasan G., and Ulyanov A. A. (1994) Ion microprobe studies of Efremovka CAIs-I: Magnesium isotope composition. *Geochim. Cosmochim. Acta* 57, 431-447.
- Srinivasan G., Ulyanov A. A., and Goswami J. N. (1994) ^{41}K Excess in Efremovka CAIs. *Lunar Planet. Sci.*
- Goswami J. N. and Srinivasan G. (1994) Isotopic analysis of early solar system objects by an ion microprobe: Parametric studies and initial results. *Proc. Ind. Acad. Sci. (EPS)* 103.
- Srinivasan G., Ulyanov A. A., and Goswami J. N. (1994) ^{41}Ca in the early solar system. *Astrophysical Journal Lett.* (submitted).
- Srinivasan G., Ulyanov A. A., Hutcheon I. D., and Goswami J. N. (1994) Excess ^{41}K in CV3 Chondrites. *Meteoritics*.